

RECEIVED

JUN 12 1997

IL GEOL SURVEY

INVESTIGATION OF THE HYDRAULIC EFFECTS OF DEEP-WELL INJECTION OF INDUSTRIAL WASTES

Edward Mehnert, Craig R. Gendron, and Ross D. Brower



ENVIRONMENTAL GEOLOGY 135
HWRIC RR 051 1990

ILLINOIS GEOLOGICAL
SURVEY LIBRARY

JAN 28 1991

Department of Energy and Natural Resources
Illinois State Geological Survey
Hazardous Waste Research and Information Center



LIBRARY

ILLINOIS STATE GEOLOGICAL SURVEY



3 3051 00005 4753

INVESTIGATION OF THE HYDRAULIC EFFECTS OF DEEP-WELL INJECTION OF INDUSTRIAL WASTES

Edward Mehnert, Craig R. Gendron, and Ross D. Brower
Illinois State Geological Survey

Final Report

Prepared for

United States Environmental Protection Agency
Office of Drinking Water
David Morganwalp, Project Officer
EPA Cooperative Agreement No. CR-813508-01-0

and

Hazardous Waste Research and Information Center
Department of Energy and Natural Resources
Jacqueline Peden, Project Officer
ENR Contract No. HWR 86022


1990
ENVIRONMENTAL GEOLOGY 135
HWRIC RR 051

ILLINOIS STATE GEOLOGICAL SURVEY
Natural Resources Building
615 East Peabody Drive
Champaign, Illinois 61820

HAZARDOUS WASTE RESEARCH AND INFORMATION CENTER
One East Hazelwood Drive
Champaign, Illinois 61820

ILLINOIS GEOLOGICAL
SURVEY LIBRARY

JAN 28 1991



Digitized by the Internet Archive
in 2012 with funding from
University of Illinois Urbana-Champaign

<http://archive.org/details/investigationofh135mehn>

CONTENTS

FIGURES	iv
TABLES	vi
ACKNOWLEDGMENTS	vii
ABSTRACT	viii
EXECUTIVE SUMMARY	ix
GLOSSARY	xi
1. INTRODUCTION	1
Background	1
Purpose	2
2. GEOLOGY OF THE INJECTION SYSTEM	3
Overview of the Geologic Environment	3
Regional Geology and Hydrogeology	14
3. HYDROGEOLOGIC INVESTIGATION OF THE INJECTION SYSTEM	23
Stratigraphic and Structural Definition of the Injection System	23
Field Investigations	32
4. NUMERICAL MODELING	48
Model Selection	48
Model Description	48
Input Data	49
Modeling Results	54
Model Projections for Long-Term Injection	58
Hypothetical Conduits	61
5. SUMMARY AND CONCLUSIONS	64
Evaluation of Injection Scenarios	64
Evaluation of Monitoring Strategies	64
REFERENCES	66
APPENDIX A Theory and practical application of geophysical logging instruments	70
APPENDIX B Reduction and analysis of geophysical log data	81
APPENDIX C Brucite formation: proposed mechanism of formation	88
APPENDIX D Sensitivity analysis	96

FIGURES

1	Location of investigation site	2
2	Generalized areal geology of the bedrock surface	5
3	Generalized statewide cross sections of Illinois	6
4	Description of rock units and their hydrogeologic roles	8
5	Geologic structures in Illinois	10
6	Seismic risk map for Illinois	11
7	Earthquake epicenters in Illinois	12
8	Oil and gas fields of the Illinois Basin	13
9	Location of underground gas storage projects in Illinois	15
10	Generalized thickness and distribution of the Maquoketa Group	16
11	Cross section from Rockford to Cairo showing position of base of the USDW	17
12	Generalized thickness and distribution of the Hunton Supergroup and the TDS boundary for USDW	18
13	Generalized thickness and distribution of the New Albany Group	19
14	Generalized thickness and distribution of the Mississippian System and the TDS boundary for USDW	21
15	Well locations	25
16	Geologic column for the injection system at WDW2	26
17	Stratigraphic correlation utilizing resistivity logs for southwest-northeast cross section	27
18	Qualitative permeability correlation utilizing permeability indicator logs for southwest-northeast cross section	28
19	Stratigraphic correlations utilizing resistivity logs for north-south cross section	29
20	Structure contour map of the top of the Lingle Formation in the vicinity of the Velsicol plant	30
21	Injection system in WDW2 indicating permeable and impermeable units delineated with available geophysical logging	31
22	Injection system in WDW2 indicating permeable and impermeable units delineated after phase I logging	33
23	Injection system in WDW2 indicating permeable and impermeable units delineated after phase II logging	37
24	Core locations for WDW2	39
25	Core permeabilities (air and water) versus depth for WDW2	41
26	Core permeabilities versus core porosities for WDW2	41
27	Unit locations for WDW2	42
28	Water level record for the Devonian Observation Well (DOW), including data from injection test	47
29	Plot of data used for Cooper-Jacob analysis	47
30	Schematic for WDW2	50
31	Schematic for DOW	51
32	Relationship between waste viscosity and specific gravity	52
33	The compressibility of water and various NaCl solutions versus temperature	53
34	Comparison of model-predicted drawdowns with results from Theis analysis	55
35	Comparison of model-predicted drawdowns versus time with Hantush analysis	55
36	Conceptual model 1 of the injection system	56
37	Comparison of model-predicted Δh versus field data	59
38	Head buildup versus radial distance for $q = 1.82 \times 10^{-4} \text{ m}^3/\text{sec}$	59
39	Injection scenario 1: head buildup and decline with time at the DOW	59
40	Injection scenario 2: head buildup and decline with time at the DOW	60
41	Injection scenario 2: head buildup and decline with time at WDW2	60
42	Conceptual model 2 of the injection system	61

43	Effect of microannulus on the head buildup at the WDW2	63
44	Effect of microannulus on the head buildup at the DOW	63
45	Effect of microannulus on the head buildup in the "Carper sand"	63
46	Head buildup in the "Carper sand" versus radial distance from WDW2	63
A-1	Caliper Log tool which utilizes a dual potentiometer configuration	70
A-2	Continuous Spinner Flowmeter Log tool	71
A-3	Generalized Sonic Log tool	73
A-4	Idealized schematic of receiver (R) signal	73
A-5	Generalized Borehole Compensated Sonic Log tool	74
A-6	Generalized Compensated Neutron Log tool	75
A-7	Generalized two-detector Density Log tool	76
A-8	Schematic diagram of induction log principles	77
A-9	Schematic diagram of lateral logging system	78
A-10	Schematic diagram of normal logging system	78
A-11	Schematic diagram of spontaneous potential circuit	79
B-1	"Tornado" chart for Dual Induction-Focused Log analysis	81
B-2	Neutron porosity lithologic correction chart	81
B-3	Compensated Neutron Log and Borehole Compensated Acoustilog porosity crossplot	82
B-4	Determination of the cementation factor	85
B-5	Rm-Rmf-Rmc relationships	86
B-6	NaCl concentration for different temperatures and fluid resistivities	87
B-7	Core porosity versus log porosity (phase I, cross-plotted porosity) for WDW2	87
B-8	Core water saturation versus log water saturation for WDW2	87
C-1	Injection system in WDW2 indicating permeable and impermeable zones delineated with the aid of geophysical logging	89
C-2	Core composition: dolomite, brucite for WDW2	91
C-3	SEM photograph for core at 2,484.5 feet KB (x58.5)	92
C-4	SEM photograph for core at 2,484.5 feet KB (x1,050)	93
C-5	SEM photograph for core at 2,479.5 feet KB (x80)	93
C-6	SEM photograph for core at 2,479.5 feet KB (x1,080)	94
C-7	SEM photograph for core at 2,456.5 feet KB (x113)	94
C-8	SEM photograph for core at 2,456.5 feet KB (x1,160)	95
D-1	Conceptual model 1 of the injection system	96
D-2	Conceptual model 2 of the injection system	97
D-3	Sensitivity analysis: effect of injection rate	99
D-4	Sensitivity analysis: effect of rock compressibility	99
D-5	Sensitivity analysis: effect of fluid compressibility	100
D-6	Sensitivity analysis: effect of hydraulic conductivity	100
D-7	Sensitivity analysis: effect of anisotropy	100

TABLES

1	Wells used in study	24
2	Data from geophysical logs run in the DOW	34
3	Data from existing geophysical logs run in WDW2	35
4	Summary of important formation characteristics	36
5	Fluid loss percentage calculated from CSFL	36
6	Core location and analysis	38
7	Results of core analysis	40
8	Summary of hydrogeological data for a portion of the disposal zone	43
9	Additional hydrogeological data for primary injection sections	45
10	Selected chemical and physical properties of water injected during injection test	46
11	Volume injected into WDW2 during injection test	46
12	Analysis of injection test	46
13	Selected parameters for fluids injected via WDW2	51
14	Chemical analysis of waste and brine	53
15	Compressibility of waste and brine	54
16	Input data for the Theis solution	55
17	Input data for leaky aquifer simulation	56
18	Selected input data for model calibration	56
19	Comparison of transmissivity (T) and storativity (S) values	57
20	Permeability of the microannulus	62
B-1	Data from geophysical logs run in the DOW	81
B-2	Data from existing geophysical logs run in WDW2	84
B-3	Summary of important formation characteristics	85
C-1	Core porosities and brucite concentration	90
C-2	Effect of brucite concentration on total flow	90
D-1	Effect of boundary conditions on head buildup	97

ACKNOWLEDGMENTS

We thank the following people for their assistance throughout this project.

Jeffrey S. Brown, Robert Colvin, and Thomas Capps, Velsicol Chemical Corporation, for allowing us access to their site and assistance in the completion of the field tests conducted on-site.

Frank Brookfield and Lance Perry, Hazardous Waste Research and Information Center (HWRIC), for their tireless assistance with the PRIME computer—from debugging and compiling code to not complaining when we monopolized the computer time.

Richard A. Cahill, Beverly Seyler, Robert R. Frost, Herbert Glass, and William R. Roy, Illinois State Geological Survey (ISGS), for performing various chemical and physical analyses on samples of the core, waste stream, and native formation brine. These analyses included thermodynamic modeling, x-ray fluorescence, microprobe, scanning electron microscopy, and x-ray diffraction.

Lynn R. Evans, ISGS, for compiling the data regarding the chemical and physical characteristics of the UIC wastes.

David Morganwalp, project manager for the U.S. Environmental Protection Agency, for his assistance and patience during this project.

Jackie Peden, HWRIC project manager, and Gary D. Miller, former project manager, for their assistance and patience during this project.

Adrian Visocky, Illinois State Water Survey, for his advice regarding the analysis of the data from the injection test.

Anne M. Graese, Bruce R. Hensel, Timothy H. Larson, Janis D. Treworgy, and Steven T. Whitaker, ISGS, for their insightful review of this report.

ABSTRACT

A numerical modeling study was conducted to investigate the hydraulic effects of liquid waste injection on an injection system. The site investigated was a chemical refinery with an operational Class I well and an observation well, both completed in Devonian limestone. Input data for the model were obtained from available records and field investigations.

The regional geologic investigation indicated that the injection system (defined here as the injection zone and its associated confining units) was laterally continuous. The hydraulic response of the injection system was numerically modeled under two injection scenarios: average historical injection rate and maximum average permitted rate. For both scenarios, pressure buildup from waste injection during the simulated 30-year injection and 30-year postinjection periods did not approach the pressure calculated to be necessary to initiate or propagate fractures in the injection system. Therefore, injected waste would be contained, and waste injection at this site and for the scenarios modeled would not endanger human health or the environment.

This analysis assumes that hydraulic conductivity remains constant; however, the formation of brucite within the injection zone may invalidate this assumption and the preceding analysis. Brucite formation within the injection zone requires additional study.

The model was also used to investigate the response of the injection system when a hypothetical conduit was introduced. This hypothetical conduit connected the uppermost injection zone with an overlying aquifer. Differences in head buildup were not monitorable in the injection well or in an observation well completed in the injection zone. Monitorable head differences were observed only in the overlying aquifer, when the hydraulic conductivity of the hypothetical conduit was greater than or equal to $1 \times 10^{-10} \text{ m}^2$.

EXECUTIVE SUMMARY

Concern over the potential for groundwater contamination from waste injection prompted a multi-faceted research effort funded by the U.S. Environmental Protection Agency (USEPA) and industry. The research will provide the USEPA with data needed to determine if underground injection of hazardous waste endangers human health or the environment. One facet of this research effort was an investigation of the hydraulic effects of deep-well injection on the injection system.

The injection system includes the geologic units constituting the injection zone and the upper and lower confining units. The site of this investigation was a chemical refinery in Illinois that has an operational injection well and an observation well completed in Devonian limestone.

Data Collection and Analysis

Before numerical modeling could be conducted, a hydrogeologic description of the site was developed from available records and geophysical logs. Numerous records and logs were available from oil- and gas-related tests and wells within a 10-mile radius of the site. Logs and records for on-site wells were also used.

In addition, hydraulic tests and geophysical logs were run to obtain detailed hydrogeologic data on the injection system. Two hydraulic tests were run in the injection well: a continuous spinner flowmeter survey and a 15-day injection test. Sidewall cores were also retrieved from the injection well. The following geophysical logs were run in the observation well: Compensated Neutron Log, Borehole Compensated Sonic Log, Minilog, Dual Induction Spherically Focused Log, and Gamma Ray Log.

Although analyses of the data from these logs and tests yielded much information concerning the hydrogeologic character of the injection system, there was one discrepancy—the results of the spinner flowmeter indicated that the waste was flowing through different zones of the injection system than had been theorized from the results of geophysical logging. To clarify this discrepancy, we conducted additional analyses (x-ray diffraction and scanning electron microscopy). The discrepancy can be explained briefly as follows. Because of its high pH, the injected wastewater reacts with the Mg^{2+} present in the injection zones or in solution, forming brucite ($Mg[OH]_2$). Brucite accumulation reduces the permeability of the injection zone. Greater amounts of brucite apparently formed in the injection zones where the flow of fluid was greater; thus the zones with higher permeability were affected first. Additional work beyond the scope of this project is needed to verify the brucite-formation hypothesis. Also, the long-term effect of this decrease in permeability on injectivity needs to be investigated.

Numerical Modeling

Site Analysis

A description of the regional and site-specific stratigraphy, structural geology, and hydrogeology of the injection system was generated from a review of available data and the field work conducted during this project. This description formed the basis of input for the numerical model. Model input also included data on the physical and chemical characteristics of the injected wastewater and the native brine in the injection system.

These data were employed as input data for a three-dimensional groundwater flow model (HST3D). Before the effects of various injection scenarios were evaluated, HST3D was verified with respect to two analytical solutions and calibrated by the use of data collected during a 2-week injection test. Both verification and calibration were considered satisfactory.

Once calibrated, the model was used to predict the effects of various injection scenarios. The effect of long-term injection was investigated at two constant injection rates—the average historical rate ($1.15 \times 10^{-2} \text{ m}^3/\text{sec}$) and the maximum average rate permitted under Class I regulations ($2.21 \times 10^{-2} \text{ m}^3/\text{sec}$). With both scenarios, significant head buildup was observed at the injection well and radially from it. During the simulated 30-year injection period, steady state was approached but not obtained for both injection scenarios. During the subsequent 30-year postinjection period, dropoff in head buildup was fairly rapid, falling to half in less than 2,000 hours for both scenarios. The maximum hydraulic pressures at the bottom of the well and at the base of the upper confining unit were significantly lower than the pressures calculated to initiate hydraulic fracturing. A fracture gradient of $1.5 \times 10^4 \text{ Pa/m}$ (Pascals/meter) (0.65 psi/ft) was used to calculate the hydraulic fracture pressures.

The regional and site-specific geological analysis revealed the continuity of the stratigraphy and qualitative permeability on a regional basis. The numerical modeling indicated that injection pressures were lower than calculated pressures required to initiate hydraulic fracturing. Therefore, from a hydraulic viewpoint, waste injected into this injection system would be contained, and waste injection at this site and for the scenarios modeled would be considered protective of human health and the environment.

These results were based on an assumption that the permeability remains constant. If the hypothesis concerning the formation of brucite is correct, its formation may reduce the permeability of the injection zones and invalidate this analysis. Any reduction in permeability of the injection zones will probably increase the hydraulic pressure resulting from waste injection if the injection rate remains constant. In such a situation, hydraulic fracturing may be of concern. Because of the potential ramifications, formation of brucite within the injection zone requires additional geochemical analysis.

Effects of Hypothetical Conduit

The model was also used to investigate the hydraulic response of the injection system to the introduction of a hypothetical conduit. The conduit, a microannulus (0.01 m wide) at the injection well, hydraulically connects the uppermost injection zone and an aquifer immediately overlying the upper confining unit. To determine the impact of the microannulus, the head buildup with the microannulus present was compared with the buildup from runs with the microannulus not present. Differences in head buildup at selected positions and for certain times were computed. Differences in the head buildup were considered unmonitorable at the injection well and the observation well. The difference in head buildup in the overlying aquifer was monitorable only when the microannulus had a hydraulic conductivity greater than or equal to $1.00 \times 10^{-10} \text{ m}^2$. The head buildup in the overlying aquifer is a function of its hydraulic conductivity, the hydraulic conductivity of the microannulus, and the radial distance from the microannulus. Thus for the scenario modeled, leakage via a microannulus could not be hydraulically monitored by use of the injection well or an observation well completed within the injection zone. This leakage was monitorable only through the use of an observation well in the overlying aquifer.

GLOSSARY

AIF	aquifer influence boundary
b	thickness
DOW	Devonian Observation Well
GL	ground level
HST3D	Heat and Solute Transport Model
ISGS	Illinois State Geological Survey
k	permeability
K	hydraulic conductivity
KB	Kelly Bushing
m	modulus of shear for the medium
Pa	Pascals
POR	porosity
psi	pounds per square inch
q	pumping rate
S	storativity
SEM	scanning electron microscopy
SWIFT	Sandia Waste Isolation Flow and Transport Model
SWIP	Survey Waste Isolation Program
T	transmissivity
TDS	total dissolved solids
USDW	underground sources of drinking water
USEPA	United States Environmental Protection Agency
WDW2	Waste Disposal Well 2
α	matrix compressibility
β	fluid compressibility
Δh	head buildup
ρ	fluid density
μ	fluid viscosity

1. INTRODUCTION

Background

Liquid waste is disposed of through underground injection by pumping the waste into or allowing it to flow through a specially designed and monitored well. Developed by the petroleum industry in the 1930s as a method for brine disposal, the technique was adapted by other industries in the 1950s for the disposal of industrial waste streams. As regulations for the disposal of waste into landfills and surface waters became more stringent, the volume of waste disposed of by underground injection increased.

Regulatory agencies have classified injection wells according to the purpose of the wells and the proximity of injection reservoirs to the lowermost underground source of drinking water (USDW). The five classes of injection wells are:

- Class I — wells used to inject hazardous and nonhazardous wastes below the lowermost USDW (this report is concerned with this class of wells).
- Class II — wells associated with the production and storage of oil and gas below the lowermost USDW.
- Class III — wells used in special process (mining) operations to inject fluid above, into, or below an USDW.
- Class IV — wells used to inject hazardous waste into or above an USDW (this class of wells is currently banned).
- Class V — wells used to inject all other wastes into or above an USDW.

According to the U.S. Environmental Protection Agency (USEPA), there were 429 Class I injection wells active in 1986 (USEPA 1986). Although the volume of waste disposed of nationwide via these wells is difficult to estimate, accurate figures are available from some states. In Illinois, nine Class I wells were used in 1984 to dispose of 310 million gallons of waste (Brower et al. 1989).

With the promulgation of the Hazardous and Solid Waste Amendments of 1984, the level of interest in underground injection increased tremendously. Provisions of the act mandated that the administrator of USEPA determine if underground injection is a threat to human health and the environment for the period the waste remains hazardous. If underground injection is found to be hazardous to human health and the environment, or if the determination is not made by the Congressionally mandated date, all underground injection will be banned. Some environmental groups want situations detailed in which underground injection has endangered or may endanger human health or the environment.

The USEPA developed an extensive research agenda to examine pertinent issues. The USEPA has funded to date one or more projects in each of the following areas: identification and classification of Class I well failures; techniques to detect abandoned wells; monitoring of various aspects of the well; flow and transport modeling of various injection scenarios; geochemical modeling of injected waste, injection formation, and brine; and hydrogeologic characterization of important injection formations and associated confining formations. Industry also has conducted research into pertinent topics of underground injection.

In this project, a numerical model was used to investigate the hydraulic effects of waste injection on the geologic reservoir. The site of the investigation is a chemical refinery located near Marshall, Illinois, in north-central Clark County (fig. 1). The chemical company used the injection well

to dispose of alkaline ($\text{pH} > 12$) waste. An observation well, which is completed in the same formation as the injection well, is located 506 meters north of the injection well.

Purpose

The primary purpose of this project was to investigate the pressure response (flow modeling) of an actual injection formation and its associated confining formations due to waste injection via a Class I well. Modeling of solute transport was not investigated here but was addressed by other researchers sponsored by USEPA and industry. Flow modeling requires detailed characterization of the site hydrogeology, so this project bridged two areas of concern—flow modeling and hydrogeologic characterization. In addition, the effectiveness of pressure-monitoring systems to detect movement of fluid beyond the injection formation was evaluated.

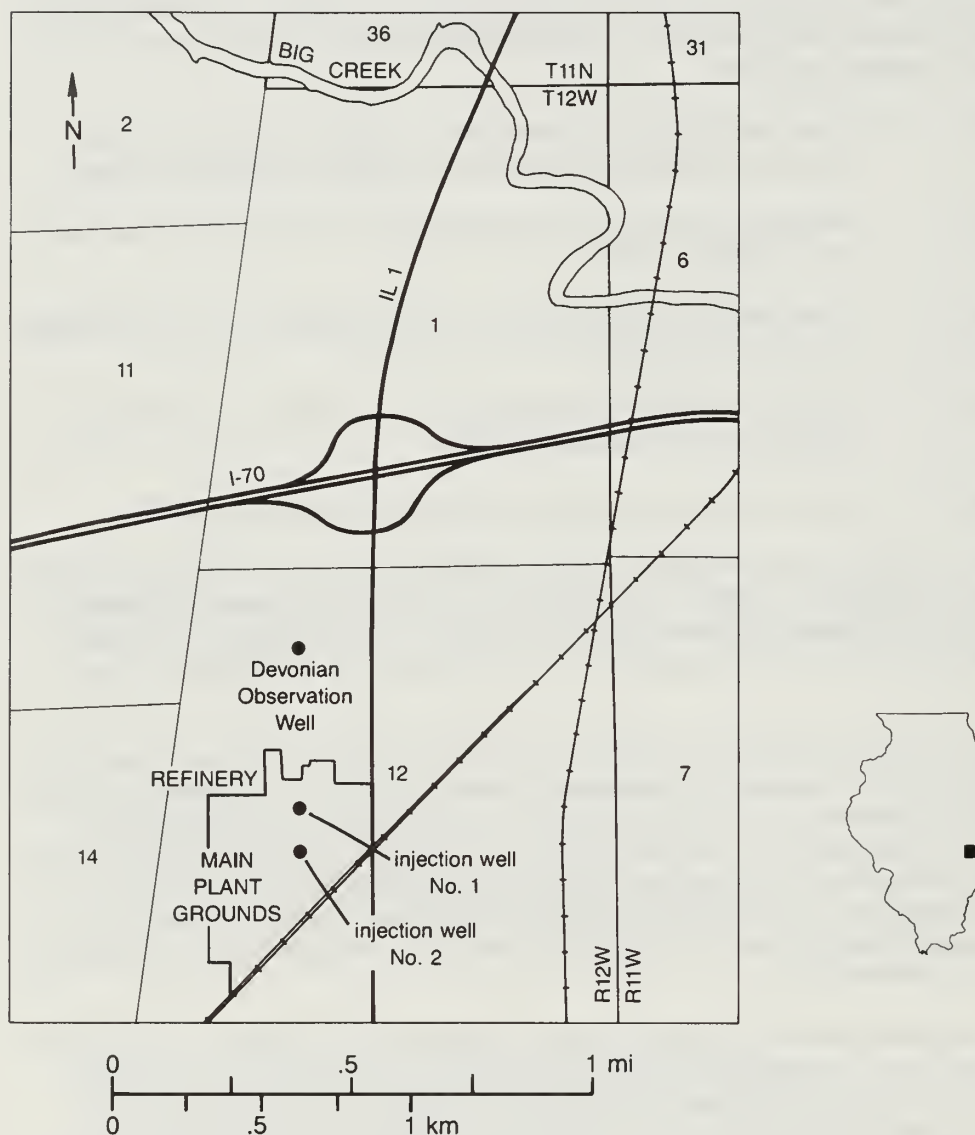


Figure 1 Location of investigation site.

2. GEOLOGY OF THE INJECTION SYSTEM

The geologic environment of an injection well site controls many aspects of the disposal operation and the fate of the injected wastes. This section includes a summary of the regional geology and hydrogeology of the units involved with the deep-well injection operation. The geologic setting is described within the context of the regional geology to show regional trends and the degree of uniformity in geologic conditions.

Only those aspects of geology pertinent to underground injection are described. The major emphasis is on the hydrogeology of the confining units and the injection interval, specifically, the hydrogeology of the upper confining unit (New Albany Group), the lower confining unit (Maquoketa Group), and the injection interval (Hunton Supergroup). The Borden Siltstone, which overlies the New Albany Group, acts as an additional confining zone.

Overview of Geologic Conditions Affecting Waste Injection

The principal geologic factors for the regional evaluation are those affecting (1) the capacity of geologic units in the injection system to accept and confine injected waste, (2) the chemical interaction of the waste with injection system components, (3) the generation of dislocations that developed during the forming of structural features or seismic events, and (4) the use of subsurface space and commercial grade resources in the area of disposal influence.

In this section we have focused on the broader regional issues that relate to local geologic conditions. Broadly defined lithologic units form a key component of the regional discussion. These units have been described in the literature, and the uniformity of their general geologic conditions and structural trends have been established by oil, gas, water, and mineral resource exploration activities in the region.

The character and trends of the regional geology have been determined from data gathered from key well records, reports, and publications. This information reveals the distribution of aquifers that meet regulatory requirements for Class I injection, i.e., aquifers that contain saline water (>10,000 mg/L total dissolved solids [TDS]) and that have confining intervals capable of protecting all USDW from contamination by injection activities. Injection is limited to selected aquifers in the southern two-thirds of Illinois, including the Hunton Supergroup and the Salem Limestone, which have been used for disposal at the study site. Injection system response to waste injection is primarily controlled by porosity and permeability characteristics, which can be directly related regionally to specific geologic units.

Porosity and permeability develop during sedimentation processes and are modified by other geologic processes. Thus porosity and permeability have a general relationship with specific lithologies. Each geologic unit in the region exhibits a range of values and areal trends. The sedimentary geologic units in east-central Illinois exhibit relatively uniform characteristics over large areas; however, both vertical and radial trends are noted within each unit. Similar patterns can also be expected within the subdivisions of each unit, but determining this would require a detailed study of subsurface records.

The lithology of the geologic units forming the injection system plays an important role in the chemical interaction between the injected waste and injection system. Chemical interaction between injected waste and the injection system can affect flow conditions (porosity and permeability) and under certain disposal conditions can compromise the integrity of the confining intervals. However, beneficial interactions may also occur that would improve flow conditions, involve retention of some waste components near the well, and provide treatment for selected, undesirable components in the waste.

This discussion focuses on the general regional characteristics of principal geologic units and relates these characteristics to hydrogeologic parameters for characterizing flow in the injection system. An effective evaluation by numerical modeling requires that the hydrogeologic character of the geologic units accepting and retaining injected waste be predictable and relatively uniform throughout the area influenced by injection. A more detailed description of the character and radial uniformity of the units in the injection system is presented in chapter 3.

General Geologic Setting

The geologic framework of Illinois in which deep-well disposal is practiced can be described as a sequence of areally extensive sedimentary rock units deposited in a large midcontinent basin known as the Illinois Basin. The study site, in the east-central part of the basin, is immediately east of the axis of the Marshall-Sidell Syncline and about 14 miles east of the La Salle Anticlinal Belt, the most dominant structural feature in the area. Figure 2 shows the generalized geology of the bedrock surface in Illinois. Generalized geologic cross sections of Illinois are depicted in figure 3. Figure 4 provides a generalized geologic column and comments on the stratigraphy, lithology, hydrogeology, and groundwater geochemistry of the geologic units associated with or protected from waste injection. Additional details on geologic units covered in this report are available in the *Handbook for Illinois Stratigraphy* (Willman et al. 1975), the *Bibliography of Illinois Geology* (Willman et al. 1968) and reports prepared by Brower et al. (1989), Cluff et al. (1981), Gray et al. (1979), and Piskin and Bergstrom (1975).

In Illinois, lithologies range from very fine- to coarse-grained clastics, a variety of carbonates, and a few evaporites and organics. Relatively uniform lithologic characteristics exist on a regional basis within individual units as a whole and within the subdivisions of each unit.

Many processes have been involved in forming, altering, and structurally readjusting these units from the time of deposition to the present day. Sedimentary deposition began early in the Paleozoic Era on the eroded surface of igneous and metamorphic rock of the Precambrian basement complex. Deposition and some erosion continued throughout the Paleozoic. Several episodes of deposition in the Mesozoic and Cenozoic Eras produced nonlithified sedimentary units. The present-day landscape has developed principally on these nonlithified sediments. Marine carbonate and clastic lithologies are dominant in the Paleozoic units, but terrestrial clastics and some organic deposits are present in the upper part of the Paleozoic (Mississippian and Pennsylvanian Systems).

The thickness of the sedimentary sequence in Illinois ranges from approximately 2,000 feet northwest of Rockford to more than 20,000 feet in the southeastern corner of the state, the deepest part of the Illinois Basin (Sargent and Buschbach 1985). In the project area, the total thickness of the sedimentary units is approximately 8,500 feet. Lithologies include dolomite, limestone, sandstone, siltstone, shale, and some coal and evaporite. The stratigraphic column in figure 4 provides a summary of the typical sedimentary sequence in the Illinois Basin.

Widespread carbonate lithologies are dominant in the lower part of the Paleozoic, and a few sandstones and some shales are interbedded with these carbonates. Most of the carbonates become sandy to the north, and a few grade into sandstones in the far northern part of the state. Greater variations in regional lithology exist in the upper part of the Devonian through the middle part of the Mississippian. Cyclic deposits of fine-grained clastics (shales and siltstones), some carbonates, and some coarse-grained clastics (sandstones) accumulated in the upper part of the Mississippian and in all of the Pennsylvanian as numerous sea-level oscillations shifted shorelines across shallow-marine and flat-lowland terrestrial environments.

The study site is in the Marshall-Sidell Syncline (see fig. 5), a broad structural feature of low relief between the La Salle Anticlinal Belt, about 14 miles to the west, and the Kankakee Arch more than 90 miles to the northeast. These two structures are reflected in the distribution of the boundaries of the geologic units exposed at the bedrock surface (fig. 2). The regional dip of the units in the study area is to the southwest from the Kankakee Arch and into the Illinois Basin, but

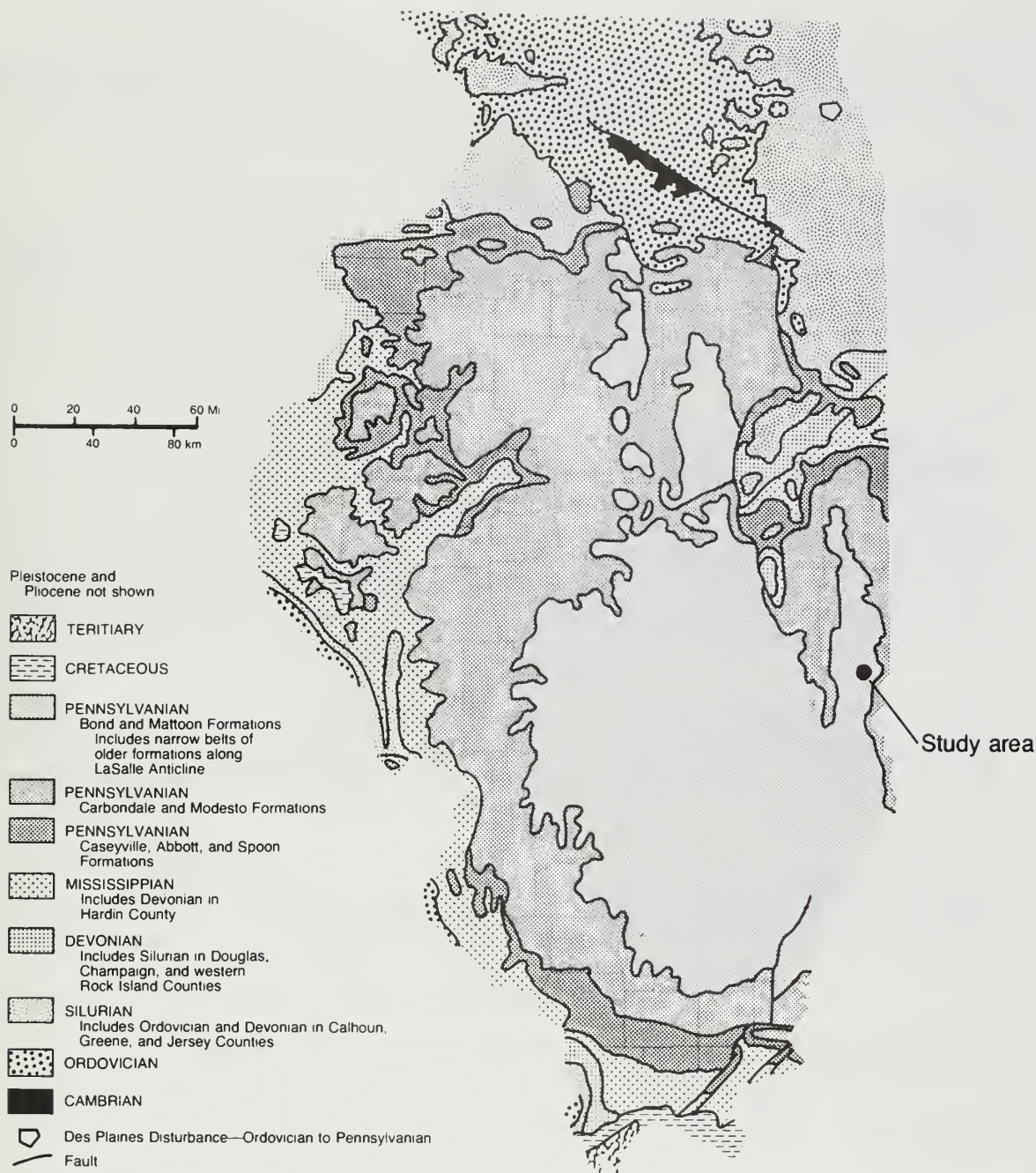
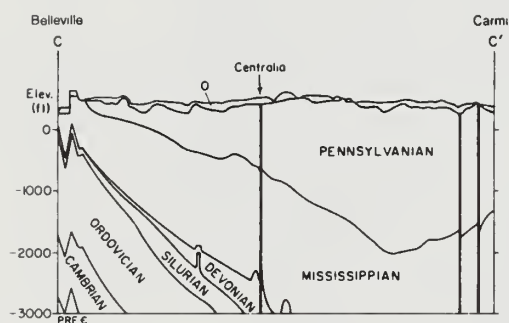
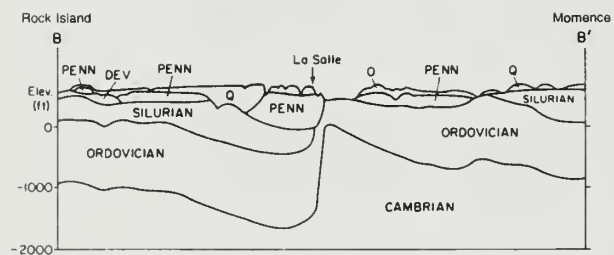
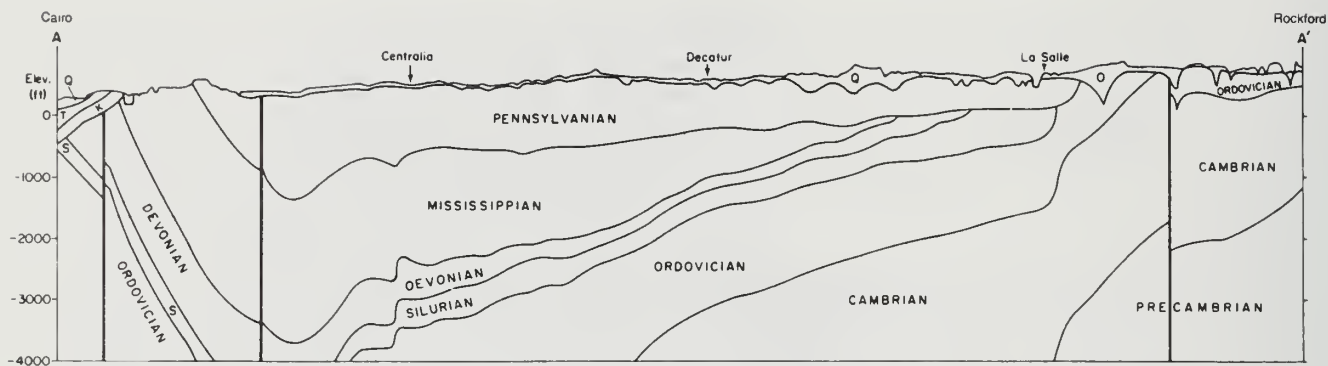


Figure 2 Generalized areal geology of the bedrock surface (from Willman and Frye 1970).

boundaries of the geologic units exposed at the bedrock surface (fig. 2). The regional dip of the units in the study area is to the southwest from the Kankakee Arch and into the Illinois Basin, but locally the units dip gently in a south-to-southwesterly direction toward the axial trend of the Marshall-Sidell Syncline.

Waste Injection Potential In Illinois

Some sequences of Paleozoic units possess sufficient porosity, permeability, and confinement to accept and retain wastes injected at moderate to high injection rates. Criteria for acceptable injec-



Q - Quaternary T - Tertiary PENN - Pennsylvanian
K - Cretaceous S - Silurian DEV - Devonian

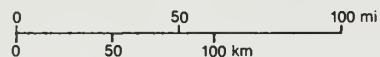


Figure 3 Generalized statewide cross sections of Illinois (from Willman et al. 1975).

Protection Act (Title 35, Illinois Administrative Code). Within Illinois, the base of the USDW ranges in depth from 500 to slightly more than 3,000 feet. All units below the lowermost USDW contain groundwater with a TDS content exceeding 10,000 mg/L (milligrams/liter). Injection is feasible only in portions of Cambrian through basal Pennsylvanian units that meet the criteria for waste injection established in the Illinois Environmental Protection Act.

In the study area, the base of the USDW has been established at a depth of about 500 feet (Pis-kin 1986). In the immediate vicinity of the study site, significant injection potential for the Salem and Hunton carbonate units has been proved by oil exploration and waste-injection testing conducted to a depth of 6,000 feet. Recently, injection has been limited to the Devonian portion of the Hunton. Very limited groundwater supplies have been obtained from the uppermost part of the Pennsylvanian bedrock. The City of Marshall obtains a moderate to large water supply from a shallow sand and gravel aquifer in the nearby valley of Big Creek.

Seismic Activity in Illinois

Earthquake waves traveling through earth materials can affect deep-well disposal systems. Earthquakes are infrequent in Illinois, and most have been low to moderate in magnitude and intensity (fig. 7). Several earthquakes of low-to-moderate magnitude recently occurred in the vicinity of the Wabash Valley Fault System, which extends northward into Edwards and Wabash Counties from southeastern Illinois (fig. 5). The largest earthquakes affecting Illinois in recorded history occurred near New Madrid, Missouri, in 1811 and 1812 (Heigold 1968, 1972). Although faulting is reported in other areas of Illinois, field studies and drilling records available to the Illinois State Geological Survey indicate that no faults are mapped at the surface or known to have occurred in the subsurface in the vicinity of the study area.

The greatest likelihood for major damage from earthquakes exists in 14 southern Illinois counties (figs. 6 and 7). This region of the state is in Area 3 on the Seismic Risk Map (fig. 6) compiled by Algermissen (1969). The project site is near the southern margin of Area 1, the area in which the damage expectancy from potential earthquakes is rated as minor.

Subsurface Resources

Subsurface resources in Illinois exclusive of groundwater resources include mineral deposits, hydrocarbon deposits, and subsurface storage space. Many of the geologic units containing subsurface resources also qualify as potential disposal horizons. The regulations for deep-well disposal require a review of all subsurface resources of commercial value in order to reduce the potential for conflicts between injection and resource extraction.

Oil and limited natural gas resources have been exploited in numerous permeable units above the St. Peter Sandstone. Oil production is mainly associated with Mississippian units; however, significant production has come from other Paleozoic units. The petroleum-producing regions in Illinois are confined to the Illinois Basin (fig. 8). Wells drilled for production provide valuable information about subsurface conditions; however, if not properly sealed, these wells can be potential avenues for fluid movement into overlying geologic units.

Oil has been produced in the Weaver Field about 9 miles to the east-southeast of the study area and in several small fields on the La Salle Anticlinal Belt, more than 14 miles to the west. Exploratory wells have been drilled throughout the vicinity of the study site; a few of these wells are within the 2.5-mile area of review of the disposal well. No commercial oil pools have been reported in the Marshall-Sidell Syncline in the vicinity of the study site.

Coal deposits are more widespread than petroleum deposits in the Pennsylvanian units, and multiple coal deposits are often found where Pennsylvanian units are present. Although more than 50 potential coal horizons have been found in Illinois, only a few are thick enough for commercial development. The coals in the project area tend to be relatively thin and deeply buried. Most coal deposits mined in Illinois are shallow (less than 500 ft) and lie within units designated as USDW.

Rock Units and Their Hydrogeologic Roles

Southern Illinois

Geologic Column

Hydrogeologic Description

Geologic Column

Hydrogeologic Description

Formation Member	Thickness Feet
---------------------	-------------------

Thickness
Feet

**Formation
Member**

SYS.SER.

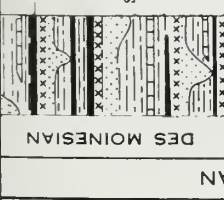
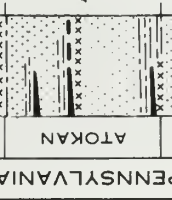
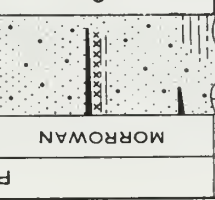
Group

QUAT.	PLEIS.	Glacial drift, loess, and alluvial deposits	0-300	Confining Bed/Aquifer: Quaternary — unconsolidated deposits; glacial pebbly clay (till), silt, clay, loess, sand and gravel; alluvial silt, sand, and gravel; major source of drinking water with larger yields from sands and gravels along present-day streams and in buried bedrock valleys; well yields are variable to more than 2,000 gpm; a few inches to more than 400 ft thick; tills and clays from uppermost confining interval.
TERTIARY	PLI.	"Lafayette" Gravel	0-50	
	Eocene	Wilcox Fm.	0-300	
		Porters Creek Clay	75-150	
CRETACEOUS	PALEO.	Clayton Fm.	5-10	Aquifer: Cretaceous-Tertiary — sands, clays, silts, and some gravels; aggregate maximum thickness of 900 ft; occurrence limited to southern tip of Illinois; McNairy and Tuscaloosa Formations are the most productive; local drinking water source with yields up to 1,000 gpm.
		Owl Creek Fm.	0-10	
	GULFIAN	McNairy Sand	125-500	
MISSOURIAN		Tuscaloosa Gravel	0-20	
	VIRGILIAN	Greenup Ls.		
		Shumway Ls.		
		Mattoon Fm.	700 +	
		Omega Ls.		
		Milleraville Ls.		
	MISSOURIAN	Bond Fm.	100-350	
		Shoal Creek Ls.		
		No. 8 Coal Modesto Fm.	200-500	
		Piasa Ls. No. 7 Coal		
No. 6 Coal Carbondale Fm. No. 6 Coal		200-400		
PENNSYLVANIAN				Confining Bed/Aquifer: Pennsylvanian — mainly shale, with some sandstone, siltstone, and coal; maximum thickness of 2,500 ft; forms the bedrock surface in most of the area; sandstone in upper few hundred feet constitutes a source of drinking water; commonly yields less than 10-15 gpm locally near outcrop area in southwest; yields of 50-100 gpm are possible; water is highly mineralized below depth of about 500 ft.

Aquifer/Confining Bed: Valmeyeran — predominantly limestones with some sandstones, siltstones, shales, and dolomites; underlies most of central and southern Illinois; thin in west, more than 800 ft thick in north-central part of region, and more than 1,800 ft thick in southeastern Illinois; constitutes a drinking water source in outcrop areas in western part and southern margin of the state; variable yields, typically less than 30 gpm but locally up to 1,800 gpm; highly mineralized at depth away from outcrop area.

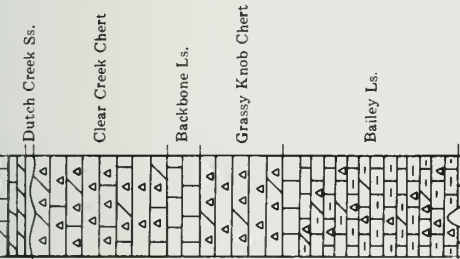
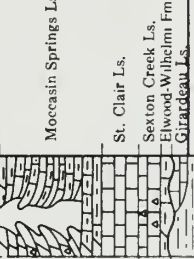
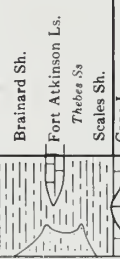
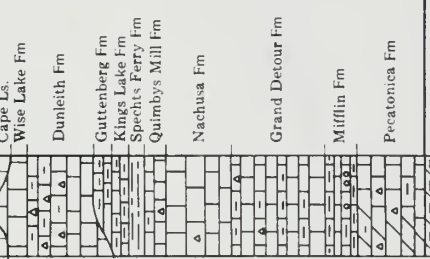
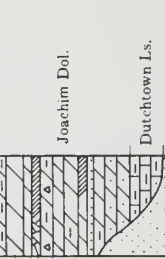
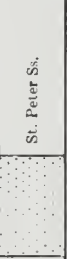
Confining Bed: New Albany — black, gray, and green shale; covers almost entire southern half of the state; over 300 ft thick.

(continued from previous page)

PENNSYLVANIAN	DES MOINESIAN	 No. 8 Coal DeKoven Coal Davis Coal Spoon Fm. Curtis Ls. Murray Bluff Ss. Abbott Fm. Grindstaff Ss. Pounds Ss. Caseyville Fm. Battery Rock Ss. Luak Sh.	10-350	Kewanee	MISSISSIPPIAN
	ATOKAN	 Grove Church Sh. Kinkaid Ls. Degonia Ss. Clare Fm. Palestine Ss. Menard Ls. Waltersburg Fm. Vienna Ls. Tar Springs Ss. Glen Dean Ls. Hardinsburg Ss. Haney Ls. Fraileys Sh. Beech Creek Ls. Cypress Ss. Ridenhower Fm. Bethel Ss. Dowreys Bluff Ls.	0-65 110-180 40-100 50-110 30-140 30-150 35-80 0-15 30-150 10-70 15-180 10-80 50-100 2-25 30-160 30-75 5-120 5-30	McCormick	
	MORROWAN	 Glen Dean Ls. Hardinsburg Ss. Haney Ls. Fraileys Sh. Beech Creek Ls. Cypress Ss. Ridenhower Fm. Bethel Ss. Dowreys Bluff Ls.	0-65 110-180 40-100 50-110 30-140 30-150 35-80 0-15 30-150 10-70 15-180 10-80 50-100 2-25 30-160 30-75 5-120 5-30	McCormick	

Alternating Sequence of Confining Beds/Aquifers: Chesterian — limestone-shale alternates with sandstone-shale; underlies much of the southern half of Illinois; thickness southward to more than 1,400 ft in southern part of Illinois Basin; some limestones and especially sandstones constitute sources of drinking water in outcrop areas along the perimeter of the Illinois Basin; commonly yields less than 25 gpm; at depth away from outcrop areas, water is highly mineralized.

(continued from previous page)

DEVONIAN	LOWER	 Dutch Creek Ss. Clear Creek Chert Backbone Ls. Grassy Knob Chert Bailey Ls.	0-15 0-600 30-150 120-250 250-450	Aquifer: Silurian-Devonian (Hunton Supergroup) —predominantly limestone with dolomite, siltstone, shale and chert; thickness of 200 ft in the west to more than 1,800 ft in the southeast part of the region; constitutes drinking water source from fractured limestones in outcrop areas; Devonian cherts are sources for small to moderate supplies in southern and western parts of the region; well yields range from moderate to maximum of 300 gpm; away from outcrop areas units are highly mineralized.
		 Moccasin Springs Ls. St. Clair Ls. Sexton Creek Ls. Elwood-Wilhelm Fm Girardeau Ls.	100-800 20-100 15-80 0-60 0-40	
		 Brainard Sh. Fort Atkinson Ls. Thebes Ss Scales Sh.	0-150 0-50 50-150	
ORDOVICIAN	CHAMPLAINIAN	 Cape Ls. Wise Lake Fm Dunleith Fm Guttenberg Fm Kings Lake Fm Specht's Ferry Fm Quimbys Mill Fm Nachusa Fm Grand Detour Fm Mifflin Fm Pecatonica Fm	0-20 0-50 100-150 0-20 0-15 0-15 15-35 40-75 50-210 15-120 0-140	Aquifer/Confining Bed: Maquoketa — mainly shale, some limestone and sandstone; underlies almost all of southern Illinois; more than 300 ft thick along eastern margin of state. Aquifer/Confining Bed: Galena-Platteville — dominantly limestone, some dolomite, shales and cherts; a possible source of drinking water where these units form upper bedrock along the western-southwestern boundary of Illinois; thickness increases southward to a maximum of about 725 ft in southeastern part of region; away from outcrop area this sequence contains highly mineralized water.
		 Joachim Dol. Dutchtown Ls. St. Peter Ss.	60-385 0-200 65-300	
		 Joachim Dol. Dutchtown Ls. St. Peter Ss.	60-385 0-200 65-300	

Aquifer/Confining Bed: Joachim-Dutch-town-St. Peter (Anceal Group) — dolomite, limestone, sandstone with a few anhydrite or gypsum deposits; underlies southern half of Illinois; reaches maximum thickness of 700 ft in the southern tip of the region; St. Peter thins southward as carbonate units become thicker; constitutes a limited source of drinking water in extreme western Illinois.

FIGURE 4. Description of rock units and their hydrogeologic roles (Brewer et al., 1988)

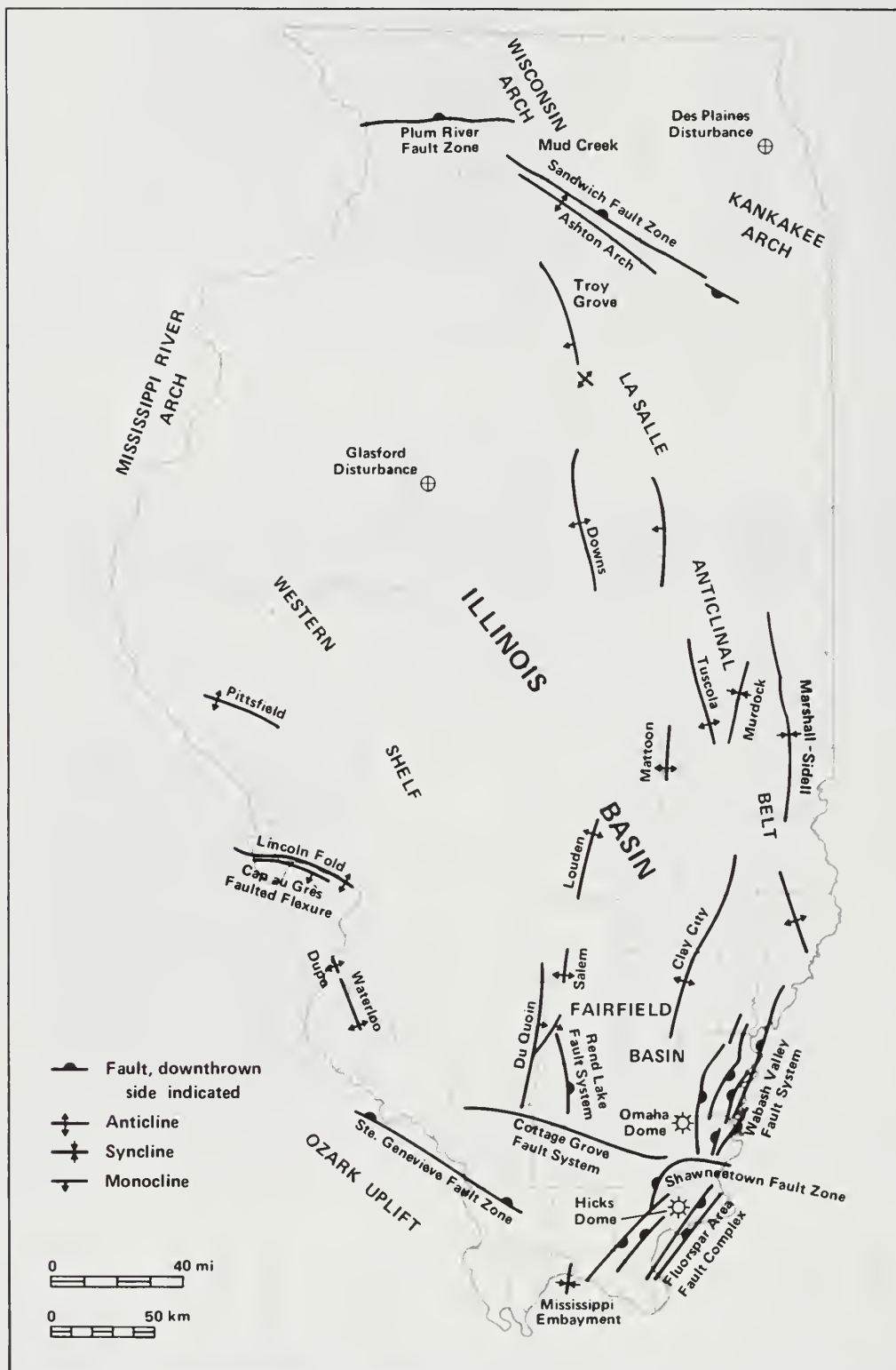


Figure 5 Geologic structures in Illinois (compiled by J. Treworgy 1979).

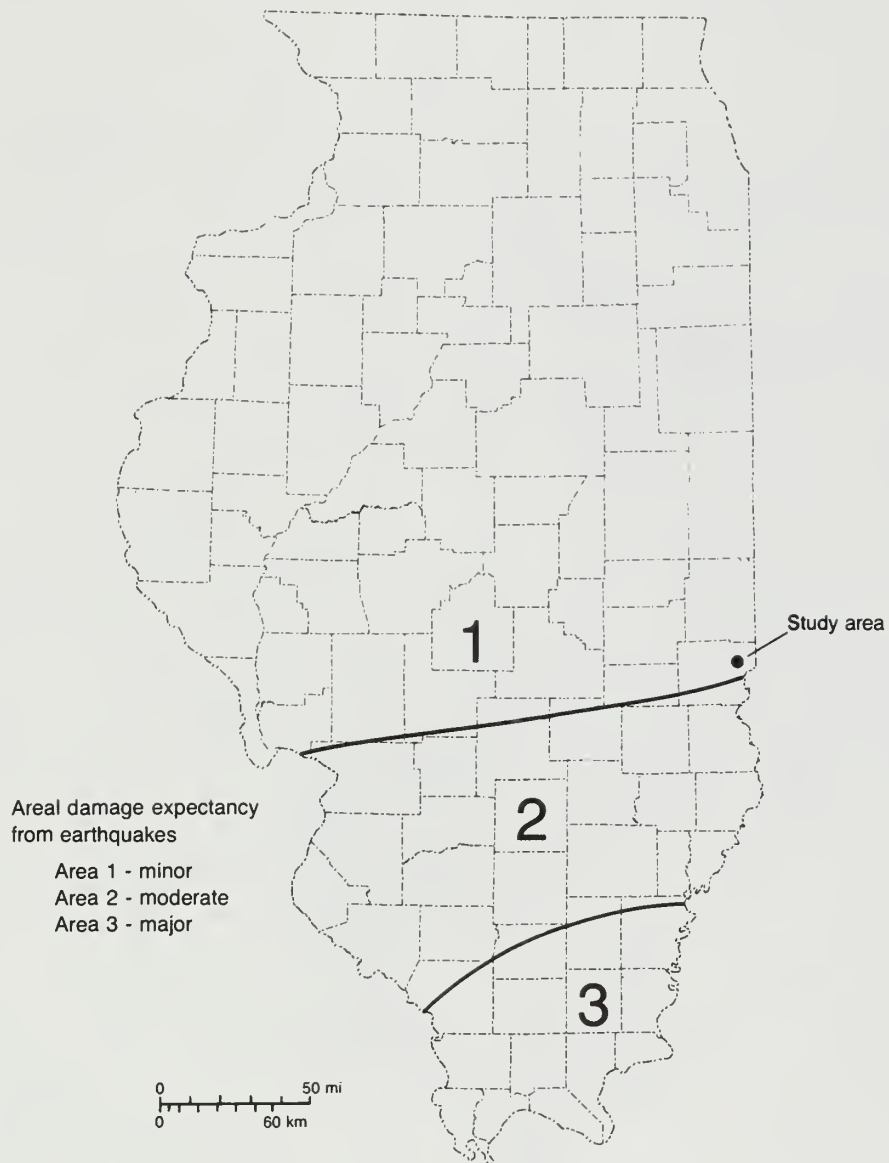


Figure 6 Seismic risk map for Illinois (after Algermissen 1969).

Other mineral resources, including building stone, agricultural lime, clay, sand, sand and gravel, metals, fluorite, barite, and tripoli, have been mined commercially throughout Illinois (Samson 1983, 1989). Most of the mining operations are at or near the land surface. Only limited surface mining (for aggregate and stone) has been done near the study area, and apparently neither the mining nor the injection operations have affected each other.

Natural gas storage fields in aquifers having localized structural closure features are scattered throughout the state. Three storage fields are located about 10 miles north and northeast of the study site (fig. 9). Aquifers of sandstone and limestone strata of Cambrian through Pennsylvanian age have been used for storage. Drilling and testing records from the Nevins, State Line, and Elbridge storage facilities have provided much useful information about subsurface geologic and

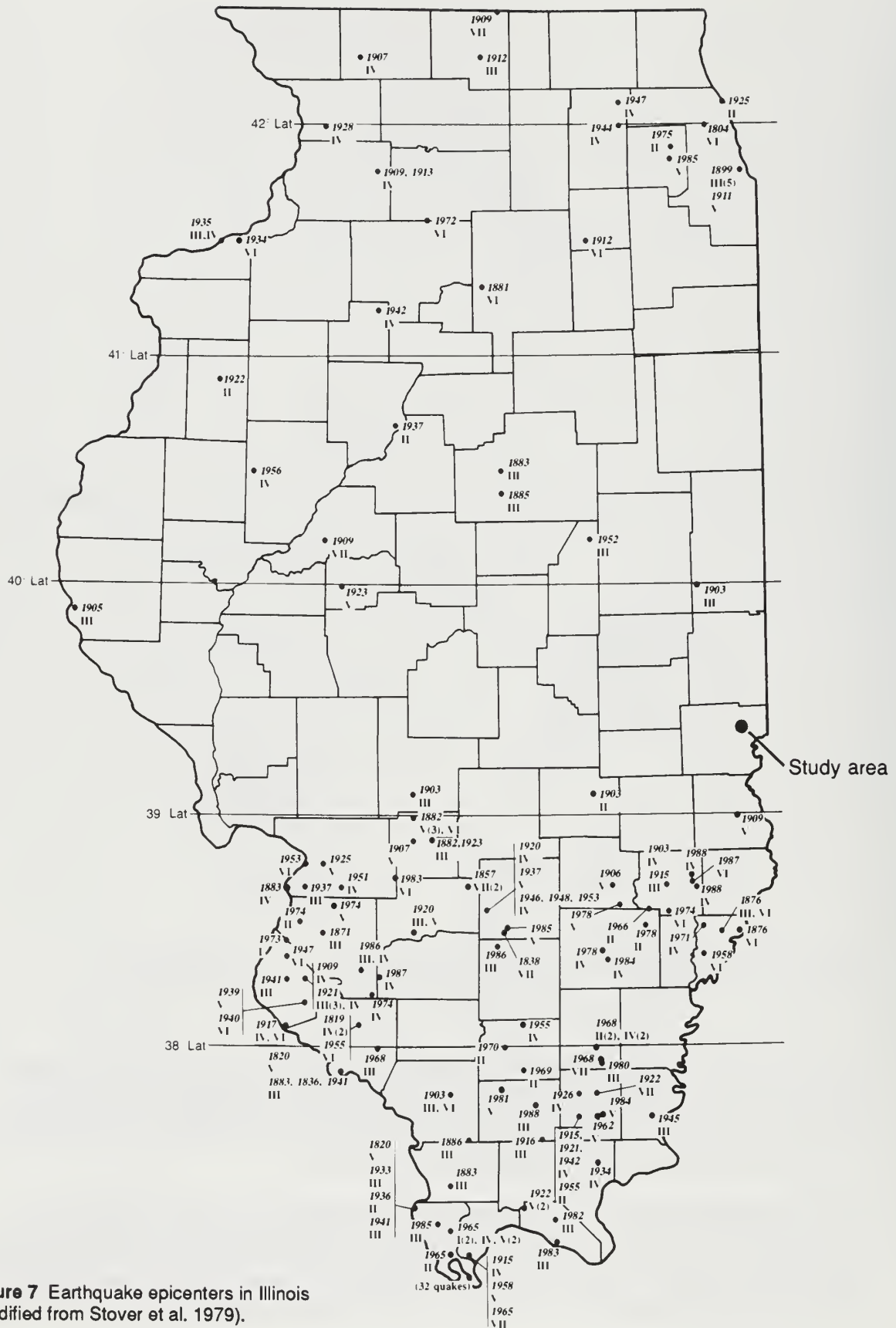


Figure 7 Earthquake epicenters in Illinois (modified from Stover et al. 1979).

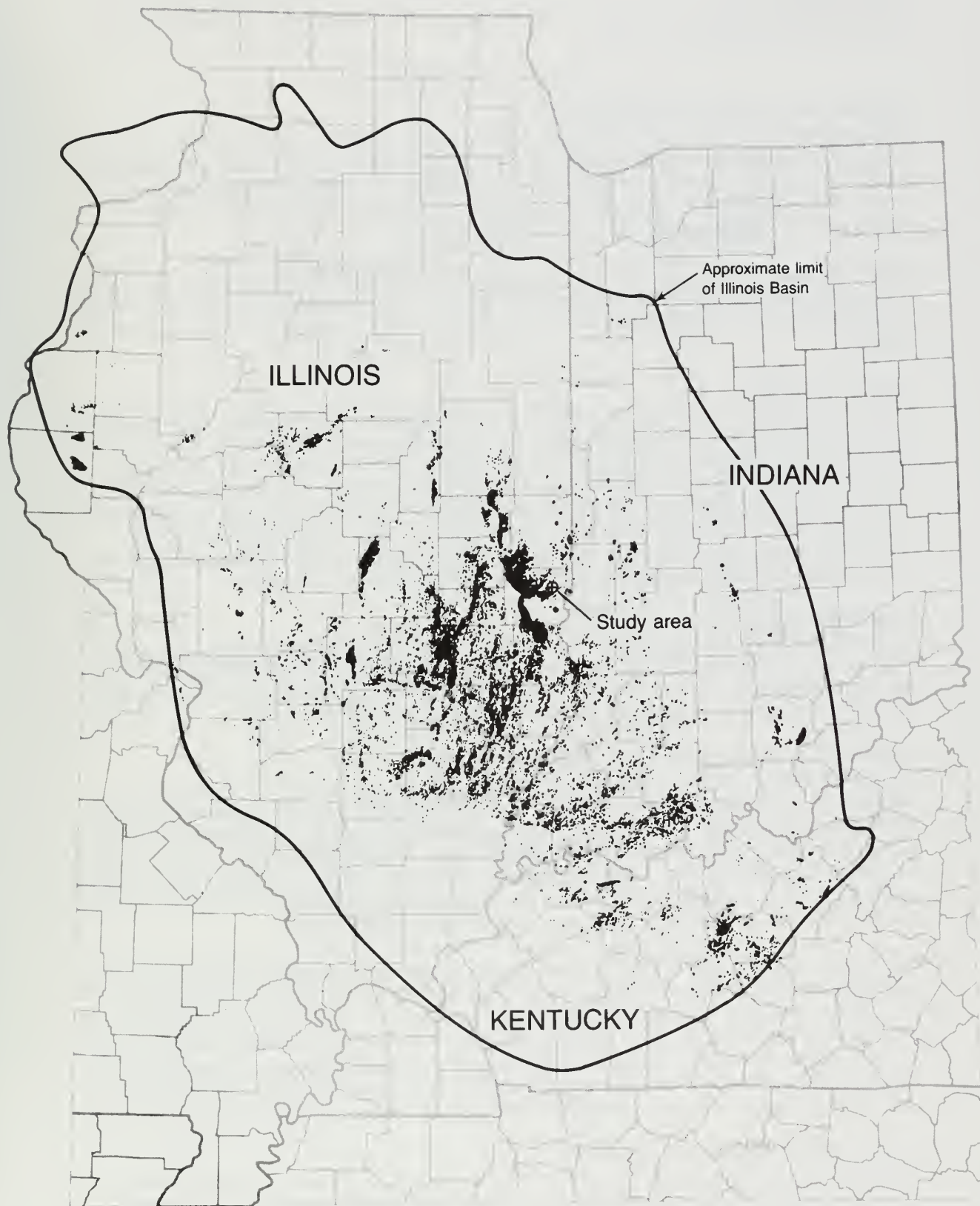


Figure 8 Oil and gas fields of the Illinois Basin (from Leighton et al. in press).

hydrogeologic conditions at the study site. Injection activities in the nearby natural gas storage fields and at the study site do not appear to affect each other significantly, although both utilize the same units of the Hunton.

Regional Geology and Hydrogeology

The units that are part of the injection system and are penetrated by the disposal well include the basal confining interval (Maquoketa Group), the injection interval (Hunton carbonate sequence), and the upper confining interval (New Albany shale sequence). Additional impermeable units and some aquifers lie between the upper confining interval and land surface. The first significant aquifer above the injection interval is the Salem Limestone.

Waste Disposal Well 2 (WDW2) was originally drilled to 6,000 feet (Eminence-Potosi Dolomites). It was plugged back into the uppermost unit of the Silurian limestone part of the Hunton because the immediately overlying Devonian limestone was the deepest, most receptive injection interval available.

Ordovician System

Ordovician strata (fig. 4) range in thickness from 700 feet (in northern Illinois) to more than 6,000 feet (in southern Illinois). The thickness increases gradually toward the south. Dolomites and limestones are the predominant lithologies; however, several distinct sandstones are found in the lower (Gunter and New Richmond Sandstones) and middle (St. Peter Sandstone) parts of the Ordovician. A thick shale-shaly carbonate sequence (Maquoketa Group) forms the upper part of the Ordovician. Many of the units below the Maquoketa are relatively impermeable and act as aquitards. The St. Peter Sandstone, a thin (50-ft), fine-grained, low-permeability sandstone in Clark County, is the first significant aquifer below the Hunton injection interval.

Maquoketa Group (Lower Confining Unit)

The Maquoketa Group (fig. 4) consists of two shale units and an interbedded shaly limestone-dolomite unit. The thickness of the Maquoketa ranges from approximately 150 feet in the western part of the state, where the top is eroded, to nearly 300 feet along the eastern edge of the state (fig. 10). In the vicinity of Marshall, the Maquoketa is less than 300 feet thick.

Hydrologic Characteristics of the Ordovician System

In northern Illinois, carbonate units of the Ordovician that are at or near land surface have moderate to relatively low permeabilities. As the burial depth of these units increases toward the south, the permeabilities of the units generally decrease. Carbonate units lying below freshwater zones (groundwater with less than 10,000 mg/L TDS) are essentially aquitards. Figure 11 shows the basal position of USDW in a north-south cross section from Rockford to Cairo. The southward-pointing tongue of USDW in the Ordovician lies in the St. Peter Sandstone. The TDS level of the St. Peter in the Marshall area is greater than 50,000 mg/L (Meents 1952).

Porosities in carbonate units in the southern half of the state are generally less than 10 percent; permeabilities in the more permeable units rarely exceed 1 to 30 millidarcys (Ford et al. 1981, Mast 1967). Porosities and permeabilities across vertical sections of the St. Peter are quite variable. The more permeable horizons measured in northern Illinois had porosities ranging from 12 to 17 percent and permeabilities ranging from 25 to 250 millidarcys. In the south, where the St. Peter is thinner, finer-grained, and more shaly, porosity and permeability values can be expected to be smaller. The shale units in the Maquoketa Group are expected to be very tight (<1 millidarcy).

Hunton Supergroup (Injection Interval)

The limestone and dolomite units of the Silurian and Devonian Systems have similar lithologic and hydrogeologic characteristics and thus are considered one large unit, the Hunton Supergroup. The thickness of the Hunton ranges from a featheredge along the Mississippi River to more than 1,800 feet near the southern tip of the state. Figure 12 shows the thickness and dis-

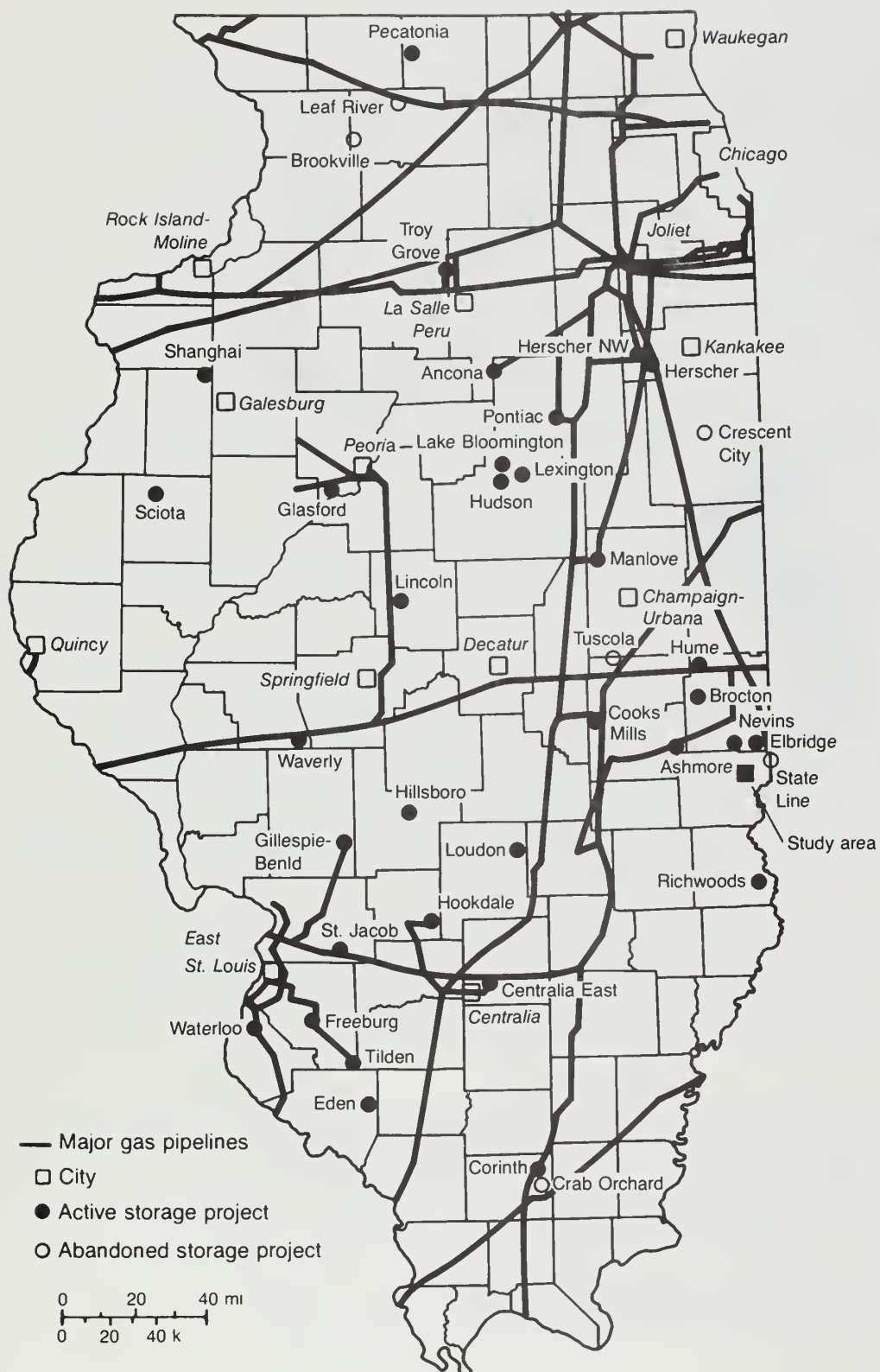


Figure 9 Location of underground gas storage projects in Illinois (after Buschbach and Bond 1974).

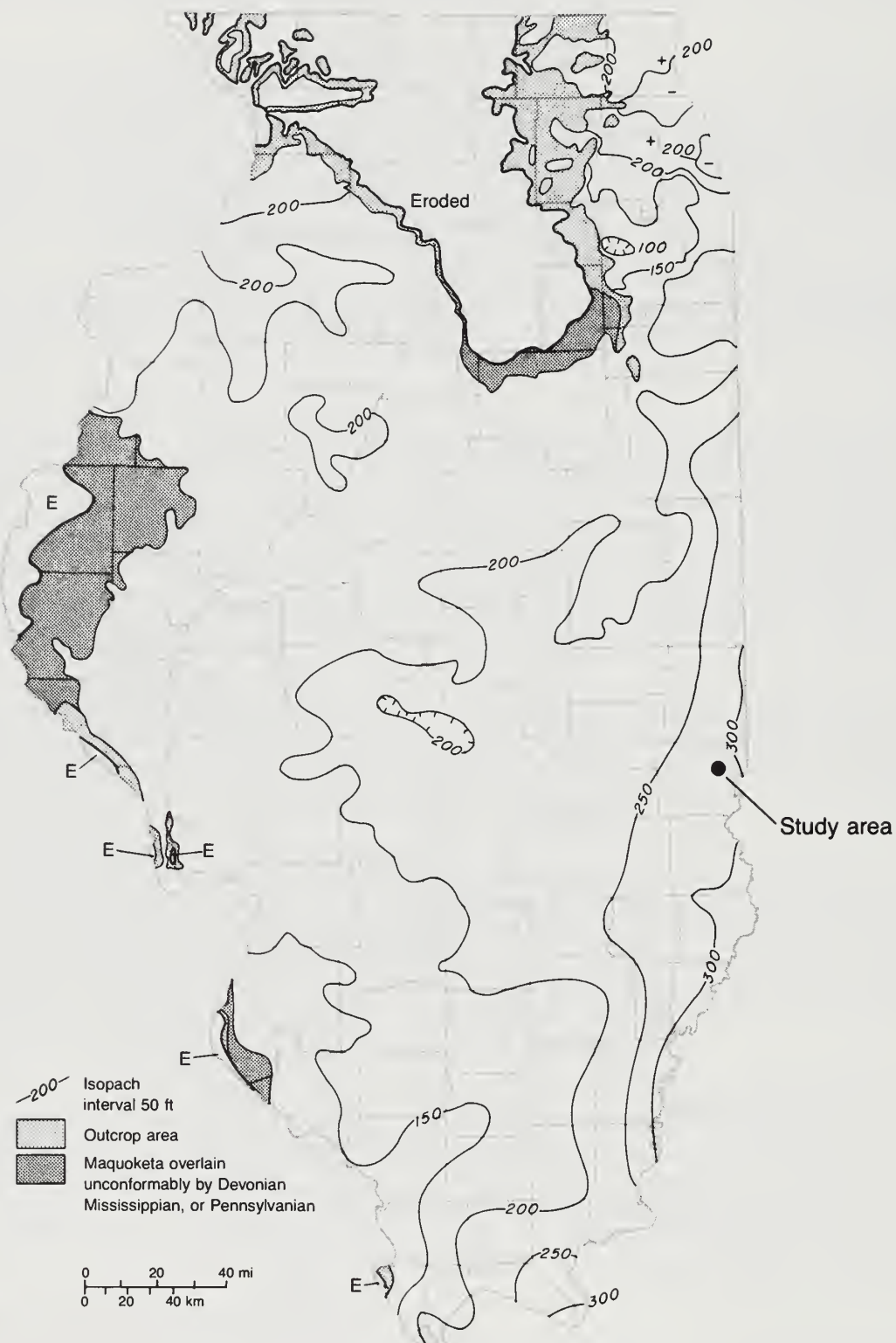


Figure 10 Generalized thickness and distribution of the Maquoketa Group (after Willman et al. 1975).

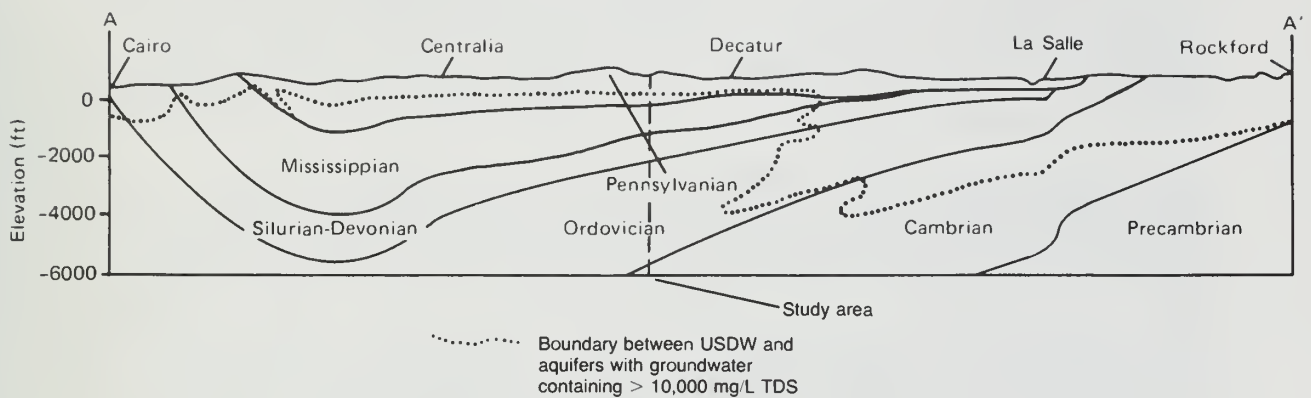


Figure 11 Cross section from Cairo to Rockford (see fig. 3) showing the position of base of the USDW (Brower et al. 1989).

tribution of this unit. Note that erosion has truncated the Hunton in a large area in the northern third of the state. Near the project site the Hunton is about 800 feet; its upper 350 feet includes units of the Devonian System.

Silurian Part of Hunton Supergroup

The Silurian consists of Alexandrian (lower part) and Niagaran (middle part) units and thickens eastward from an erosional featheredge in western Illinois to more than 700 feet in the east-central part of the state. In places, pinnacle reefs may increase the thickness to 1,000 feet. Units of the Cayugan (upper part) are thin or missing in Illinois. The Niagaran, the principal unit of the Silurian, consists of three dominant carbonate facies: shaly dolomite in the south, intermediate-purity carbonate in the north-central and northeast, and relatively high-purity carbonate in the northwest. Reefs are found throughout the Silurian units, and those in the southern part of the state (particularly in the southwestern part) may be oil-bearing (Whitaker 1988).

The uppermost Silurian unit in the study area is the Moccasin Springs Formation (fig. 4). The Moccasin Springs consists mostly of red (or red-and-gray-mottled), very silty, argillaceous limestone and calcareous siltstone; shale is common near the top. The Moccasin Springs contains numerous reefs, dominantly limestone, which have well-defined flank structures. The Moccasin Springs is commonly 160 to 200 feet thick and is more than 160 feet thick in the study area.

Devonian Part of the Hunton Supergroup

The Devonian part of the Hunton is composed of a basal sequence of four cherty limestones (including the Bailey Limestone) and an upper sequence of two limestones (the Grand Tower Limestone and the Lingle Formation). The Bailey Limestone is a silty, cherty, thin-bedded, hard limestone that begins along a southwesterly trending featheredge in central Illinois. Southeast of Marshall, additional cherty carbonate units were successively deposited above the Bailey. The combined thickness of these units reaches 1,200 feet in the southern part of the state. The Bailey is 144 feet thick in the Marshall area. The overlying Grand Tower Limestone and Lingle Formation begin along a southwesterly trending featheredge 75 miles northwest of Marshall and thicken southward to more than 400 feet in Gallatin County. Near Marshall, these two units have a total thickness of 96 feet; the Lingle is 22 feet thick.

Hydrogeology of the Hunton Supergroup

Fresh water is found at or near the surface in the Hunton in the northern half of the state and along the margins of the Illinois Basin. Well yields vary, depending mostly on the degree of fracture development. Variations in primary porosity and permeability can be related to lithology, which exerts some control on the degree of fracture development. Fracture development is greatest near the surface and generally decreases as depth of burial increases, particularly where the Hunton is overlain by impermeable shale units of the New Albany and Pennsylvanian.

The boundary marking the base of USDW in the Hunton is shown in figure 12. Typically, groundwater mineralization increases rapidly southward from this boundary. However, in Clark County the rate of increase in the TDS of the brine is relatively lower southwest of the USDW boundary, resulting in a TDS content of approximately 16,000 mg/L in the permeable Devonian units. Increased groundwater circulation in units with higher permeabilities allows less mineralized water to advance greater distances downdip (Brower et al. 1989). Other examples of this phenomenon are shown in figure 11; tongues of fresher water in the St. Peter Sandstone (Ordovician), the Ironton-Galesville Sandstone (Cambrian), and in certain shallow units (Silurian through basal Pennsylvanian near Cairo) move downdip into the Illinois Basin (Student et al. 1981). In the deeper parts of the basin, the mineral content of groundwater in the Hunton may reach from 150,000 to more than 200,000 mg/L TDS (Graf et al. 1966).

Drilling records and testing for the region show that the Lingle, portions of the Grand Tower, and a major part of the Silurian are relatively tight. The Bailey and several horizons in the Grand Tower and the Silurian have significant zones of permeability. Selected intervals of higher permeability in the Bailey have been used for disposal at the study site.

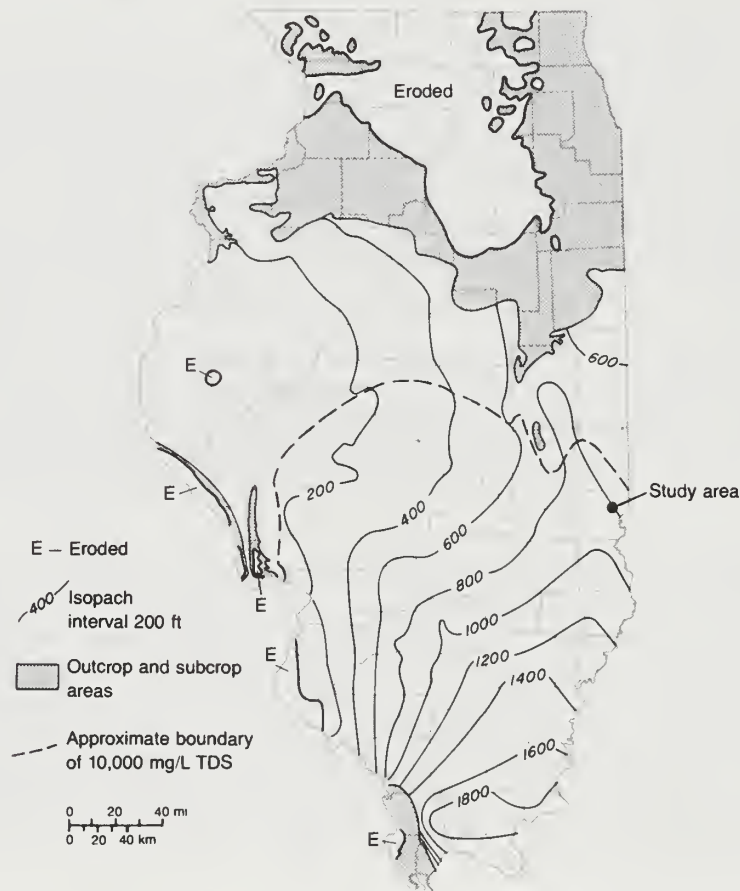


Figure 12 Generalized thickness and distribution of the Hunton Supergroup (after Willman et al. 1975) and the TDS boundary for USDW (Brower et al. 1989).

Porosity and permeability data obtained from tests run on samples collected from oil exploratory and gas storage wells scattered around the state show a mean porosity of 13 percent and a mean permeability of 40 millidarcys (Mast 1967). These data included values obtained from units in the Galena Group. Ford et al. (1981) reported porosity values of 12 to 19.5 percent and permeability values of 50 to 300 millidarcys for 269 wells completed in Devonian carbonate reservoirs of Illinois.

Evaluation of geophysical logs and sample cuttings conducted during the course of this study and for related studies of the disposal wells indicated that discrete, areally extensive horizons having high, moderate, and low permeabilities occur in the Bailey. Pore sizes range from 5 microns (μm) to over 300 (average range, 10 to 25 μm), and the pores have a fair degree of interconnection.

New Albany Group

Sedimentation during Late Devonian and Kinderhookian (Mississippian) time produced widespread accumulation of black, gray, and green shales and some limestones and siltstones. The rock units that accumulated during this time attained a total thickness of 100 to 450 feet through central and southeastern Illinois (fig. 13). Cluff et al. (1981) identified three formations present in east-central Illinois. The Blocher Shale, the basal unit, appears several miles west of the study area and thickens toward the southeast. The Blocher consists of calcareous-to-dolomitic, pyritic shale that is rich in organic matter. The Blocher is overlain with the Sweetland Creek Shale, which thickens from about 50 feet at an erosional cutoff in the central part of the state to more than 350 feet in Hardin County in southern Illinois. The Sweetland Creek is dark gray (in some places, green) and has poorly developed, laminated bedding. The unit is similar in



Figure 13 Generalized thickness and distribution of the New Albany Group (after Cluff et al. 1981).

appearance to both the Blocher and the overlying Hannibal Shale, but has widely traceable key beds. The overlying Hannibal Shale or its equivalent is less than 10 feet thick and indistinctly bedded. These formations are not differentiated at the study site.

Hydrogeology of the New Albany Group

The units of this group are very tight and therefore serve as an upper confining interval for the Hunton Supergroup. Natural gas storage fields completed in the Hunton utilize the low porosity and very low permeability of these units to retain gas in the underlying storage reservoirs (Buschbach and Bond 1974). The shale units in this group have essentially no water- or oil-yielding potential.

Mississippian Units

Mississippian units cover the southern two-thirds of the state and reach a maximum thickness of 3,300 feet in Williamson and Saline Counties (fig. 14). The widespread, thin, irregularly bedded Chouteau Limestone (Buschbach 1952) rests on the top of the New Albany and marks the base of three simultaneously deposited units: (1) the deltaic, tongue-shaped Borden Siltstone trending southwesterly across the state from the west-central part of Indiana; (2) the Burlington-Keokuk Limestones to the northwest; and (3) the Fort Payne Formation and Ullin Limestone to the southeast. The Borden consists of siltstone, some silty shale, and a few beds of fine sandstone and coarse siltstone. The "Carper sand" is present in places near the base of the Borden. The Ullin or its equivalent overlaps the top of the Borden with 150 feet of limestone and some shale in the Marshall area. Widespread limestone units, including the Salem, St. Louis, and Ste. Genevieve Limestones, accumulated between the Borden and the overlying alternating sequences of shale-limestone and shale-sandstone units that were deposited during Chesterian time.

The Mississippian section above the Chouteau is approximately 1,200 feet thick in the Marshall area and includes 450 feet of Borden Siltstone. The "Carper sand" is approximately 20 feet thick and lies very near the base of the Borden.

Hydrogeologic Conditions in the Mississippian

Mississippian units are used extensively for small (and some moderate) water supplies in and near outcrop areas. Most wells are finished at shallow depths, typically less than 300 to 500 feet. Groundwater mineralization increases rapidly with increasing depth of burial and in a down-dip direction toward the Illinois Basin (Meents 1952).

The Borden Siltstone is a thick unit of very low-permeability material that provides confinement in addition to the New Albany Group, the primary confining unit of the Hunton injection interval. The "Carper sand" provides the first somewhat permeable horizon above the top of the Hunton. Several thin, fine-grained sandstones also lie near the top of the Borden. Available porosity logs suggest that porosities of about 8 to 12 percent can be expected in these sandstones. At the study site, the Salem Limestone is the first overlying aquifer having significant permeability; it has been used for waste injection in the past. The measured static water level in the Salem is about 50 feet lower than the water level in the Bailey. The mineral content of the Salem and the Bailey in the Marshall area is similar (about 15,000 to 16,000 mg/L TDS). The groundwater in these units has an anomalously low mineral content, which appears to be related to the relatively high porosity and permeability of these units. Figures 12 and 14 show the location of the USDW boundary in Hunton and Mississippian units. The less permeable units of the Mississippian, particularly those in the upper part, contain groundwater with a much higher mineral content.

Pennsylvanian Units

The bedrock surface in the southern two-thirds of the state has been formed on Pennsylvanian units. Shale and clay units (more than 50% of the total thickness), sandstones and siltstones (more than 25%), limestones (less than 10%), and coals comprise more than 500 distinguishable units. Pennsylvanian strata reach a maximum thickness of 2,500 feet in the south-central part of the basin. Sandstones are interbedded with the shale throughout the Pennsylvanian but are most

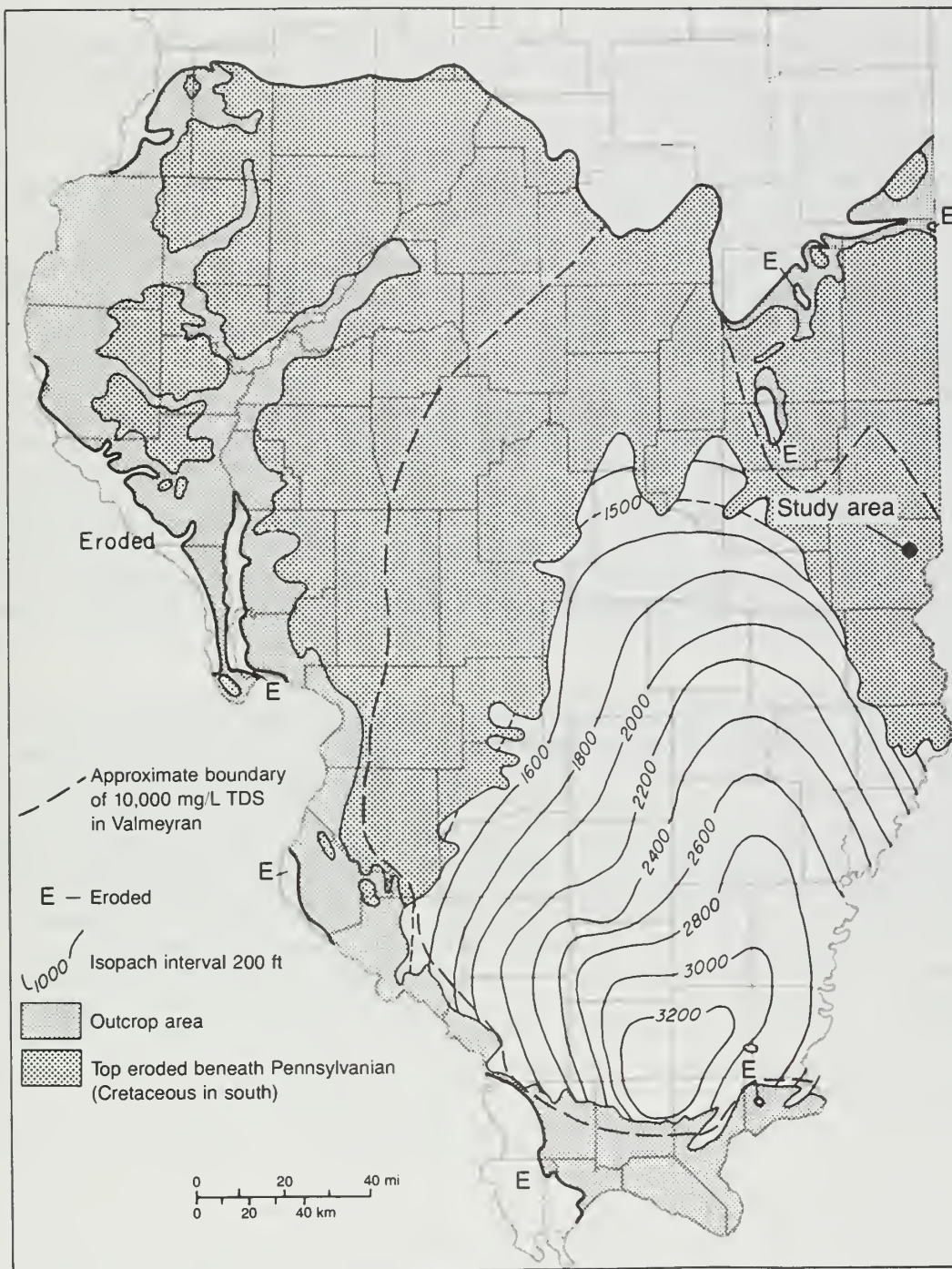


Figure 14 Generalized thickness and distribution of the Mississippian System (after Willman et al. 1975) and the TDS boundary for USDW (Brower et al. 1989).

abundant in the lower two of seven formations. Limestones are more abundant in the second formation from the top, and the most well-developed coal units are in the middle (fourth) formation.

In the Marshall area, the Pennsylvanian is about 1,050 feet thick. The thicker sandstones are found near the base of the Pennsylvanian. Coal units are present but thin. The more prominent coals occur below a depth of 400 feet.

Hydrogeologic Conditions in the Pennsylvanian Units

Fresh water exists in the upper 300 to 500 feet of the Pennsylvanian units and is a principal source for low-volume water supplies where no potential for supply exists in overlying glacial deposits. Near the margins of the basal formations, the more permeable sandstones contain fresh water to depths of more than 1,000 feet. In the Marshall area, mineralization of groundwater increases rapidly below depths of 50 to 75 feet, and water wells rarely penetrate to depths below 100 to 200 feet. The base of USDW is estimated from geophysical logs to lie about 500 feet below the surface (Piskin 1986).

Sandstones in the upper three-fourths of the Pennsylvanian are thin and widely spaced and yield very little water. The basal sandstones in the Marshall area may yield up to 20 gpm; however, water from these sandstones has a very high mineral content (38,000 mg/L TDS) (ISGS UIC files).

Porosity and permeability values measured from cores and wells collected from or finished in all types of Pennsylvanian units range from 9 to 25 percent and 10 to 10,000 millidarcys (Ford et al. 1981). Porosities measured in oil-producing sandstones are relatively uniform, averaging 17 to 20 percent (Whiting et al. 1964). Whiting also reported permeabilities of 100 to 400 millidarcys, which decrease as depth of burial increases.

Quaternary System

Glacial deposits consisting of loess, silt, clay, till, sand, and gravel cover a large part of the bedrock surface of Illinois. In the Marshall area, the drift is less than 10 to 50 feet thick in the upland areas and up to 30 to 100 feet thick in the larger stream valleys. Peoria Loess (2 to 6 ft thick) and Roxana Silt (0 to 3 ft thick) mantle the Glasford Formation (clay, sand, and till, 0 to >21 ft thick) on the upland. The Banner Formation (clay and till 0 to >20 ft) underlies Glasford Formation till where thicker drift is present in the upland areas (ISGS UIC files 1981). Cahokia Alluvium (silt, sand, and clay) overlies Henry Formation (outwash sand and gravel up to 70 ft thick) in the valley of Big Creek. Very limited to small water supplies are available from the upland glacial deposits. Moderate to large water supplies are available along some segments of Big Creek valley. Marshall obtains its water supply from the Henry Formation, about 2.25 miles east of the study site.

3. HYDROGEOLOGIC INVESTIGATION OF THE INJECTION SYSTEM

This chapter briefly discusses techniques used to collect and analyze hydrogeologic data. Details of the techniques and analyses are in appendices A and B. Specifically, stratigraphic correlations within the injection system from regional (5 to 10 miles) and local (3 miles) perspectives are discussed, along with methods used to collect additional data from the site of the injection well. These methods include geophysical logging, sidewall coring and associated analysis, and hydraulic testing. A hydrogeologic description of the injection system at the site is also given.

Stratigraphic and Structural Definition of the Injection System

The injection system consists of the geologic materials constituting the injection zone and its associated upper and lower confining units. To evaluate the confining and injection potential for the Devonian injection system, data were collected from wells in three gas storage fields (Nevens, Elbridge, and State Line), wells within 5 to 10 miles from the project site, and wells within 3 miles of the site (see figure 15 and table 1). The gas storage fields are approximately 9 miles northeast of Velsicol's Waste Disposal Well 2 (WDW2). Data from these wells were used to correlate hydrogeologic units within the injection system and to construct a structure map of the top of the Lingle Formation. The injection interval for WDW2 lies within the Devonian limestone sequence, immediately below the Lingle and Grand Tower Formations.

Each of the three gas storage fields utilizes a domal structure with closure to concentrate and store the gas. Each domal structure was formed by the deposition of Devonian- and Silurian-age shelf facies sediments over Silurian-age reef facies sediments.

Although this type of structure is not present in the area immediately surrounding the Velsicol plant, the general stratigraphic relationship of the rock units near the storage fields and those near the disposal well was shown to be consistent. Inferences were then made regarding data from the gas storage fields to the disposal well at Velsicol.

Geophysical logs from wells at a 5- to 10-mile radius from the plant were used to correlate stratigraphy and to give a regional picture of the configuration of the injection system. Geophysical logs from wells within 3 miles of the injection well were used to construct a structure map consistent with regional data.

Stratigraphic Description of the Injection System

The stratigraphy of the injection system includes the Silurian-age Moccasin Springs Formation at the base through the Grassy Creek Shale, the uppermost Devonian unit of the New Albany Group. Figure 16 is a geologic column showing the stratigraphic position and hydrogeologic characteristics of these units at the waste disposal well studied. Much of the strata information is from Willman et al. (1975). Additional data were obtained for the Middle Devonian strata from North (1969) and for the strata of the New Albany Group from Cluff et al. (1981).

The Devonian strata comprise three series—the Lower, Middle, and Upper. The Bailey Limestone, basal unit of the Lower Devonian Series, is dominantly gray to greenish gray, silty, cherty, thin-bedded, very hard limestone. Some beds are argillaceous. The chert, black to dark gray, occurs in bands up to 2 feet thick. An upper zone, 0 to 100 feet thick, is limestone that is pure, white, coarsely crystalline, and only slightly cherty.

A major unconformity occurs at the Lower and Middle Devonian interface. The basal formation of the Middle Devonian Series is the Grand Tower Limestone, which is mostly coarse-grained, light gray, medium- to thick-bedded, cross-bedded, pure, fossiliferous limestone. It also contains lithographic limestone, which becomes more abundant upward. One member differentiated at the study site is the Tioga Bentonite Bed, which is found 10 to 30 feet from the top of the Grand

Table 1 Wells used in study

Well No.	Name	Location
3	Richard Lindley #1	29-11N-10W
4	Thomas Coats #2	31-10N-13W
5	C. A. Pence #1	31-10N-13W
6	Burger #1	23-10N-13W
7	H. O. Coldren #1	4-11N-11W
8	A. Kannmacher #1	24-10N-13W
9	Clifford I Morgan, et al. #1	4-11N-11W
10	Gus Birchfield #1	24-10N-13W
12	Frank Morgan, et. al. #1	19-10N-13W
13	S. M. Scholfield #1	6-11N-11W
14	Birchfield-Shumaker Comm. #1	34-11N-11W
15	Boyd #1	5-11N-14W
17	Smitley #1	7-11N-11W
19	F. Kuhn #1	8-11N-11W
21	D. M. Davison #1	8-11N-11W
23	Eugene Chenowith #1-A	9-11N-11W
25	Alfred Seidel #1	15-10N-11W
26	Russel Higginbottom, et. al. #1	34-10N-12W
27	E. P. Daly #1	8-11N-14W
28	E. F. Newman, et. al. #1	30-10N-13W
29	Ella Mae Young #1	19-10N-13W
30	Ormal Higginbotham #1	22-11N-13W
33	Fraker #1	16-11N-11W
35	Lickert #1	16-11N-11W
36	Guinnip-Keyes Comm. #1	10-11N-12W
37	Southerland Comm. #1	16-11N-11W
39	Southerland #2	16-11N-11W
43	Gunder #1	19-11N-11W
45	Monk #1	21-11N-11W
48	WDW1	12-11N-12W
49	DOW	12-11N-12W
50	Redman #1	5-11N-14W
51	Mary E. Kendall #1	22-11N-11W
52	G. and E. Herrington #1	8-11N-10W
53	Frank Morgan #2	24-10N-14W
54	WDW2	12-11N-12W
55	J. C. Yeley #1	27-12N-11W
56	Elbridge #1 (gas storage)	2-12N-11W
57	Nevins #6 (gas storage)	5-12N-11W
58	State Line #1 (gas storage)	28-12N-10W
61	Hall #1	1-11N-12W
69	Alton Blankenship #1	16-11N-12W
77	Bays #1	21-11N-12W
79	Anna Brosman #1	21-11N-12W
81	Minnie L. Jackson #1	21-11N-12W
85	John W. Dawson #1	22-11N-12W
87	Frahm-Cole-Lee Comm. #1	28-11N-12W
103	Glen Morgan #1	21-11N-12W
111	Waller Comm. #1	21-11N-11W

Tower. The Tioga is a greenish to brownish gray shale that contains biotite flakes and an abundance of silicate minerals that distinguish it from other shales. The Tioga generally is only 1 to 2 inches thick, but it may be 6 to 8 inches thick.

The Lingle Formation overlies the Grand Tower and is more argillaceous, darker, and finer-grained than the Grand Tower. At the study site, the Lingle is composed of two members, the Howardton Limestone Member and the Tripp Limestone Member. Howardton, the basal member, is gray, fine-grained, slightly silty, argillaceous limestone, most of which has thin, shaly partings. The Tripp is heterogeneous, containing limestone, dolomite, chert, siltstone, and shale. It is largely cherty, argillaceous, silty limestone, but beds of shale are abundant near its base and top. The New Albany Group overlies the Lingle Formation. The Devonian portion of this group includes the Blocher, Selmier (Sweetland Creek), and Grassy Creek Shales. These units were not

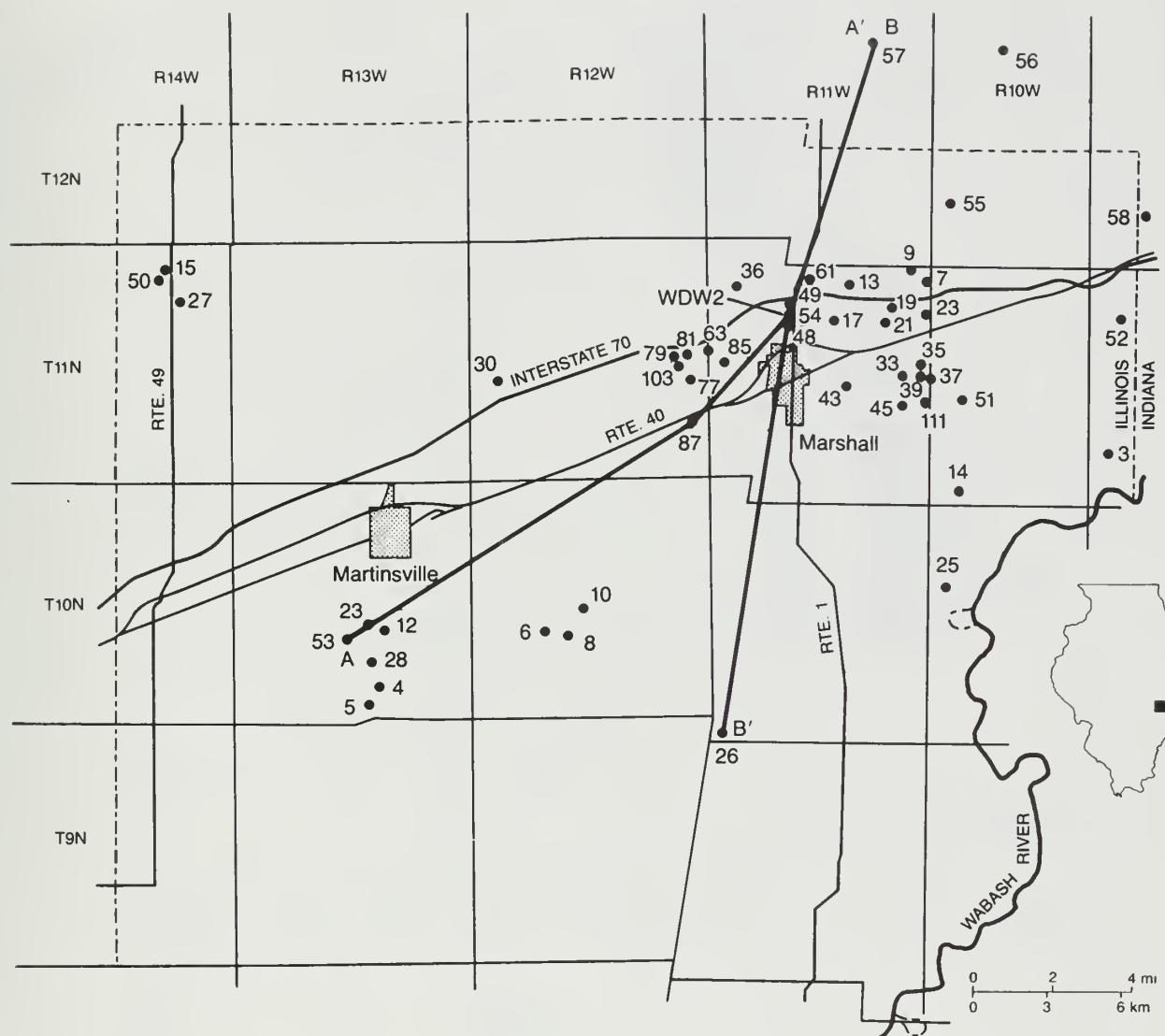


Figure 15 Well locations. Cross sections for A-A' and B-B' appear in figures 17, 18, and 19.

differentiated at the study site. The Blocher is the basal formation of the New Albany Group and is a calcareous or dolomitic black shale. The Blocher is the only shale in the New Albany containing much calcite.

The Selmier Shale Member overlies the Blocher and consists of greenish gray, dolomitic, bioturbated mudstone at the top that grades downward through an interbedded zone to black dolomitic laminated shale at the base. North (1969) placed these same units in the Sweetland Creek Member. The Selmier is conformably overlain by the Grassy Creek Shale Member.

The Grassy Creek is the uppermost Devonian unit of the New Albany Group and consists of brownish black to grayish black, finely laminated, pyritic, carbonaceous shale.

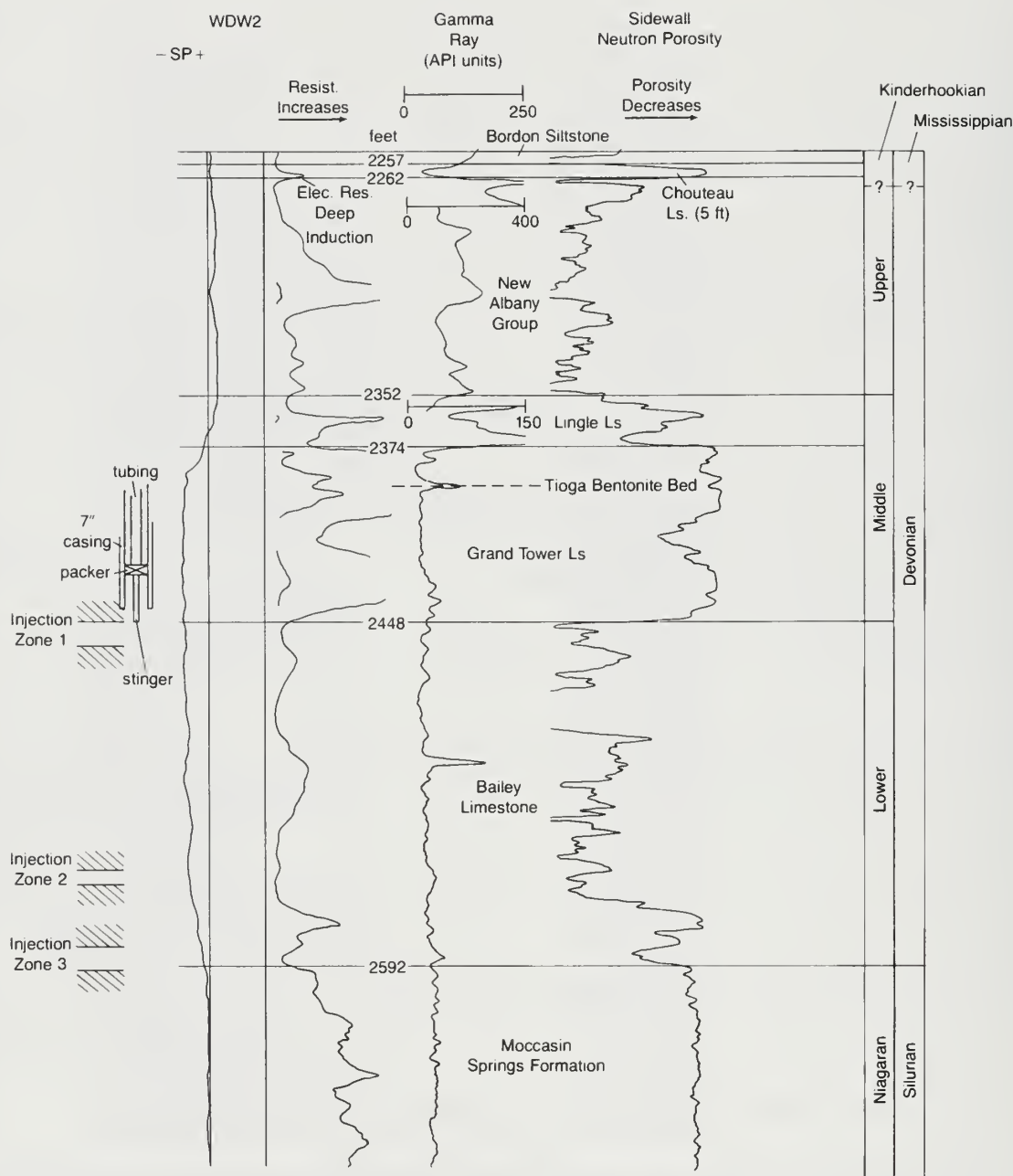


Figure 16 Geologic column for the injection system at Waste Disposal Well 2 (WDW2).

Geophysical Log Correlations

Figures 17, 18, and 19 illustrate the stratigraphic continuity of the hydrogeologic units within the injection system and the base of the New Albany Group within a 10-mile radius of WDW2. Figure 17 shows a southwest-northeast cross section based on resistivity logs, Induction Electric Logs (IEL), and Electric Logs (EL). Figure 18 is also a southwest-northeast cross section, but it is based on qualitative permeability log (Minilog) responses. Figure 19 shows a north-south cross section that is based on resistivity logs. Qualitative permeability logs were not available for all wells along this cross section.

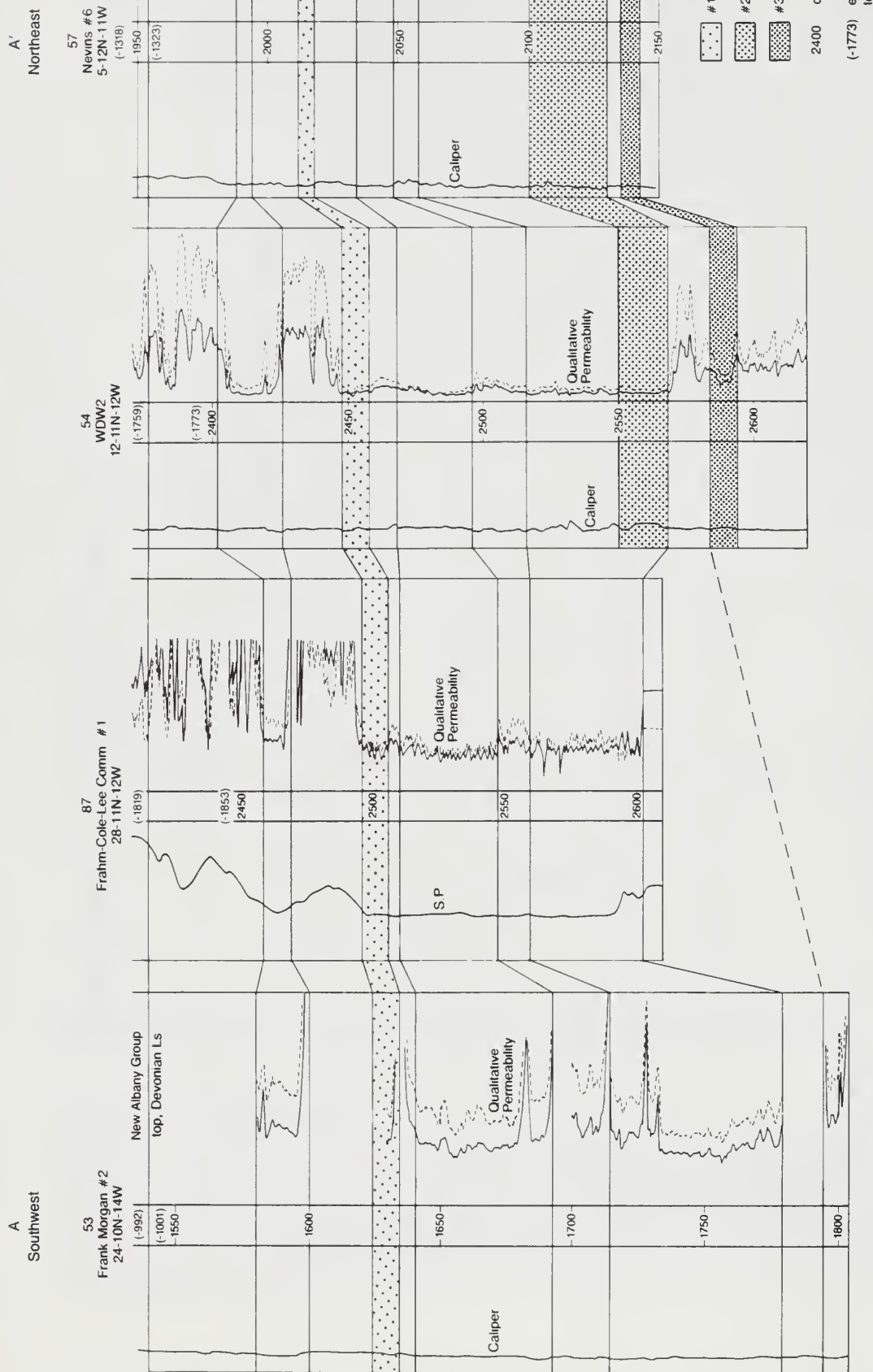


Figure 18 Qualitative permeability correlation utilizing permeability indicator logs for southwest-northeast cross section.

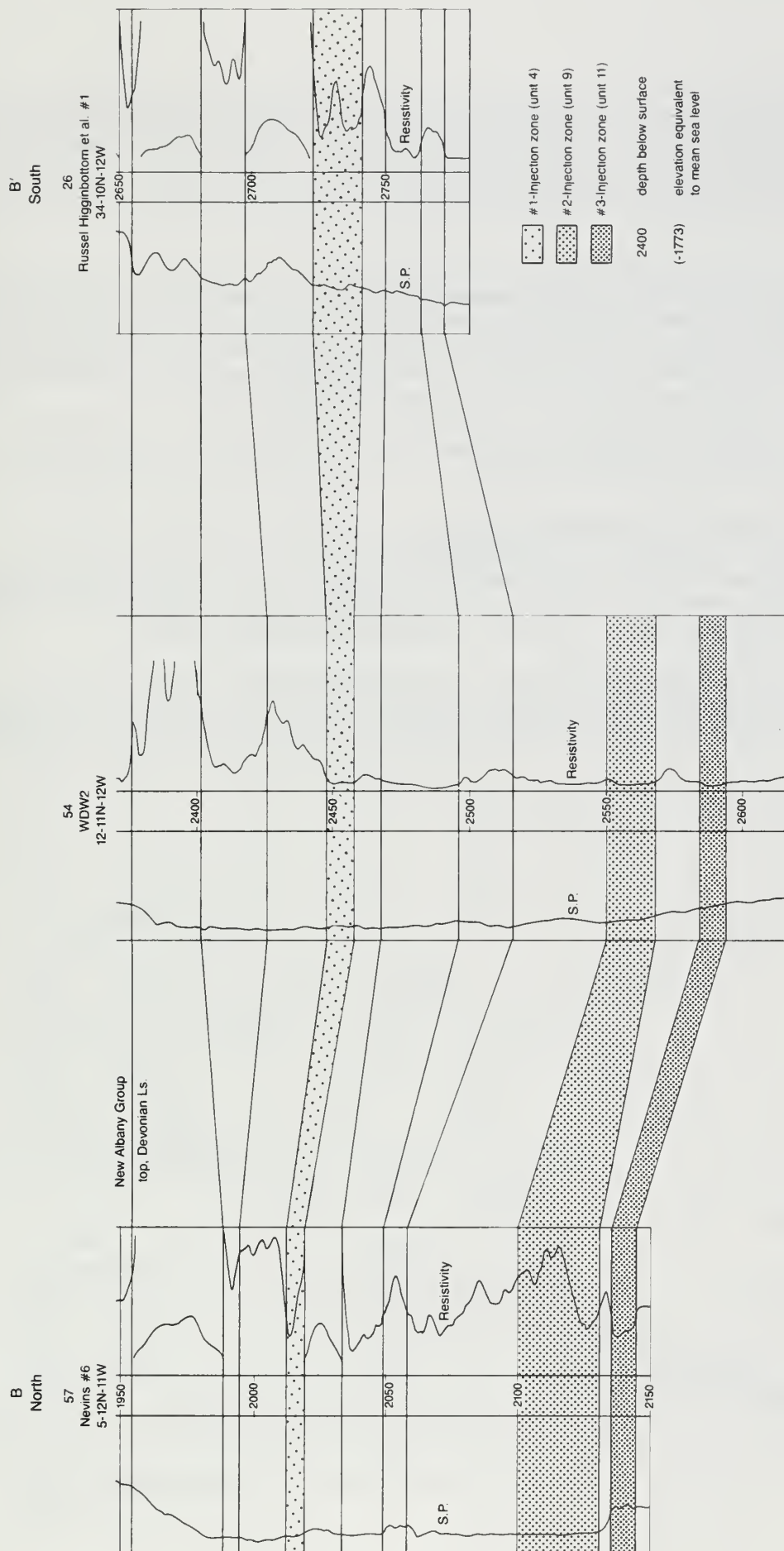


Figure 19 Stratigraphic correlation utilizing resistivity logs for north-south cross section.

The data presented in figures 17 and 19 show the hydrogeologic units within the injection system to be laterally continuous across the study area with one exception. Likewise, the continuity of the qualitative permeability of these units is inferred from figure 18. On the basis of resistivity and qualitative permeability logs, injection zone no. 2 could not be differentiated from the overlying unit in some wells in the study area. These unit designations are not included in these cross sections.

Nevertheless, the stratigraphic and qualitative permeability continuity of the Devonian limestone and the New Albany shale between the wells at Velsicol and the wells in the gas storage fields can be inferred; thus, continuity of quantitative permeability can be inferred. Analysis of core retrieved from WDW2 provided quantitative permeability data for the various hydrogeologic units. The quantitative permeability data obtained from wells at the three gas storage field wells are summarized later in this chapter (see Hydrogeology of the Site, p. 40).

A structure map of the top of the Lingle Formation was constructed (fig. 20) using information from wells within a 3-mile radius of Velsicol.

Stratigraphic and Structural Characterization

On the basis of correlations between the disposal well at Velsicol and the wells within a 5- to 10-mile radius of the plant, both the upper and lower confining units and the injection zones appear to be continuous across the study area. Although information about the thickness of the lower confining unit is limited, figures 17, 18, and 19 clearly show its stratigraphic location.

The analysis of available geophysical logs for regional hydrogeology of the injection system is summarized in figure 21. A confining unit is distinguished from an "impermeable" unit by its position with respect to the permeable units. Confining units lie directly above the uppermost perme-

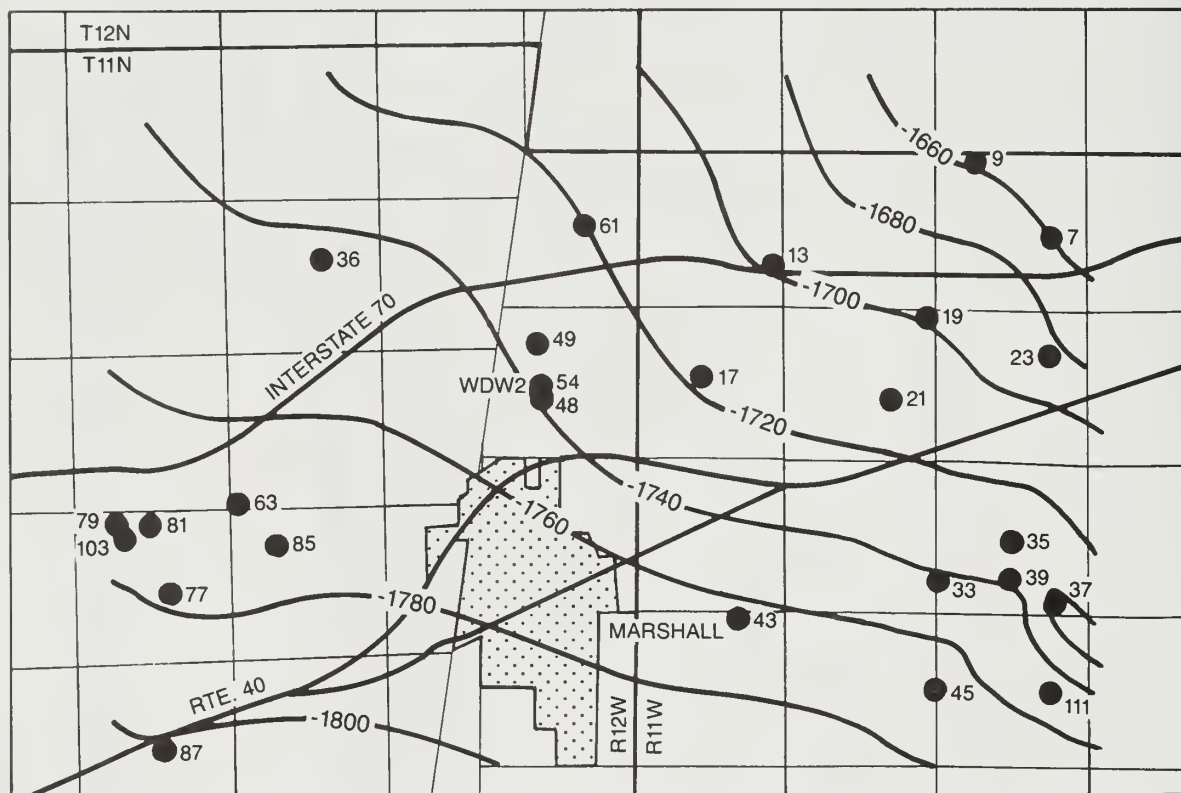


Figure 20 Structure contour map of the top of the Lingle Formation in the vicinity of the Velsicol plant.

able unit or directly below the lowermost permeable unit; impermeable units lie between permeable units. For permitting purposes, the upper confining unit includes the base of the New Albany shale and 26 feet of the Lingle Formation and Grand Tower Formation. Thickness variations for this section of the upper Devonian limestone are limited to about ± 8 feet over the 10-mile region of investigation. In terms of the hydraulic confinement of the injection interval, the upper confining unit is composed of Grand Tower Limestone. Its thickness is approximately 74 feet at WDW2.

For permitting purposes, the Maquoketa shale is considered the lower confining unit. In terms of hydraulic confinement, the lower confining unit consists of the Moccasin Springs Limestone. Its total thickness could not be determined in this study because of limited data, but it is at least 160 feet thick at WDW2, based on available geophysical log data.

It is evident from figure 20 that the structure in the Velsicol plant area is generally flat with a gradual inclination of about 25 feet/mile to the northeast.

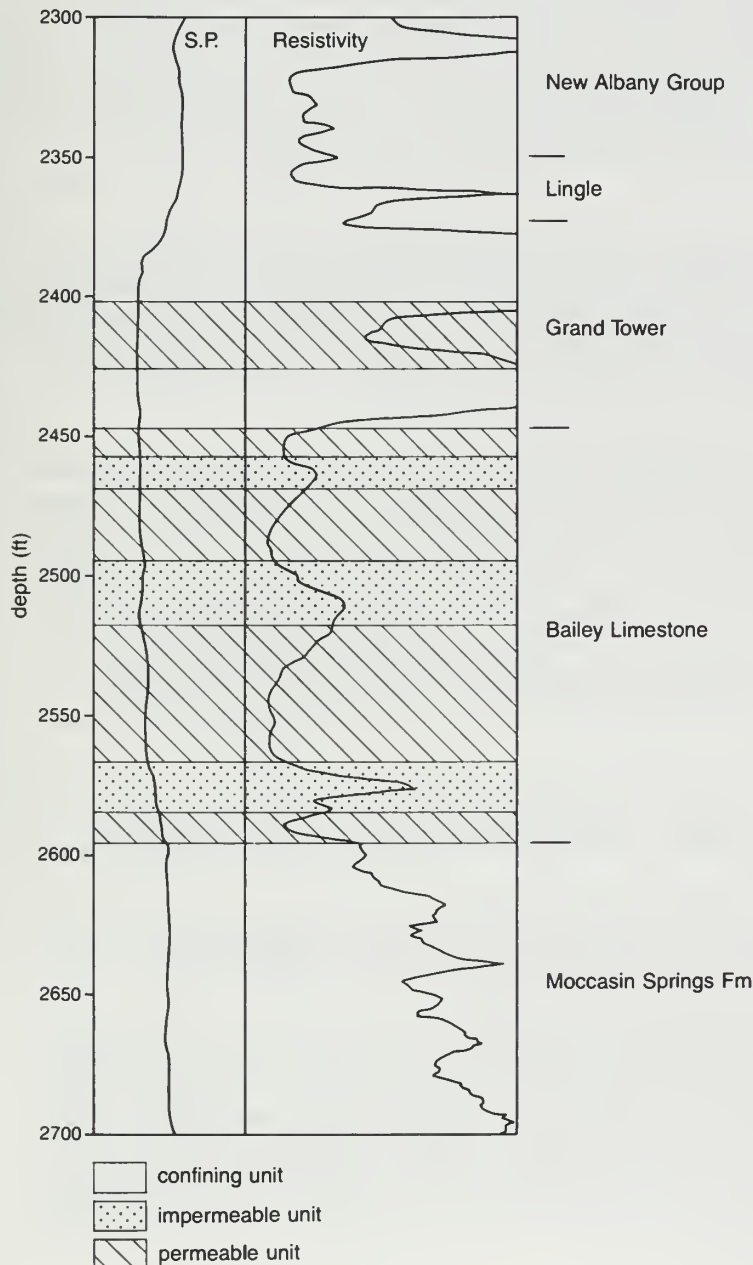


Figure 21 Injection system in WDW2 indicating permeable and impermeable zones delineated with available geophysical logging.

Determination of Horizontal Hydraulic Gradient

If the horizontal gradient is to be properly calculated, the hydraulic head within the injection system must be known for various locations. The initial reservoir pressure, obtainable from drill stem tests (DSTs), would be an excellent source of data. For initial reservoir pressure calculations, the pressure versus time chart from the DST is needed. This chart, however, was not available for wells in this area. Final flow and final closed-in pressures, as well as static water levels, were used to calculate the horizontal gradient. According to limited, high-quality data, the greatest horizontal gradient existed between wells 54 (WDW2) and 57. The hydraulic gradient (dh/dl) has a magnitude of 3.5×10^{-4} in a general direction of north to south.

Field Investigations

Two phases of geophysical logging were performed at the Velsicol site. During phase I, data on porosity and qualitative permeability, stratigraphic orientation, and the lithology of the rock units within the disposal zone were obtained from the Devonian Observation Well (DOW), Well 49. Data reduction indicated the units most favorable for fluid infiltration. Phase II was a detailed study based on information obtained from phase I. Results from phase II included quantitative data on permeability (air and water), bulk compressibility, hydraulic conductivity, specific discharge, and specific storage of the injection horizon. Those units with the greatest injection potential were further characterized for thickness, storativity, and transmissivity. In addition, hydraulic testing (flowmeter and injection testing) of the injection system was conducted.

Phase I Investigations

Records (well logs, drilling records, and other data) provided a general overview of the structure and regional continuity of stratigraphic units particularly important to waste injection and confinement. These data, however, were only one aspect of the overall integrated approach used to characterize the injection system. Additional data were needed to precisely define the character of possible confining and injection intervals. The methods and techniques used to characterize the disposal zone are discussed briefly and considered in detail in appendix A.

Existing geophysical logs. After a review of the historical records, a preliminary estimate was made of the stratigraphic location of the potential confining units (upper and lower) and the impermeable units associated with the operational waste disposal well (WDW2). These hydrogeologic units were delineated using four principal downhole geophysical logs, which were run during initial well (WDW2) construction in 1971. The logs were the Sidewall Neutron Log (SNL), Induction Electric Log (IEL), Gamma Ray Log (GRL), and Microlog (MIL). The hydrogeologic units determined from analysis of these logs are presented in figure 22. Consideration of all four logs was necessary to fully evaluate porosity, qualitative permeability, shale percentage, and lithology of the geologic materials. Interpretation methods used in the evaluation of these logs are discussed in appendix B.

Additional existing geophysical logs include the Temperature/Salinometer and GR/Neutron Logs run in the DOW in 1981 and 1973, respectively, and a Sonic Log (SL) run in WDW1 in 1965.

However, since logging instrument technology has progressed dramatically and subsequent equations and modeling of formation characteristics have advanced since these logs were run, a new suite of logs was run. Use of these geophysical logs enabled further delineation of the hydrogeologic characteristics of the injection system.

Phase I geophysical logging. A suite of logs was selected on the basis of the considerations discussed above and the physical dimensions of the casing and tubing in the three wells at Velsicol. The only well suitable for study during phase I was the DOW. Dresser Atlas performed the logging. The two types of porosity logs run were the Compensated Neutron Log (CNL) and the Borehole Compensated Sonic Log (BCS). The Minilog (MIL) was run to qualitatively determine permeability. Resistivity parameters were determined by the Dual Induction Spherically Focused

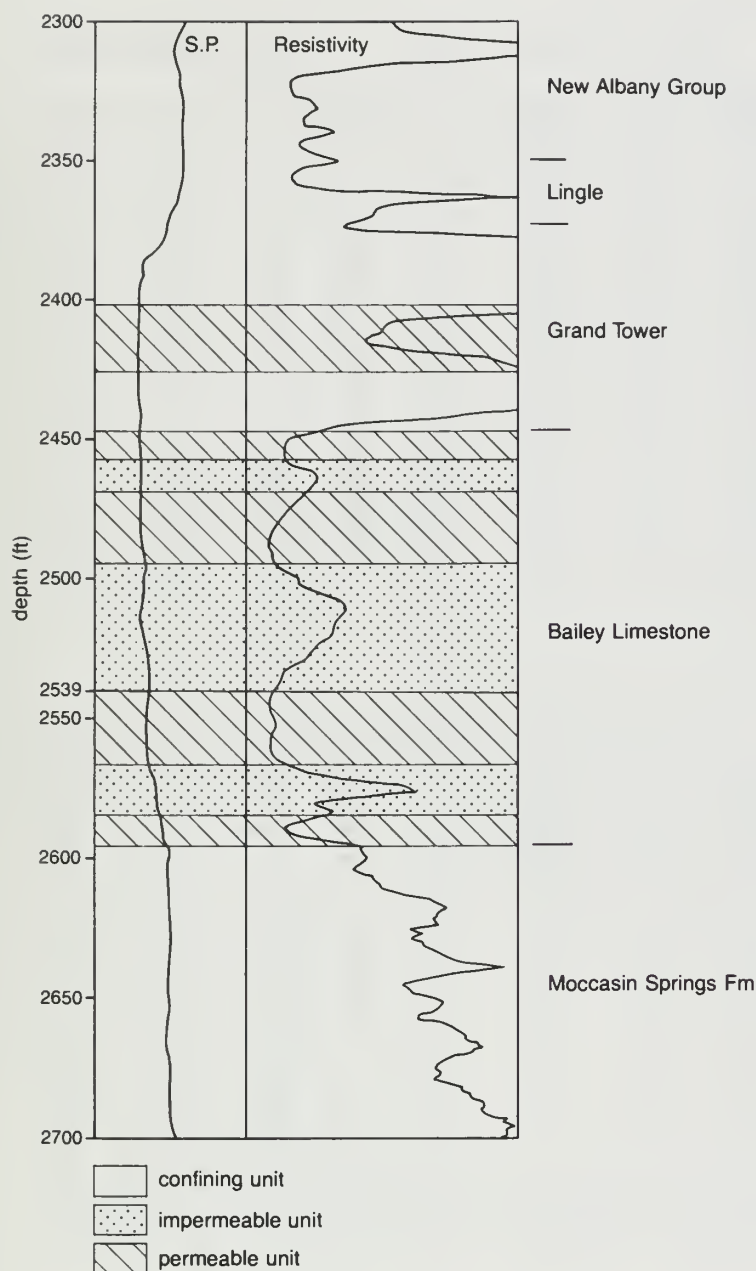


Figure 22 Injection system in WDW2 indicating permeable and impermeable zones delineated after phase I logging.

Log (DISFL). Finally, to provide the best stratigraphic correlation between the three wells at Vel-sicol, the Gamma Ray Log (GR) was run. (See appendix A for a discussion of the theory and general application of these logs.)

The techniques used to reduce the geophysical log data are discussed in appendix B. The data from these logs, analyzed and reported in 2-foot intervals, are presented in table 2. With the use of these modern logging tools and incorporation of improved analytical techniques, it was possible to obtain more accurate hydrogeologic data of the geologic materials constituting the injection interval. These data consisted of the formation's matrix-corrected CNL porosity ([POR]Ncor), matrix-corrected BCS porosity ([POR]BCScor), cross-plotted porosity ([POR]xp), secondary porosity ([POR]sec), true resistivity (Rt), matrix lithology (MA), water saturation (SW), shale volume (Vsh), and qualitative permeability (k). The same data were obtained from existing logs for WDW2 and are reported in table 3. Important parameters from these tables are summarized in table 4.

Table 2 Data from geophysical logs run in the DOW

DEPTH	GR	(POR)	(POR)		(POR)	(POR)	(POR)	RT	MA	SW	Vsh	k
GL		Nls	Ncor	t	BCScor	xp	sec					
(ft)	(API)	(%)	(%)	(sec)	(%)	(%)	(%)	(ohm-m)		(%)	(%)	
2434	28	4.3	4.3	53	3.8	4.3	0.5	50.0	LS	100	6.2	N
36	40	5.0	5.0	53	3.8	5.0	1.2	65.0	LS	100	15.4	N
38	35	12.0	12.0	60	8.8	10.0	3.2	20.0	LS	100	11.5	N
40	25	18.0	18.0	69	15.1	16.4	2.9	11.0	LS	100	3.8	N
42	30	19.0	19.0	69	15.1	16.7	3.9	7.0	LS	100	7.7	Y
44	25	23.8	23.8	77	20.8	21.7	3.0	5.0	LS	100	3.8	Y
46	22	22.6	22.6	76	20.1	21.1	2.5	4.8	LS	100	1.5	Y
48	23	23.0	17.0	70	18.2	18.2	0.0	7.0	DOL	100	2.3	N
50	30	16.0	10.0	62	12.7	12.0	0.0	10.0	DOL	100	7.7	N
52	30	17.5	11.5	57	9.3	9.7	2.2	16.0	DOL	100	7.7	N
54	22	19.0	13.0	60	11.3	11.7	1.7	13.0	DOL	100	1.5	N
56	17	22.0	16.0	62	12.7	13.3	3.3	9.0	DOL	100	0.0	N
58	20	20.6	14.6	63	13.4	13.6	1.2	10.0	DOL	100	0.0	N
60	28	21.8	15.8	61	12.0	12.7	3.8	9.0	DOL	100	6.2	N
62	27	24.6	18.6	65	14.8	15.6	3.8	7.0	DOL	100	5.4	Y
64	32	24.0	18.0	66	15.5	16.0	2.5	5.5	DOL	100	9.2	Y
66	22	25.5	19.5	70	18.2	18.5	1.3	4.8	DOL	100	1.5	Y
68	23	28.5	22.5	78	23.7	23.5	0.0	4.0	DOL	100	2.3	Y
70	17	29.2	23.2	82	26.5	26.0	0.0	3.3	DOL	100	0.0	Y
72	18	28.0	28.0	82	24.3	25.7	3.7	3.0	LS	100	0.0	Y
74	17	30.0	30.0	87	27.9	28.8	2.1	3.2	LS	100	0.0	Y
76	17	28.0	28.0	83	25.0	26.3	3.0	3.5	LS	100	0.0	Y
78	19	26.8	20.8	78	23.7	23.2	0.0	3.9	DOL	100	0.0	Y
80	17	26.3	20.3	77	23.0	22.6	0.0	4.4	DOL	100	0.0	Y
82	20	29.0	23.0	74	21.0	21.4	2.0	4.0	DOL	100	0.0	Y
84	24	23.5	17.5	71	18.9	18.5	0.0	4.6	DOL	100	3.1	Y
86	26	21.3	15.3	63	13.4	13.7	1.9	7.1	DOL	100	4.6	N
88	23	22.3	16.3	64	14.1	14.5	2.2	10.0	DOL	100	2.3	N
90	23	16.5	10.5	60	11.3	11.1	0.0	11.0	DOL	100	2.3	N
92	30	16.4	10.4	56	8.6	8.9	1.8	16.0	DOL	100	7.7	N
94	29	19.8	13.8	57	9.3	10.2	4.5	21.0	DOL	100	6.9	N
96	60	19.0	13.0	60	11.3	11.6	1.7	20.0	DOL	100	30.8	N
98	84	18.5	12.5	60	11.3	11.5	1.2	15.0	DOL	100	49.2	N
2500	52	19.3	13.3	62	12.7	12.7	0.6	14.0	DOL	100	24.6	N
2	37	18.2	12.2	57	9.3	9.8	2.9	14.0	DOL	100	13.1	N
4	33	22.0	16.0	59	10.7	11.8	5.3	11.0	DOL	100	10.0	N
6	45	23.0	17.0	64	14.1	15.1	2.9	8.0	DOL	100	19.2	N
8	30	19.8	13.8	60	11.3	12.1	2.5	9.0	DOL	100	7.7	N
10	23	20.0	14.0	58	10.0	11.3	4.0	8.5	DOL	100	13.1	N
12	20	22.8	16.8	60	11.3	13.2	5.5	8.2	DOL	100	0.0	N
14	32	20.7	14.7	64	14.1	14.4	0.6	9.0	DOL	100	9.2	N
16	30	20.1	14.1	60	11.3	12.4	2.8	10.5	DOL	100	7.7	N
18	42	20.8	14.8	62	12.7	13.6	2.1	8.5	DOL	100	16.9	N
20	38	19.0	13.0	60	11.3	12.1	1.7	10.0	DOL	100	13.8	N
22	30	20.3	14.3	56	8.6	10.4	5.7	11.0	DOL	100	15.4	N
24	23	21.7	15.7	61	12.0	13.3	3.7	10.0	DOL	100	2.3	N
26	24	20.0	14.0	60	11.3	12.2	2.7	8.0	DOL	100	3.1	N
28	23	16.0	10.0	57	9.3	9.7	0.7	9.0	DOL	100	2.3	N
30	23	19.0	13.0	61	12.0	12.5	1.0	10.0	DOL	100	2.3	N
32	21	20.4	14.4	63	13.4	13.8	1.0	12.0	DOL	100	0.8	Y

Table 2 Continued

DEPTH GL (ft)	GR (API)	(POR) Nls (%)	(POR) Ncor (%)	t (sec)	(POR) BCScor (%)	(POR) xp (%)	(POR) sec (%)	RT (ohm-m)	MA	SW (%)	Vsh (%)	k
2534	33	22.5	16.5	60	11.3	12.2	5.2	10.0	DOL	100	10.0	Y
36	27	22.0	16.0	63	13.4	13.9	2.6	7.5	DOL	100	5.4	Y
38	28	24.3	18.3	65	14.8	15.5	3.5	6.5	DOL	100	6.2	Y
40	29	24.0	18.0	63	13.4	14.2	4.6	5.8	DOL	100	6.9	Y
42	35	17.3	11.3	61	12.0	11.8	0.0	7.1	DOL	100	11.5	N
44	40	16.5	10.5	59	10.7	10.6	0.0	9.0	DOL	100	15.4	N
46	42	21.3	15.3	63	13.4	13.7	1.9	8.5	DOL	100	16.9	Y
48	40	22.5	16.5	70	18.2	17.7	0.0	6.7	DOL	100	15.4	Y
50	40	20.6	14.6	66	15.5	15.1	0.0	6.7	DOL	100	15.4	Y
52	38	15.6	15.6	65	12.3	13.3	3.3	10.0	LS	100	13.8	N
54	29	8.6	8.6	57	6.6	7.4	2.0	20.0	LS	100	6.9	N

Table 3 Data from existing geophysical logs run in WDW2¹

DEPTH GL (ft)	GR (API)	(POR) Nls (%)	(POR) Ncor (%)	t (sec)	(POR) BCScor (%)	(POR) xp (%)	(POR) sec (%)	RT (ohm-m)	MA	SW (%)	Vsh (%)	k
2582	26	8.1	8.1	63	10.9	10.1	0.0	30.0	LS	90	4.6	N
84	30	10.0	10.0	66	13.0	12.2	0.0	28.0	LS	77	7.7	N
86	34	15.0	15.0	71	16.5	16.3	0.0	17.0	LS	74	10.8	N
88	38	14.7	14.7	73	18.0	17.1	0.0	13.0	LS	81	13.8	Y
90	37	13.5	13.5	73	18.0	16.9	0.0	13.0	LS	82	13.1	Y
92	26	7.8	11.1	68	8.8	10.0	2.3	20.0	SS	100	4.6	Y
94	29	6.1	9.3	65	7.1	8.2	2.2	38.0	SS	98	6.9	N

1 All logs used for study were from WDW2 (run during well installation), except the Sonic Log (SL), which was from WDW1 (run during well installation). The methods of analysis used were the same as above. All depths measured are from Kelly Bushing (KB), which is 12 feet above GL.

From the data (see appendix B) it appeared that the host formation, the Bailey Limestone, was composed mainly of a clean dolomite with less than 20 percent shale throughout most of the interval logged. Since the Bailey Limestone is predominantly a dolomite, secondary porosity is always a consideration. A comparison of CNL and BCSL data suggested that secondary porosity may account for up to 10 percent of the total porosity. The intervals with higher relative permeability have a slightly higher secondary porosity and, in turn, total porosity.

Also, the entire interval is primarily 100 percent water saturated with a fluid resistance of approximately 0.247 ohm-m. At a formation temperature of about 80°F and depth of 2,460 feet GL, the fluid composition was estimated to be approximately 24,000 ppm NaCl.

Phase I log analysis provided qualitative data of the disposal horizon. On the basis of this analysis, an additional section of the disposal horizon (2,518 to 2,539 ft KB [Kelly Bushing]) was eliminated as a possible injection zone (fig. 23).

Table 4 Summary of important formation characteristics

(POR) _{xp,ave} = 16%	(POR) _{xp,max} = 28.8	%(POR) _{xp, min} = 8.9%
(POR) _{sec,ave} = 1.98%	(POR) _{sec,max} = 5.7%	
t _{ave} = 66.7×10^{-6} sec/ft		
t _{max} = 87×10^{-6} sec/ft		
t _{min} = 56×10^{-6} sec/ft		
R _{t,ave} = 8.6 ohm-m	R _{t,max} = 21 ohm-m	R _{t,min} = 3 ohm-m
V _{sh,ave} = 8.05%	V _{sh,max} = 49.2%	V _{sh,min} = 0.0%

Formation lithology (based on 98 feet of "higher permeability, higher porosity" unit), 61.0% dolomite, 35.0% limestone, and 4.0% sandstone.

Phase II Geophysical Logging

Phase II analysis consisted of a detailed site-specific evaluation of the injection/confining interval. Continuous Spinner Flowmeter logging (CSFL) and core analysis formed the basis of the study. Scanning Electron Microscope (SEM) analysis and formation brine/wastewater analysis were also conducted.

Continuous spinner flowmeter logging. The foregoing data were obtained exclusively from a static environment, i.e., no fluid injection into the well. For a quantitative evaluation of the response of the formation to "normal" or near-normal injection rates, a Continuous Spinner Flowmeter Log (CSFL) was run in WDW2. (An X-Y Caliper Log run prior to the CSFL provided borehole volumetric data to be used in conjunction with the CSFL data.) Again, as with the previous set of geophysical logs, borehole conditions in WDW2 restricted the interval available for logging. But work-over operations subsequent to the WDW2 logging permitted coverage of all anticipated injection zones as delineated by historical and phase I logging (fig. 23).

The CSFL data were used in two ways. First, the data enabled the delineation of specific injection zones and the calculation of the percentage of total flow into each zone. Second, the data were used to identify the lower boundary of fluid infiltration (i.e., the upper limit of the basal confining unit).

To evaluate the effect of varying injection rates, we recorded flow rates at three surficial injection rates: 75 gallons per minute (gpm), 100 gpm, and 150 gpm. The results are reported in table 5. Fluid loss is the percentage, on a volumetric basis, of fluid moving into a particular unit. For example, on average, 14 percent of the fluid flows into injection zone 1. The 150-gpm rate is the closest to the "average" waste injection rate (182 gpm) for WDW2 (see p. 58).

The repeatability of the flowmeter was verified by taking measurements as the flowmeter moved both up and down the borehole. With the flowmeter stationary, data were collected adjacent to suspected high permeability units and below the base of the anticipated injection horizon (2,594 ft KB from the other geophysical surveys). The validity of the results was checked by obtaining data with a stationary flowmeter in the 7-inch casing. At surficial injection rates of 75 gpm, 100 gpm,

Table 5 Fluid loss percentage calculated from CSFL

Injection zone no.	Depth (ft below KB)	Fluid Loss (%) Injection rates (gpm)			
		75	100	150	Average
1	2448-2458	11	15	17	14
2	2552-2558	40	38	29	36
3	2584-2594	49	47	54	50

and 150 gpm, calculated flow rates in the 7-inch casing were 81 gpm, 107 gpm, and 163 gpm, respectively (margin of error less than 10%).

The effective interval of injection at the time of logging the CSFL (from the base of the 7-inch casing to the deepest depth of penetration of the logging tool) was from 2,437 to 2,614 feet KB. If conditions remain stable, fluid should infiltrate exclusively into the zones listed in table 5 and shown on figure 23. No flow was detected below 2,614 feet.

As shown on figure 23, data from the CSFL were not consistent with the interpretation of the geophysical logs. First, the interval from 2,468 to 2,496 feet was identified from both the historical and phase I logging as a potential injection zone, but the CSFL indicated an absence of flow into this interval. Second, data from the CSFL indicated that only a portion of the potential injection interval from 2,538 to 2,568 feet allowed substantial fluid infiltration. And third, on the basis solely of porosity and permeability data, zone 3 should have accepted less fluid than either zones 1 or 2;

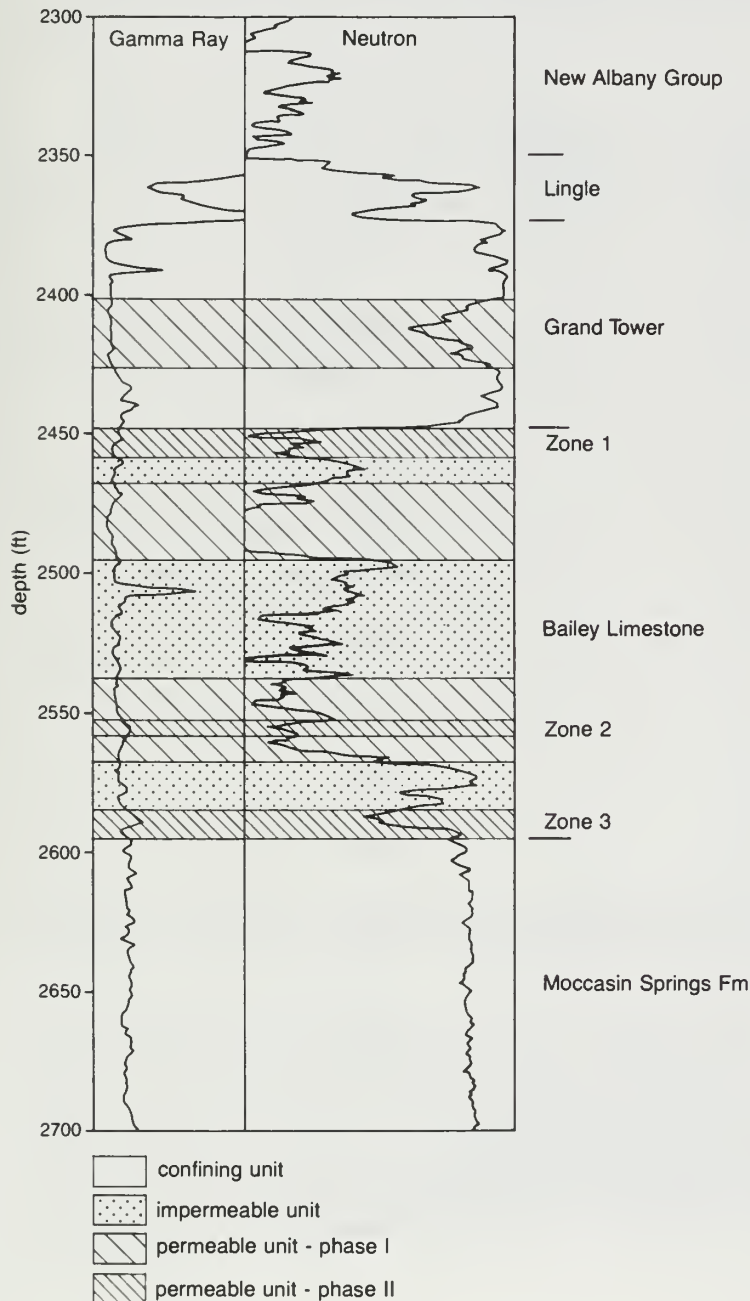


Figure 23 Injection system in WDW2 indicating permeable and impermeable units delineated after phase II logging.

however, this scenario was not supported by the CSFL data. In an effort to resolve these discrepancies and to obtain two additional parameters (quantitative permeability and bulk compressibility) essential to injection-interval evaluation, we conducted lab testing of sidewall cores.

Core retrieval and analysis. Several criteria were used to choose the coring zones. In order of decreasing priority, the selection criteria were to (1) cover all possible injection zones determined from the historical and phase I logging, (2) obtain cores from the anticipated lower confining unit indicated by logging data, and (3) cover a range of permeabilities and other physical properties present in the disposal horizon. Core depths are indicated in figure 24 and table 6.

Twenty-nine sidewall cores were retrieved with Gearhart's Hard Rock Coring tool. Gearhart Industry Inc. Corelab performed the core analysis. Additional core study was done at the ISGS. The core analysis provided data on quantitative permeability, bulk compressibility, and mineralogic composition, and provided a means to evaluate the accuracy of the downhole geophysical methods employed. The results of the core analysis are reported in table 7 and figures 25 and 26.

Table 6 Core location and analysis

Core no.	Core depth	kw ¹ (Y,N)	Strength ² test (Y,N)	Comments ³
1	2663.0	N	N	No ka
2	2622.0	Y	Y	
3	2620.0	Y	N	
4	2617.5	N	N	
5	2606.0	N	N	No ka
6	2605.0	Y	Y	
7	2588.5	Y	N	
8	2573.5	Y	N	
9	2572.5	N	N	No ka
10	2560.5	N	N	
11	2556.5	N	N	
12	2555.0	Y	Y	
13	2551.5	N	N	No ka
14	2539.5	N	N	
15	2509.5	Y	Y	
16	2508.5	N	N	
17	2491.5	N	N	No ka
18	2490.5	N	N	
19	2484.5	Y	Y	
20	2482.5	N	N	
21	2481.0	N	N	No ka
22	2479.5	N	N	
23	2478.5	N	N	
24	2463.5	N	N	
25	2462.5	N	N	No ka
26	2457.5	N	N	
27	2456.5	N	N	
28	2451.5	Y	Y	
29	2450.5	N	N	No ka

- 1 Water permeabilities (kw) derived from air permeabilities (ka) by applying a Klinkenberg correction.
- 2 Separate test which yields Poisson's ratio, Young's modulus, and bulk compressibility (corrected for in situ pore and confining pressures).
- 3 Basic analysis and x-ray diffraction performed on all cores. Basic analysis consists of ka, total porosity, water saturation (Sw), and fluorescence. X-ray diffraction identifies all minerals that have an abundance of 1% or more by weight and the total clay percentage.

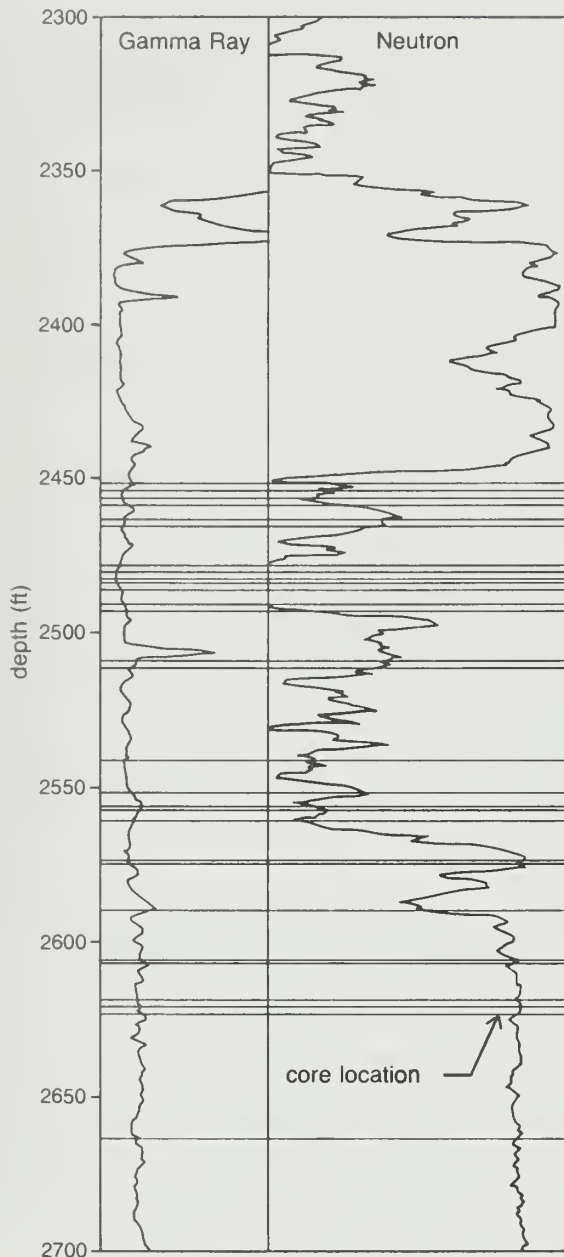


Figure 24 Core locations for WDW2.

Available data indicate that the discrepancies between the injection zones identified from phase I and phase II are due to the presence of brucite ($\text{Mg}(\text{OH})_2$). The supporting data used to develop the brucite-formation hypothesis are summarized below and more fully described in appendix C.

Mineralogic analysis of sidewall cores identified brucite (up to 45% by weight) to be present in potential injection zones, as identified from phase I logging. Brucite, not present in the injection system prior to well operation, forms during waste injection. Brucite apparently formed in zones having the highest potential for fluid flow, as identified from phase I logging. Brucite formation does not reduce porosity (as identified from geophysical logs) but does reduce the permeability significantly. Flow rates in the different injection zones appear from CSFL results to be proportional to the brucite concentration within that zone, i.e., zones with higher brucite concentrations have lower flow rates.

Table 7 Results of core analysis

Depth (ft KB)	POR (%)	ka (md)	kw (md)	Compress $\times 10^{-12}$ (cm sec ² /gm)
2450.5		24.2		
51.5	26.1	0.640	0.476	15.5
56.5	27.7	62.54		
62.5	13.2	0.0076		
63.5	11.5	0.0087		
79.5	26.4	0.178		
81.0	24.8	0.017		
82.5	56.1			
84.5	30.8	14.97	12.940	8.70
90.5	29.4	2.292		
91.5	24.2	0.457		
2508.5	9.9	0.0089		
09.5	11.4	0.017	0.001	3.36
39.5	17.7	0.203		
51.5	8.9			
55	18.0	0.060	0.017	8.41
60.5	17.1	0.095		
73.5	5.2	0.0050	0.00013	
88.5	16.6	0.021	0.004	11.9
2605	3.1	0.0055	0.00042	4.71
06	4.6	0.0029		
17.5	4.8			
20	4.6	0.0034		
22	3.8	0.0038		
63	6.7			

The source of ions for brucite formation is not clear. The source of OH^- is the injected waste ($\text{pH} > 12$), but the source of Mg^{2+} is unclear. Two possible sources are the waste fluid or the dolomite within the injection zones.

Hydrogeology of the site. Having developed a hypothesis to explain brucite formation, we quantified the hydrogeologic characteristics of the injection system, which allowed the data to be used as parameter input for the numerical model. The disposal interval was divided into 12 units based on hydrogeologic characteristics (fig. 27 and table 8), using data derived from figure 23. These 12 units were used for differentiating the stratigraphic cross sections (figs. 17, 18, and 19). Local and regional stratigraphic/structural studies, presented in Stratigraphic and Structural Definition of the Injection System, page 23, were also considered to ensure that the units chosen were not localized anomalies (i.e., noncontinuous).

Table 8 lists the units and their associated characteristics. Permeability, air (k_a) and water (k_w), and bulk compressibility data were obtained from core analysis. Hydraulic conductivity (K) and specific storage (S_s) measurements were derived from these results. The porosity measurements (POR) were taken from table 2 (geophysical logging results) and core analysis results. Storativity (S) and transmissivity (T) data were calculated only for the three injection zones delineated previously (table 9). Units 2, 9, and 11 in table 8 correspond to injection zones 1, 2, and 3, respectively. The thicknesses (b) for units 2, 9, and 11 were determined from figure 27.

The three gas-storage field wells mentioned in Stratigraphic and Structural Definition of the Injection System, page 24, provided additional permeability data for the intervals corresponding to unit 1 and the overlying strata (above 2,402 feet KB). Values for vertical water permeabilities of

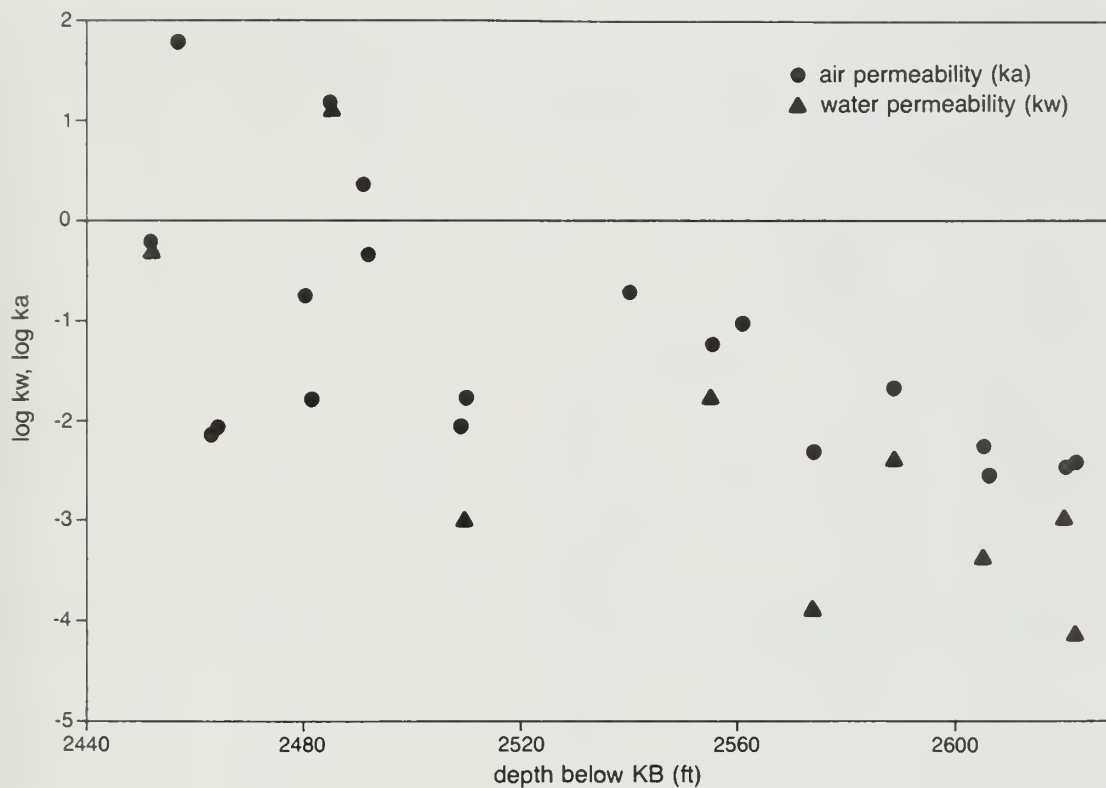


Figure 25 Core permeabilities (air and water) versus depth for WDW2.

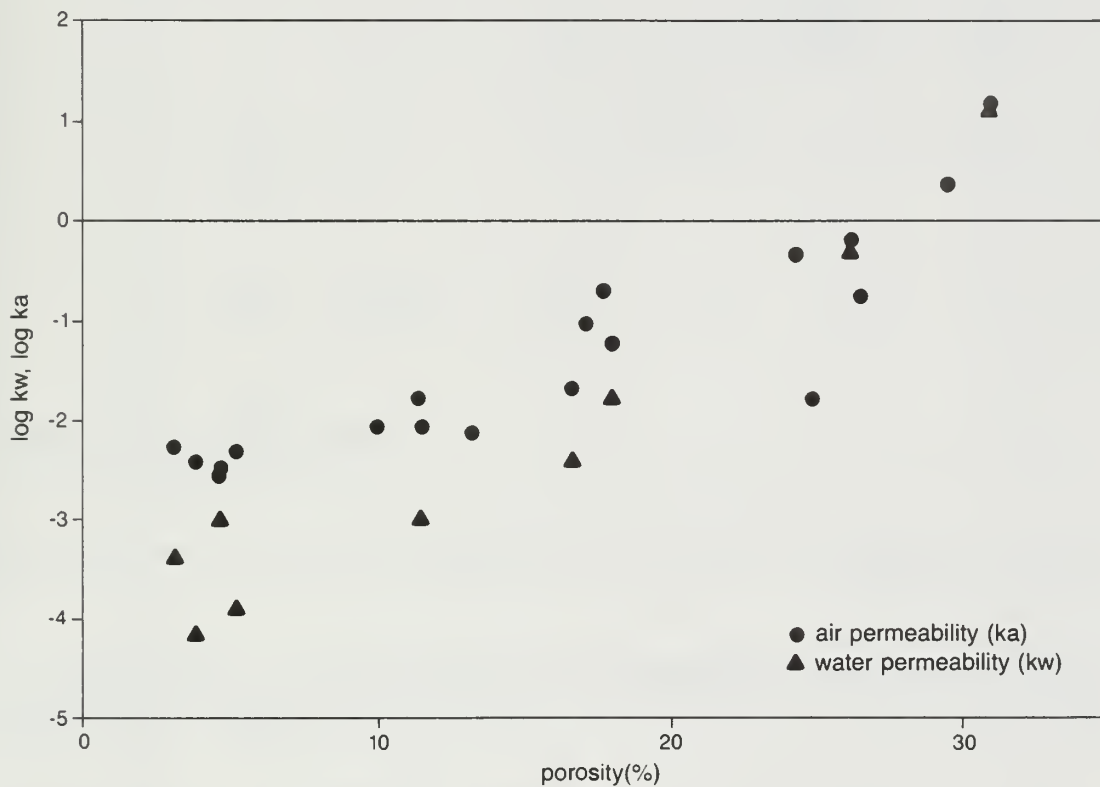


Figure 26 Core permeabilities versus core porosities for WDW2.

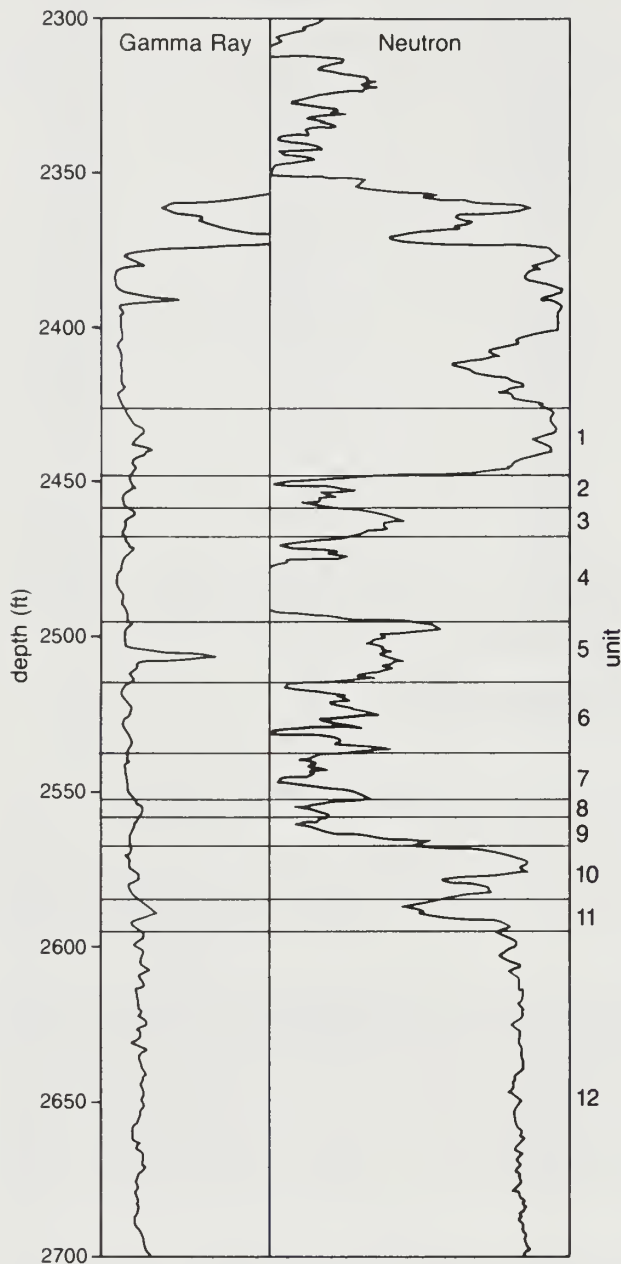


Figure 27 Unit locations for WDW2.

7.85×10^{-5} md (millidarcys) for the interval corresponding to unit 1 and 3.51×10^{-5} md for the overlying strata were obtained.

Long-Term Injection Test

A long-term injection test was conducted to obtain T and S values for the injection formation. An injection test is similar to a standard pump test except that water is injected into the well instead of being withdrawn from it.

The injection test started at 10 a.m., July 9, 1987, and was completed at 7 a.m., July 24, 1987. The test ended at this time because of a power outage scheduled by the power company. Velsicol

Table 8 Summary of hydrogeological data for a portion of the disposal system

Depth (ft KB)	POR (%)	ka (md)	kw (md)	Compress $\times 10^{-12}$ (cm sec ² /gm)	K ^a $\times 10^{-9}$ cm/sec	Ss ^b $\times 10^{-9}$ cm ⁻¹	Unit
2432	2.0						1
34.5	2.0						1
36	4.0						1
38	2.0						1
40	7.8	7.85 $\times 10^{-5}$ **					1
42	4.0						1
44	4.3						1
46	5.0						1
48	10.0						1
50	21.7						1
50.5	24.2						1
51.5	26.1	.640	.476	15.5	52.73	2.67	2
52	21.1						2
54	18.2						2
56	18.2						2
56.5	27.7	62.54					2
57.5	18.2						2
58	15.0						2
60	12.0						3
62	9.7						3
62.5	13.2	.0076					3
63.5	11.5	.0087					3
64	11.7						3
66	13.3						3
68	13.3						3
70	15.6						4
72	16.0						4
74	18.5						4
76	18.5						4
78	23.5						4
79.5	26.4	.178					4
80	26.0						4
81	24.8	.017					4
82	25.7						4
82.5	56.1						4
84	28.8						4
84.5	30.8	14.97	12.940	8.70	1434	2.21	4
86	26.3						4
88	23.2						4
90	22.6						4
90.5	29.4	2.292					4
91.5	24.2	.457					4
92	21.4						4
94	18.5						4
96	13.7						5
98	14.5						5
2500	11.1						5
02	8.9						5
04	10.2						5
06	11.6						5
08	11.5						5
08.5	9.9	.0089					5
09.5	11.4	.017	.001	3.36	.111	.831	5
10	12.7						5
12	9.8						5
14	11.8						5
16	15.3						6
18	11.0						6
20	11.0						6

Table 8 Continued

Depth (ft KB)	POR (%)	ka (md)	kw (md)	Compressx10 ⁻¹² (cm sec ² /gm)	K ^a x10 ⁻⁹ cm/sec	Ss ^b x10 ⁻⁹ cm ⁻¹	Unlt
22	14.3						6
24	9.5						6
26	9.5						6
28	12.2						6
30	14.2						6
32	14.2						6
34	11.9						6
36	9.3						6
38	12.0						6
39.5	17.7	.203					7
40	14.1						7
42	12.2						7
44	13.9						7
46	15.5						7
48	14.2						7
50	11.8						7
51.5	8.9						7
52	10.6						8
54	13.7						8
55	18.0	.060	.017	8.41	1.88	1.62	8
56	17.7						8
56.5	17.0						8
58	15.1						8
60	13.3						9
60.5	17.1	.095					9
62	17.8						9
64	14.5						9
66	7.0						9
68	6.2						9
70	4.0						10
72	1.0						10
73.5	5.2	.0050	.00013		.0144		10
74	1.0						10
76	1.0						10
78	6.2						10
80	5.0						10
82	5.0						10
84	5.5						11
86	8.9						11
88	9.8						11
88.5	16.6	.021	.004	11.9	.443	1.90	11
90	7.0						11
92	4.0						11
94	4.0						11
96	4.0						12
98	4.0						12
2600	4.0						12
02	4.2						12
04	4.4						12
05	3.1	.0055	.00042	4.71	.0465	.597	12
06	4.6	.0029					12
17.5	4.8						12
20	4.6	.0034					12
22	3.8	.0038					12
63	6.7						12

** Average vertical water permeability (kaw) and POR from three gas injection wells in the study area.

Table 9 Additional hydrogeological data for primary injection zones

Section	b (ft)	$S^c \times 10^{-6}$ (-)	$T^d \times 10^{-6}$ (cm ² / sec)
2	10	8.14	161
8	6	2.96	3.44
10	10	5.79	1.35

Explanation for tables 8 and 9:

(a) $K = kwpg / \mu$

where

K = hydraulic conductivity

kw = water permeability (Klinkenberg corrected air permeability)

ρ = water density = 0.997 gm/cm³*

g = acceleration due to gravity = 980 cm/sec²

μ = water viscosity = 0.008705 gm/cm sec*

* temperature used to determine ρ and μ was taken to be 26°C. This came from Temperature Log run in WDW2 assuming the cooling effect due to past injection was extremely localized (see appendix A).

(b) $Ss = \rho g (\alpha + n\beta)$

where

Ss = specific storage

α = matrix bulk compressibility

β = fluid bulk compressibility* = 4.513×10^{-11} cm-sec²/g

n = porosity

* temperature used to determine β was taken to be 26°C (see note above).

(c) $S = Ssb$

where

S = storativity

Ss = specific storage

b = zone thickness

(d) $T = Kb$

where

T = transmissivity

K = hydraulic conductivity

b = zone thickness

injected water from its stormwater retention ponds during the test. Table 10 shows the physical and chemical properties of the fluid injected during the in injection test (Velsicol, 1987). Table 11 shows the volume and rate of fluid injected. The average injection rate was 288.4 gpm.

Head data were collected at the DOW using a Stevens water level recorder (fig. 28). The water level recorder was set with a 1:1 gearing and an 8-day chart.

Data obtained from the DOW were analyzed by two techniques: Theis analysis and Cooper-Jacob analysis (see Todd 1980 or Freeze and Cherry 1979 for a detailed explanation of these techniques). Theis analysis is a curve-fitting technique; therefore, the T and S values obtained from this method depend on the analyst's judgment. The Cooper-Jacob technique is somewhat less subjective since the data plot is a straight line on semilog paper.

Table 10 Selected chemical and physical properties of water injected during injection test (Velsicol 1987)

Suspended solids	29 mg/L
Dissolved solids	1205 mg/L
Sodium chloride	794 mg/L
Sodium hydroxide	235 mg/L
pH	8.0
Specific gravity	1.004
Sample temperature	58°F

Table 11 Volume injected into WDW2 during injection test

Reporting date	Hours operated	Volume injected (gallons)	Injection rate (gpm)
7/10/87	21	340,673	270.4
7/11	24	414,607	287.9
7/12	24	422,409	293.3
7/13	24	419,684	291.2
7/14	24	423,836	294.2
7/15	24	419,042	290.8
7/16	24	401,760	278.8
7/17	24	418,939	290.8
7/18	24	411,973	285.9
7/19	24	413,270	286.9
7/20	24	411,616	285.7
7/21	24	410,420	284.9
7/22	24	424,717	294.8
7/23	24	424,211	294.4
7/24	24	419,352	291.0
Average		411,767	288.4

Table 12 Analysis of injection test

Method	S (-)	Transmissivity (m ² /min)
Theis	2.75×10^{-4}	0.385
Cooper-Jacob (r = 0.960)	2.47×10^{-4}	0.386

r = correlation coefficient for the linear regression

For the Cooper-Jacob technique, head buildup was plotted versus log time (fig. 29). Linear regression was used to calculate the parameters (S and t_0) for this method. An iterative approach was taken since the data used in the analysis depend on the outcome of the analysis. For the Cooper-Jacob method, u ($u = r^2 S / (4Tt)$) must be less than to 0.01. From the definition of u and the value of T and S , a minimum time can be determined (i.e., only field data where $t > t_{\min}$ can be used). Thus, an iterative technique was necessary to calculate T and S . Table 12 shows the results of the analyses (only the values for the final iteration of the Cooper-Jacob analysis are presented). Note the good agreement between the Theis and Cooper-Jacob analyses. The values obtained by the Cooper-Jacob technique are considered to be the more accurate since this technique is less subjective.

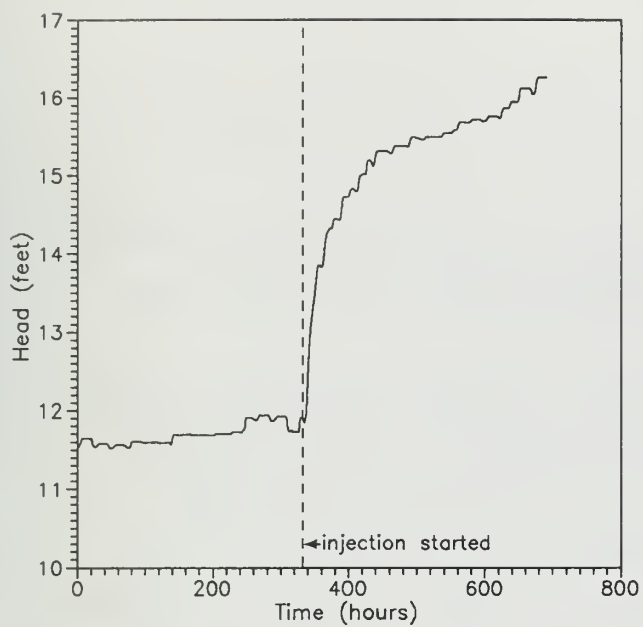


Figure 28 Water level record for DOW, including data from injection test.

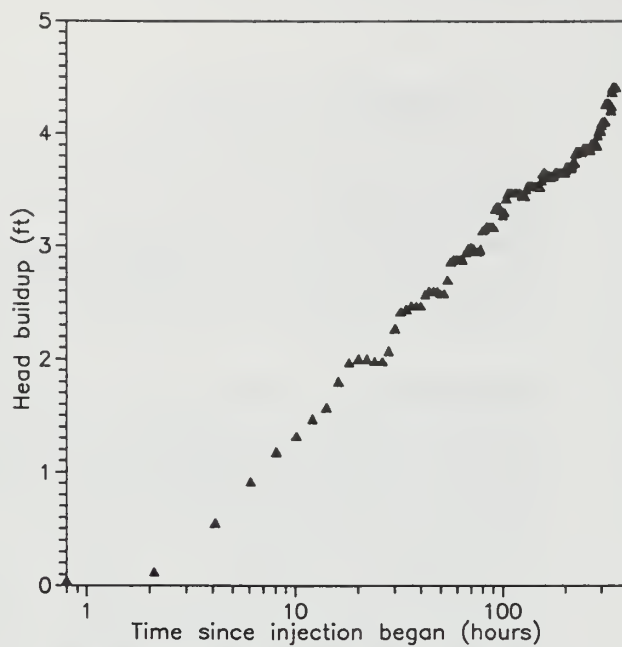


Figure 29 Plot of data used for Cooper-Jacob analysis.

4. NUMERICAL MODELING

Model Selection

Model selection is an important step in conducting a modeling investigation of a groundwater flow problem. The model should be able to handle all significant physical processes of the groundwater flow system. If the model does not incorporate these processes, it cannot be expected to simulate the field situation with any degree of accuracy.

The literature contains descriptions of many general and specialized numerical models. At the outset of this project, it was thought that a model capable of simulating three-dimensional (3D) flow and flow through complex hydrogeologic regimes would be required. Several 3D groundwater flow models have been developed, including the Sandia Waste Isolation Flow and Transport Model (SWIFT) (Reeves and Cranwell, 1981) and the Heat and Solute Transport Program (HST3D) (Kipp 1987). SWIFT and HST3D are finite difference groundwater flow and transport models that are independent modifications of SWIP (INTERCOMP, 1976). This original model, developed to model the effects of deep-well waste injection, includes sophisticated well functions rarely incorporated into other models. Although SWIFT and HST3D have a more general focus than does their predecessor, both models retain these well functions, and either model could be used for this project. Since a version of HST3D compatible with the Prime 9650 computer used in this project was available before a similar version of SWIFT (II), HST3D was selected.

Model Description

HST3D is a descendent of the Survey Waste Isolation Program (SWIP) written for the U.S. Geological Survey by INTERCOMP Resource Development and Engineering Consultants. HST3D represents a complete rewrite of SWIP with many major and minor modifications, improvements, and corrections.

Overview of Model

HST3D simulates saturated groundwater flow and associated heat and solute transport in three dimensions. The following equations are solved numerically: the saturated groundwater flow equation, formed from combining the conservation of total fluid mass and Darcy's Law for flow through porous media; the heat transport equation from the conservation of enthalpy for the fluid and porous medium; and the solute transport equation from the conservation of mass for a single solute, which may adsorb onto the porous medium and/or decay (Kipp 1987). These equations are coupled through the dependence of advective transport on the interstitial fluid velocity field, fluid viscosity on temperature and solute concentration, and fluid density on pressure, temperature, and solute concentration.

For the dependent variables of pressure, temperature, and mass fraction, numerical solutions are obtained successively using a set of modified equations that more directly link the original equations through the velocity, density, and viscosity coupling terms. Finite difference techniques are used for the spatial and temporal discretization of the equations. When supplied with appropriate boundary and initial conditions and system-parameter distributions, a wide variety of heat and solute transport simulations can be performed (Kipp 1987).

The basic source-sink term represents wells. A complex well-flow model may be used to simulate specified flow rate and pressure conditions at the land surface or within the aquifer, with or without pressure constraints. Types of boundary conditions include specified value, specified flux, leakage, heat conduction, an approximate free surface, and two types of aquifer influence functions. All boundary conditions may be functions of time (Kipp 1987).

Assumptions Incorporated into the Model

Since this project was concerned with simulation of fluid flow and not heat and/or contaminant transport, only the assumptions incorporated into the flow model will be discussed. Kipp (1987) incorporated the following assumptions into the partial differential equation describing groundwater flow:

- Groundwater fully saturates the porous medium within the region of groundwater flow.
- Groundwater flow is described by Darcy's Law.
- The porous medium and the fluid are compressible.
- The porosity and permeability are functions of space.
- The coordinate system is chosen to be aligned with the principal directions of permeability tensor so that this tensor is diagonal for anisotropic media.
- The coordinate system and the principal directions of the permeability tensor are orthogonal.
- The coordinate system is right-handed with the z-axis pointing vertically upward.
- The fluid viscosity is a function of space and time through dependence on temperature and solute concentration.
- Density-gradient diffusive fluxes of the bulk fluid are neglected relative to advective-mass fluxes.
- Dispersive-mass fluxes of the bulk fluid from spatial-velocity fluctuations are excluded.

Input Data

Input data required by HST3D for modeling fluid movement may be categorized as follows: hydrogeologic properties of the aquifer, physical dimensions of the aquifer, physical dimensions of the well(s), hydraulic properties of the well(s), and physical and chemical properties of the fluid. Additional input data are required for any attempts to model solute and/or heat transport.

Physical Configuration of the Injection System

As defined here, the injection system refers to the geologic deposits that constitute the injection zone and its associated confining units. The hydrogeology of the site is described in chapter 3. The physical dimensions and hydrogeologic properties of the injection system used as model input will be described where appropriate in each section.

Description of the Injection and Observation Wells

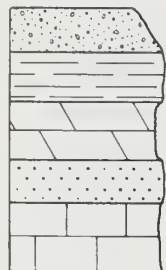
Waste Disposal Well 2 (WDW2) at the Velsicol Chemical Corporation's Marshall Plant was modeled. WDW2 is a packer-annulus-type well completed in Devonian limestone (fig. 30). Originally, the well was drilled to a total depth of 6,007 feet and was completed open-hole from 2,440 to 2,737 feet. Preceding the phase II field testing of the well, Velsicol completed extensive well workover procedures to remove debris, which had partially filled the well. These procedures included a high-pressure jet wash of the well bore. In addition to suspending and removing the debris in the well, the tool scoured the well bore. Thus it is assumed that the skin effect for this well would be negligible. Access for geophysical tools to total depth was blocked at 2,610 feet, presumably due to bridging of materials sloughed from the well face. However, the bridging probably did not plug the well from a hydraulic standpoint.

Located 506 meters due north of WDW2 is the Devonian Observation Well (DOW), which was completed open-hole starting near the top of the Devonian limestone (fig. 31). Total depth for this well is 2,580 feet. Water-level data were collected from this well during this project.

Physical and Chemical Properties of the Fluids

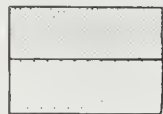
HST3D requires input of various physical properties of the fluids, including density, temperature, viscosity, and compressibility. These data are required for the fluid injected and the native fluid in the formation (brine). Fluid-compressibility data for injected wastes and/or brines were generally not available but were estimated on the basis of the chemical composition of these fluids. Much of these required input data were available from a database compiled by the ISGS.

Lithology



Unconsolidated
Shale
Dolomite
Sandstone
Limestone

Aquifers (USDW)



Primary freshwater aquifer
(0-2,500 mg/l)
Secondary aquifer
(2,500-10,000 mg/l)

Stratigraphic Units

Q	Quaternary
P	Pennsylvanian
M	Mississippian
Mc	Chesterian sandstone
Msg, sl	Ste. Genevieve Limestone
Msa	St. Louis Limestone
Mb	Salem Limestone
Mch	Borden Siltstone
	Chouteau Limestone
M/D	Mississippian/Devonian
M/Dna	New Albany Group
D	Devonian
Dlgb	Lingle Limestone
	Grand Tower Limestone
	Bailey Limestone
S	Silurian
Sm	Moccasin Springs Fm
Su	Undifferentiated dolomite
O	Ordovician
Om	Maquoketa Shale
Ogp	Galena-Platteville dolomite
Osp	St. Peter Sandstone
Opdc	Prairie du Chien dolomite
€	Cambrian
€ep	Eminence-Potosi dolomite

Injection System Components

M/Dna	Upper confining unit
Dlgb	Injection unit
Sm	Lower confining unit

Waste Disposal Well #2

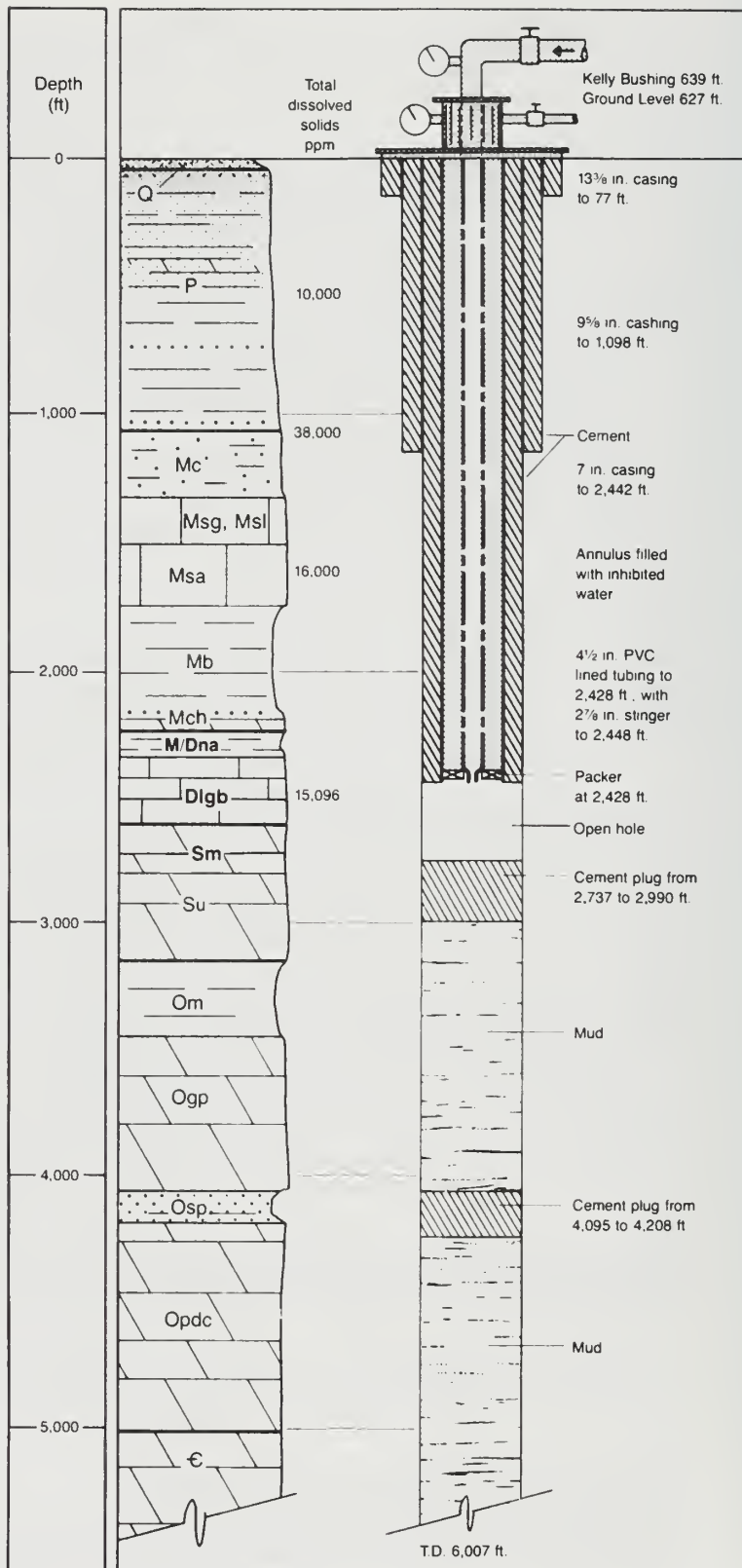


Figure 30 Schematic for WDW2 (modified from Brower et al. 1989).

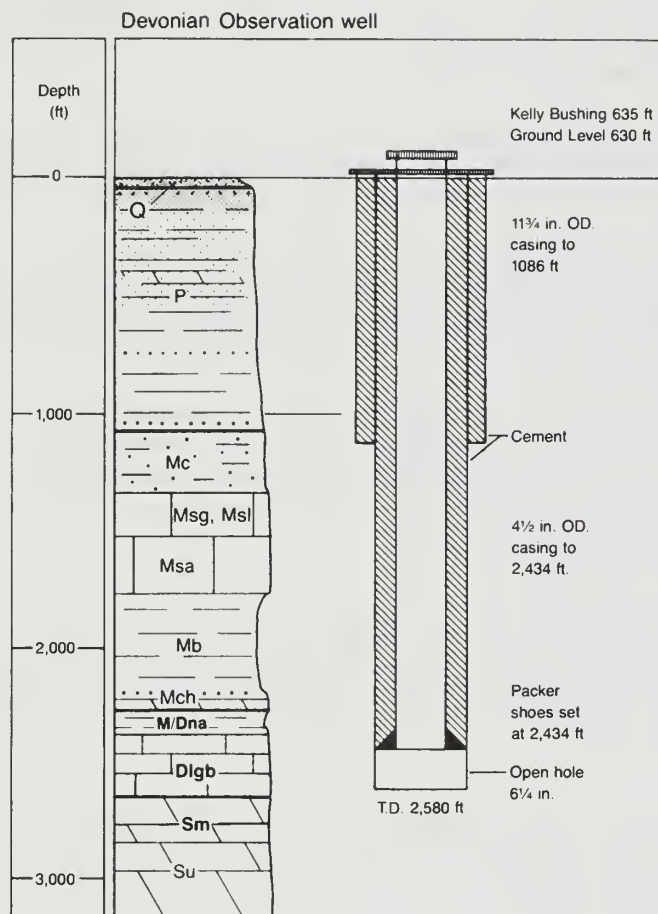


Figure 31 Schematic for DOW (Velsicol 1984).

General Parameters

Velsicol injected hazardous waste consisting of production wastewater and surface runoff water from on-site process areas. Chlorinated pesticides were produced at this site. The waste was highly alkaline (pH > 12) and contained pesticides and other chlorinated hydrocarbons. The relative concentrations of constituents in the waste were NaCl > NaOH > hexachlorocyclopentadiene (hex) > chlordane.

Velsicol has been required by permit to sample and analyze the waste injected into WDW2 and the brine from the DOW. Thus an extensive database of physical and chemical properties of the injected fluid and brine is available. This database was compiled by the ISGS and used extensively in this project. For WDW2, available data date back to early 1973, when operating reports were first required. Data for dissolved solids, specific gravity, and viscosity are presented in table 13.

Table 13 Selected parameters for fluids injected via WDW2

Parameter (unit)	Range	Average	Standard deviation	Number
Dissolved solids (mg/L)	200 - 254,000	38,346	35,388	671
Specific gravity (-)	0.9948 - 1.14	1.027	0.025	538
Viscosity (centipoise)	0.7161 - 0.9822	0.7857	0.0700	33

Data for dissolved solids in table 13 show the variability of the injected fluid, which is predominantly storm water runoff. Brower et al. (1989) attributed this variation in dissolved solids to variation of precipitation frequency and intensity.

A relationship between specific gravity and viscosity seems to exist (fig. 32). Linear regression of these variables produced a correlation coefficient of 0.873. If additional viscosity data had been available, this correlation might have improved.

The mean value for specific gravity of the waste was used as input for the numerical model. For comparison, Devonian brine sampled during construction of WDW2 had a specific gravity of 1.011. The linear relationship between viscosity and specific gravity was assumed to be valid; thus, viscosity was determined using the mean specific gravity of the waste (fig. 32).

All modeling was conducted under isothermal conditions. Although the temperature of the injected fluid varied throughout the year, it was assumed that the temperature of the formation would not change significantly from its mean temperature because of injection. The formation temperature was determined from a temperature log run down the DOW on December 18, 1986. The mean formation temperature was 34.4°C (94°F).

Compressibility of the Fluids

Lab-determined values for the compressibility of the waste and brine were not available; however, compressibility values for common saline solutions were available in the literature. Millero et al. (1974) published compressibility values for NaCl, MgCl₂, NaSO₄, and MgSO₄ as a function of temperature and molality. Figure 33 depicts the fluid compressibility in relation to temperature and molality for NaCl solutions.

Roy et al. (1989) characterized the brine and waste as predominantly NaCl solutions. Table 14 shows the chemical analysis of the Velsicol waste, Velsicol dilute waste, and Devonian brine. In this context, waste refers only to the fluids from the plant processes. Dilute waste, typically the fluid injected, comprises fluids from the plant processes and surface runoff. The sample of Devonian brine was obtained from the DOW in June 1987.

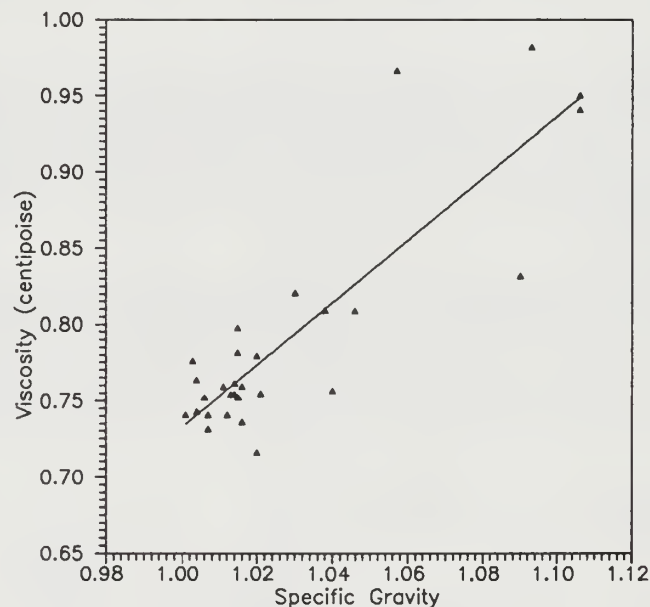


Figure 32 Relationship between waste viscosity and specific gravity.

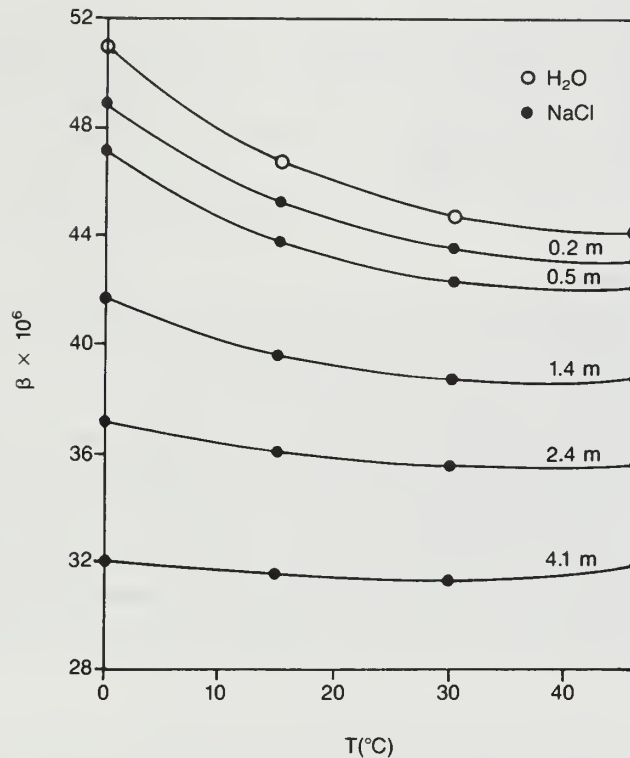


Figure 33 The compressibility of water and NaCl solutions versus temperature (Millero et al. 1974).

Table 14 Chemical analysis of waste and brine

Parameter (unit)	Waste	Dilute waste	Brine
pH	12.92	12.85	9.07
Eh (mV) ^a	+572	+572	-154
EC (mmhos @ 25°C)	403	56 ^b	22
TDS (mg/L)	215,900 ^b	37,300 ^b	—
Cl (mg/L)	112,664	15,400	12,700
F (mg/L)	151	—	20.1
Na (mg/L)	86,350	—	8,370
SO ₄ (mg/L)	61.5	—	182
NO ₃ (mg/L)	274	—	25.1
Mg (mg/L)	<0.07	—	117.0

a: relative to a standard ZoBell solution

b: Mravik (1987)

from Roy (1987)

Concentrations of the major anion and cation were used to determine the molality of each fluid. Compressibility of each fluid was determined on the basis of the molality and two assumptions: (1) that the temperature was 34.4°C and (2) that the fluids could be considered NaCl solutions. Table 15 shows the molality and compressibility of the three fluids.

Review of the TDS data for the waste and dilute waste indicated that the "average" waste injected into WDW2 (TDS = 38,346 mg/L) had a slightly higher TDS concentration than the dilute waste. Thus the compressibility of the "average" waste should be close to, but slightly lower than, the compressibility of the dilute waste. (See table 18 for the value used.)

Table 15 Compressibility of waste and brine

Fluid	Molality (moles/kg)	Compressibility (1/Pa)
Waste	3.76	3.185×10^{-10}
Dilute waste	0.799	4.105×10^{-10}
Brine	0.703	4.145×10^{-10}
Waste	—	4.46×10^{-10}

Volume of Injected Waste

Since waste injection began in March 1972, Velsicol (1987) reported that 1.4623×10^9 gallons of fluid have been injected via WDW2. Simple volumetric equations were used to determine the extent to which these fluids have moved within the injection zone.

Cross-plotted analysis of geophysical logs indicated that the thickness-averaged porosity of the injection zone is 12.5 percent. Assuming that waste has flowed through the entire thickness (174 ft) of the injection zone and radially from the well, the pore volume of the injection zone from WDW2 to the DOW (1,660 ft) is 1.406×10^9 gallons. Thus the cumulative volume of injected fluid is equivalent to 1.04 pore volumes. To account for this fact, model input of fluid data was based on the physical properties of the waste. In this project, only groundwater flow was simulated; thus, the properties of the fluid must be homogeneous throughout the injection system. To consider nonhomogeneous fluids, one would need to model solute transport.

Modeling Results

Most numerical modeling studies of groundwater flow include several modeling phases, which have also been followed in this study. First, verification of the model is conducted. In this stage, the model is used to simulate known analytical solutions. This phase is typically followed by history matching or model calibration. Here, the model was used to simulate field data, usually collected during a pump test. Sensitivity analysis generally follows model calibration. During this phase, the effect of pertinent parameters is quantified. The final stage is the prediction stage, which is an exercise in "what if." For example, what will the pressure buildup be at the well if a certain flow rate is continued for 30 years. The following discussion describes each of these phases for this project.

Model Verification

Model verification was necessary since HST3D was a new code. Verification allowed the modeler a chance to become familiar with this new model and to check the model accuracy versus analytical solutions. HST3D was verified using two analytical solutions: unsteady radial flow in a confined aquifer with constant pumping rate (Theis 1935), and unsteady radial flow in leaky systems with no storage in the semipervious layer at a constant pumping rate (Hantush 1964).

Theis Solution. Theis solution is an analytical solution for unsteady radial flow in confined aquifers. This solution is readily available in any groundwater text and is not repeated here. Input data for the analytical solution and HST3D are listed in table 16.

A radial coordinate system was used to discretize the groundwater flow domain: 50 nodes in the r-direction and 20 nodes in the z-direction. The radius of the aquifer simulated was 24,960 m. No-flow conditions were applied at all boundaries.

Figure 34 shows the drawdown at a point 100 m from the pumping well determined by numerical and analytical methods. The two solutions are identical.

Leaky Aquifer Solution . HST3D was also verified against an analytical solution for wells in leaky systems without storage in the semipervious layer (no storage in the semipervious is an as-

Table 16 Input data for the Theis solution

HST3D	Analytical solution
aquifer thickness, $b = 3.05$ m	transmissivity, $T = 0.001$ m ² /sec
hydraulic conductivity, $K = 3.29 \times 10^{-4}$ m/sec	storativity, $S = 0.001$
porosity, $n = 0.20$	pumping rate, $q = 3.0 \times 10^{-3}$ m ³ /sec
matrix compressibility, $\alpha = 3.34 \times 10^{-8}$ Pa ⁻¹	
fluid compressibility, $\beta = 4.53 \times 10^{-10}$ Pa ⁻¹	
viscosity, $\mu = 0.001$ kg/m-sec	
fluid density, $\rho = 999.5$ kg/m ³	
pumping rate, $q = 3.00 \times 10^{-3}$ m ³ /sec	

sumption inherent to HST3D) (Hantush 1964). A radial coordinate system was used to discretize the aquifer: 50 nodes in the r-direction and 5 nodes in the z-direction. No-flow conditions were applied at the lower and radial boundaries. A leaky aquifer boundary condition is applied at the top boundary. The remaining input data for this simulation are listed in table 17.

The drawdown for a well 20 m from the pumping well was determined using the analytical and numerical solutions (fig. 35). The numerical solution tends to slightly underestimate the drawdown. These results are closer to the analytical solution than those reported by Ward et al. (1984) and are considered to be acceptable.

Model Calibration

Data used for model calibration (history matching) were obtained from the long-term injection test described in chapter 3 (p. 42). and plotted on figure 28. The conceptual model for the injection system was based on data presented in Long-Term Injection Test (p. 42) and is shown on figure 36. The hydraulic conductivity and physical dimensions in the vertical direction are also depicted on this figure. Other pertinent input data are listed in table 18. The injection system was discretized with radial coordinates: 60 nodes in the r-direction and 22 nodes in the z-direction.

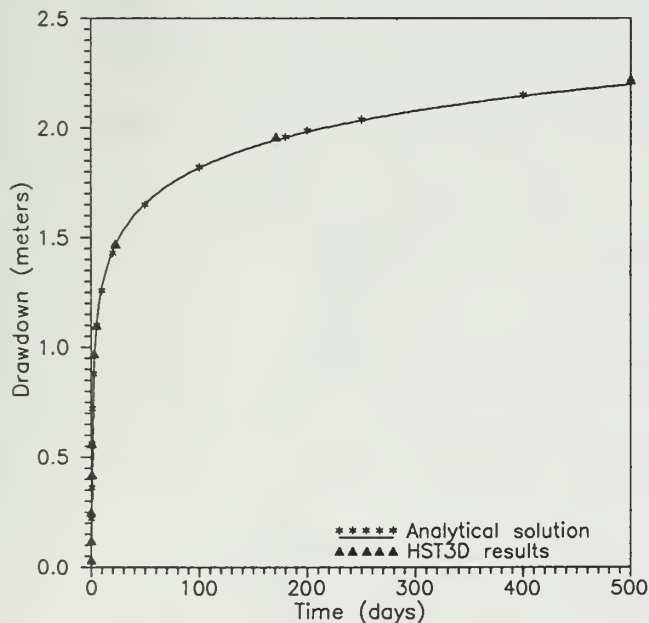


Figure 34 (left) Comparison of model-predicted drawdowns with results from Theis Analysis.

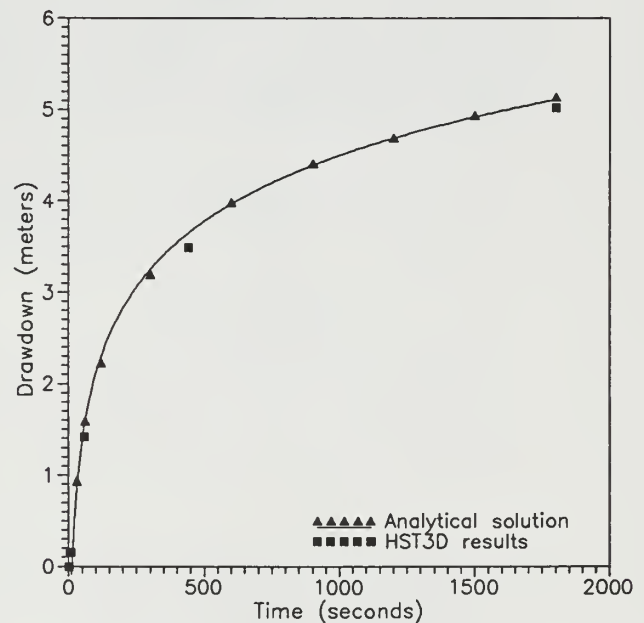


Figure 35 Comparison of model-predicted drawdowns in relation to time with Hantush Analysis.

Table 17 Input data for leaky aquifer simulation

HST3D	Analytical solution
aquifer thickness, $b = 3.05$ m	transmissivity, $T = 10^{-3} \text{ m}^2/\text{sec}$
aquifer intrinsic hydraulic conductivity, $K = 3.35 \times 10^{-11} \text{ m}^2$	storativity, $S = 10^{-4}$
matrix compressibility, $\alpha = 3.34 \times 10^{-8} \text{ Pa}^{-1}$	aquitard hydraulic conductivity, $K' = 3 \times 10^{-10} \text{ m/sec}$
fluid compressibility, $\beta = 4.53 \times 10^{-10} \text{ Pa}^{-1}$	aquitard thickness, $b' = 0.30$ m
fluid density, $\rho = 999.5 \text{ kg/m}^3$	pumping rate, $q = 0.014 \text{ m}^3/\text{sec}$
viscosity, $\mu = 1.00 \times 10^{-3} \text{ kg/m-sec}$	
aquitard intrinsic hydraulic conductivity, $K = 3.06 \times 10^{-17} \text{ m}^2$	
aquitard thickness, $b' = 0.30$ m	
pumping rate, $q = 0.014 \text{ m}^3/\text{sec}$	

Table 18 Selected input data for model calibration

radius, $r = 15870.90$ m
$\beta = 4.00 \times 10^{-10} \text{ Pa}^{-1}$
$\alpha = 4.50 \times 10^{-10} \text{ Pa}^{-1}$
$\rho = 1020 \text{ kg/m}^3$
$\mu = 7.87 \times 10^{-4} \text{ kg/m-sec}$

No-flow conditions were applied at the top and bottom boundaries, while an aquifer influence was applied at the radial boundary.

Kipp (1986) describes the use of aquifer influence boundary conditions (AIF BC) as a simple, but approximate, method for embedding an inner region of groundwater simulation within a larger region where groundwater flow may be treated in an approximate fashion. The use of aquifer influence functions reduces the size of the computational grid with a corresponding reduction in computer storage and execution time.

The natural hydraulic gradient of the Devonian limestone is very low (see p. 32); thus, the hydraulics of the injection well will dominate the groundwater hydraulics in the area surrounding the well. The flow rate across an AIF boundary is a function of the potentiometric head and hydrogeologic characteristics of the aquifer. The use of the AIF BC was favored over a specified head or flow-type BC, since the AIF is a more accurate representation of the hydraulics of the injection system.

Stratigraphy	elev. above reference (m)	Hydrogeologic Role	K (m ²)
New Albany Group, Lingle and Grand Tower Limestones	128.29	upper confining unit	4.35×10^{-21}
Bailey Limestone	55.76	upper injection zone	2.51×10^{-11}
	52.71		2.30×10^{-14}
	24.06	middle injection zone	9.65×10^{-11}
	22.23		2.99×10^{-14}
Moccasin Springs Formation	14.31	lower injection zone	7.72×10^{-11}
	11.28	basal confining unit	9.68×10^{-14}
	0		

Figure 36 Conceptual model 1 of the injection system.

The T and S values calculated on the basis of input data, as well as the values determined from field testing, are presented in table 19. The input data and field data match reasonably well. Closer agreement of the field and model T and S values probably could have been obtained with minor adjustments to the input data (chiefly K, α , and β); however, the T and S values used were considered satisfactory.

The model values for T and S were even more satisfactory considering that two of the chief input parameters, α and β , are consistent with published values. Fluid compressibility (β) has been previously discussed (p. 52).

Table 19 Comparison of transmissivity (T) and storativity (S) values

	Field test	HST3D
T (m ² /min)	0.386	0.373
S (-)	2.47×10^{-4}	2.65×10^{-4}

Our rock compressibility (α) values also agreed with values in the literature. Birch (1966) reports that $\alpha = 1.22 \times 10^{-11} \text{ Pa}^{-1}$ for dolomite. Domenico and Mifflin (1965) report α for sound rock ranges from 10^{-9} to 10^{-10} Pa^{-1} , while α for jointed rock ranges from 10^{-8} to 10^{-10} Pa^{-1} . Since secondary porosity was present in the cores retrieved, one would have expected that α for the dolomite at the study site would be slightly greater than $\alpha = 1.22 \times 10^{-11} \text{ Pa}^{-1}$. In fact, the values of the cores tested range from 1.55×10^{-10} to $3.26 \times 10^{-11} \text{ Pa}^{-1}$. Thus the use of $\alpha = 4.50 \times 10^{-10} \text{ Pa}^{-1}$ for model calibration seemed reasonable. As discussed in appendix C, the scanning electron microscopy (SEM) work indicated that secondary porosity was present, primarily in the form of vugginess and some localized microfractures. The microfractures were very small and tended to be interconnected. Because of the close spacing and size of the microfractures, modeling flow through this geologic material as flow through porous media was considered to be a valid assumption.

The intrinsic permeability values for the three injection zones ranged from 2.5×10^{-11} to $9.7 \times 10^{-11} \text{ m}^2$ (25.4 to 97.8 darcys). Schmoker et al. (1985) summarized data for limestone and dolomite petroleum reservoirs throughout the United States. These authors report that only 11 percent of all dolomite reservoirs exceed 0.1 darcy. Freeze and Cherry (1979) list 0.2 darcy as an upper permeability limit for limestone and dolomite. Clearly, the permeability values for the injection zones seem to be quite high. The permeabilities used as model input were based on the results of the injection test and were higher than the laboratory-determined permeabilities. There appear to be two explanations for the apparent high permeability values. First, the permeability values were actually calculated from transmissivity values and thickness of "permeable" units of the aquifer. The thickness of these units could have been underestimated. Another possibility was that the cores may not be representative of the overall injection system. Greater emphasis was placed on the results of the injection test, since this is an in situ measurement of the system.

In addition to aquifer transmissivity, another control on specifying intrinsic permeability was the results of the flowmeter survey conducted during phase II of the field experiments. The intrinsic permeability of the three injection zones was adjusted so that the flow into each of these three zones matched the flow profile defined by the flowmeter. Thus in the model, 48.1 percent of the injected fluid flowed into the lower injection zone, 36.2 percent into the middle zone, and 15.7 percent into the upper zone.

Figure 37 depicts the head build-up at the DOW during the injection test and the buildup predicted by HST3D versus time. The model overpredicted the head buildup at times by less than 20 hours; however, the results at later times are very close. Oscillation of the head buildup (field data) is also evident in figure 37. This oscillation is believed to be a manifestation of earth tides and not a variation in the pumping rate.

Matching model results with the later field results was considered more important because the main use of the model was to predict long-term effects of injection. The input data were reasonable, and the predicted head buildup matched reasonably well the head buildup observed in the field; therefore, model calibration was deemed successful.

Sensitivity Analysis

A rigorous sensitivity analysis as described by Yeh (1986) was not conducted. The sensitivity analysis conducted here involved varying significant parameters and noting the effect of this variation on head buildup (Δh) at the DOW, the parameter of interest. The significance of various parameters (i.e., injection rate, hydraulic conductivity) was observed during the two previous stages of this project. Based on these observations, sensitivity analysis was conducted for the following parameters: boundary conditions, injection rate, rock compressibility, fluid compressibility, hydraulic conductivity, and anisotropy. The sensitivity analysis is summarized here and described in detail in appendix D.

Injection rate and hydraulic conductivity were the most sensitive input parameters. That is, a given change in injection rate or hydraulic conductivity would produce the largest change in Δh observed at the DOW. The type of boundary condition and the location of the boundary could also significantly affect the head buildup predicted by the model. In decreasing order, the most sensitive parameters were injection rate and hydraulic conductivity, rock compressibility, anisotropy, and fluid compressibility.

Model Projections for Long-Term Injection

Using the conceptual model developed during the model calibration phase, we investigated the effects of long-term, continuous injection at two rates: 1.150×10^{-2} and 2.208×10^{-2} m³/sec. The first injection rate is the "average" rate at which the company injected waste during the life of the well. This was calculated by dividing the cumulative volume of waste injected by the length of operation for WDW2. The second injection rate is the maximum average injection rate permitted by the Illinois Environmental Protection Agency (IEPA 1987).

Embedded in this calculation of the "average" injection rate is the assumption that the well was operated on a continual basis; however, WDW2 was not in operation continually. A larger head buildup in the injection system would be produced by assuming continuous (24-hour) operation because pressure in the injection system would never bleed off.

HST3D was used to predict the head buildup in the injection system over a 30-year period. The decline in head was also modeled for an additional 30-year postinjection period. Thirty years was chosen since this is typically the length of service for an injection well. Because of problems experienced with HST3D, the injection rate during the postinjection period could not be set to zero. During the postinjection period, the injection rate was set as low as possible, $q = 1.82 \times 10^{-4}$ m³/sec. Figure 38 shows the head buildup in relation to radial distance from the injection well after 10,927 days (30 years). At the DOW, Δh after this time is 0.03 m. Thus, use of $q = 1.82 \times 10^{-4}$ m³/sec during the postinjection period did not significantly impact the pressure decline during the postinjection period.

Injection Scenario 1

Injection scenario 1 is injection for 30 years at a rate of 1.150×10^{-2} m³/sec, followed by a postinjection period in which $q = 1.82 \times 10^{-4}$ m³/sec. Figure 39 shows the response of the injection system during both 30-year periods (262,980 hours each). Head buildup at the DOW increases exponentially. After 30 years of injection, $\Delta h = 1.61$ m at the DOW. In terms of Δh , steady state was approached but not reached. The head buildup at the DOW also dropped exponentially. Approximately 900 hours after the change in the injection rate, the head buildup was approximately half of its maximum value. Nearly 7.5 years (66,000 hours) after the change in the injection rate,

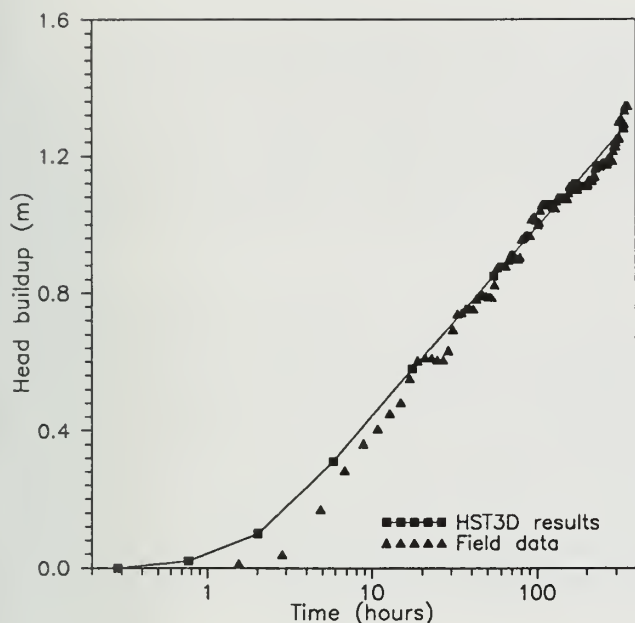


Figure 37 (left) Comparison of model-predicted Δh versus field data for DOW.

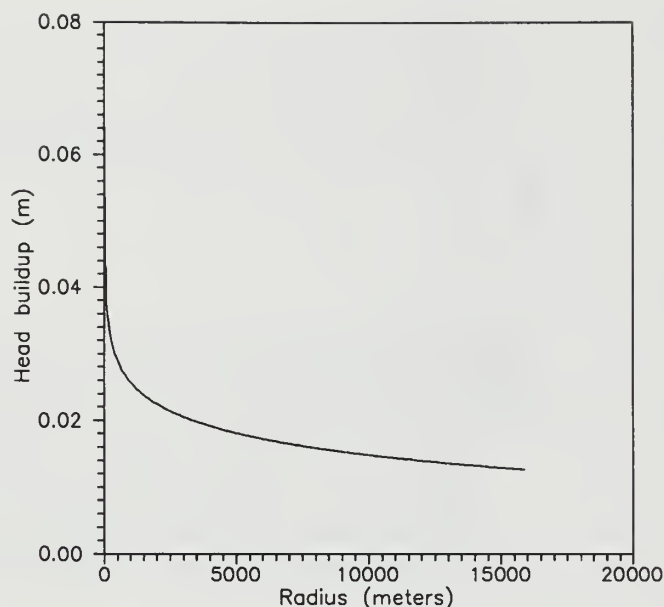


Figure 38 Head buildup versus radial distance from WDW2 $q = 1.82 \times 10^{-4} \text{ m}^3/\text{sec}$.

the head buildup was only 0.01 m, after correcting for Δh due to injection at $q = 1.82 \times 10^{-4} \text{ m}^3/\text{sec}$. During the 30-year postinjection period, the head buildup did not reduce to 0.00 m.

Injection Scenario 2

During the second injection scenario, the effects of injection for 30 years at $q = 2.208 \times 10^{-2} \text{ m}^3/\text{sec}$ were investigated. A postinjection period followed during which $q = 1.82 \times 10^{-4} \text{ m}^3/\text{sec}$. Figure 40 shows the head buildup at the DOW. The results were similar to the results for injection scenario 1. The head buildup increased exponentially to a maximum $\Delta h = 3.20 \text{ m}$ after 30 years of injection. Also, after the injection rate was reduced, the head fell exponentially. The head buildup approached but did not go to 0.00 m during the postinjection period.

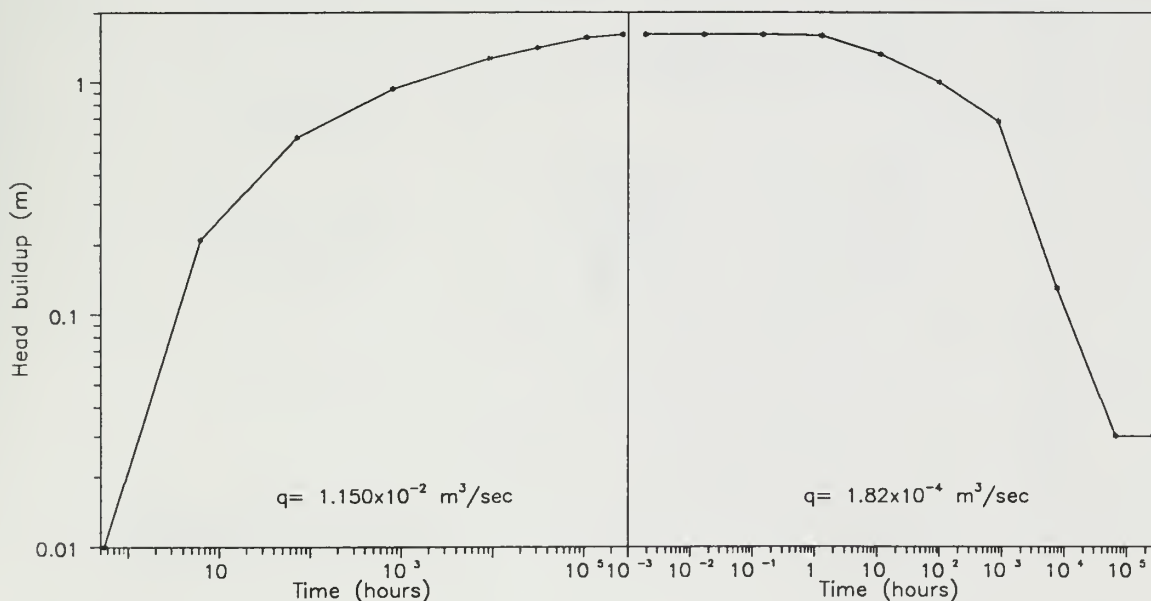


Figure 39 Injection scenario 1: head buildup and decline with time at the DOW.

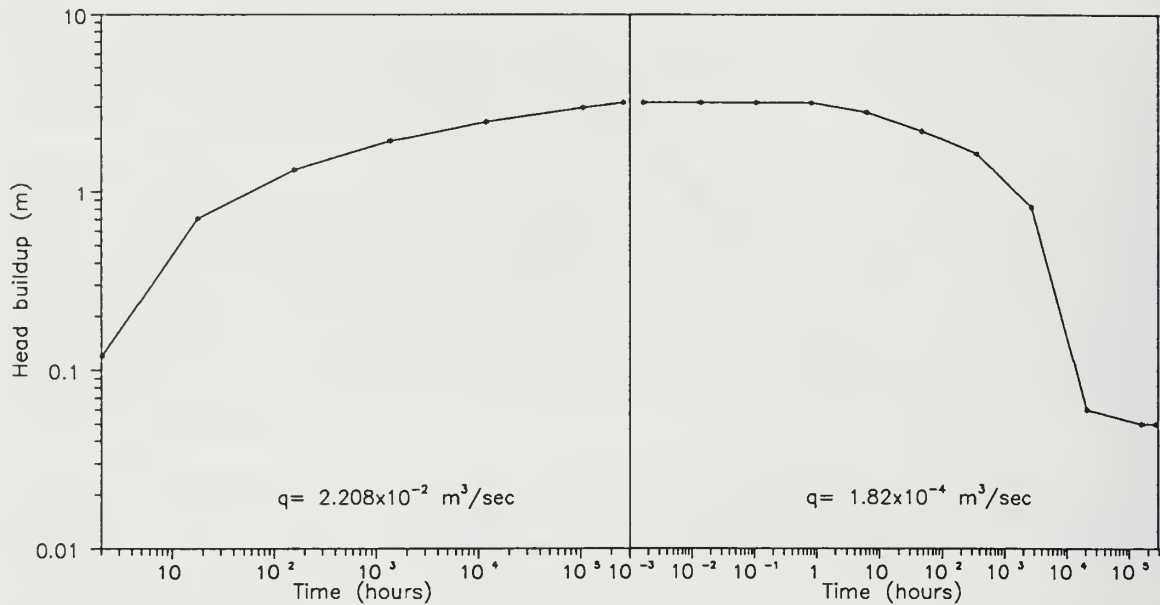


Figure 40 Injection scenario 2: head buildup and decline with time at the DOW.

Figure 41 shows the head buildup at the WDW2 during the injection and postinjection periods. The results were similar to the results shown in figure 40 except the magnitude of the head buildup was greater at the injection well. After 30 years of injection, Δh at WDW2 was 7.88 m. For comparison, Δh at WDW2 for injection scenario 1 was 4.22 m.

Maximum hydraulic pressure was 7.081×10^6 Pa (1,027 psi) and occurred at the bottom of the well after 30 years of injection under injection scenario 2. The pressure at the base of the confining layer equaled 6.687×10^6 Pa (970 psi). The pressure increase due to 30 years of injection was 7.73×10^4 and 6.69×10^4 Pa at the bottom of the well and the base of the confining unit, respectively. The pressures resulting from injection scenario 1 ($q = 1.150 \times 10^{-2}$ m³/sec) were slightly lower than those listed here.

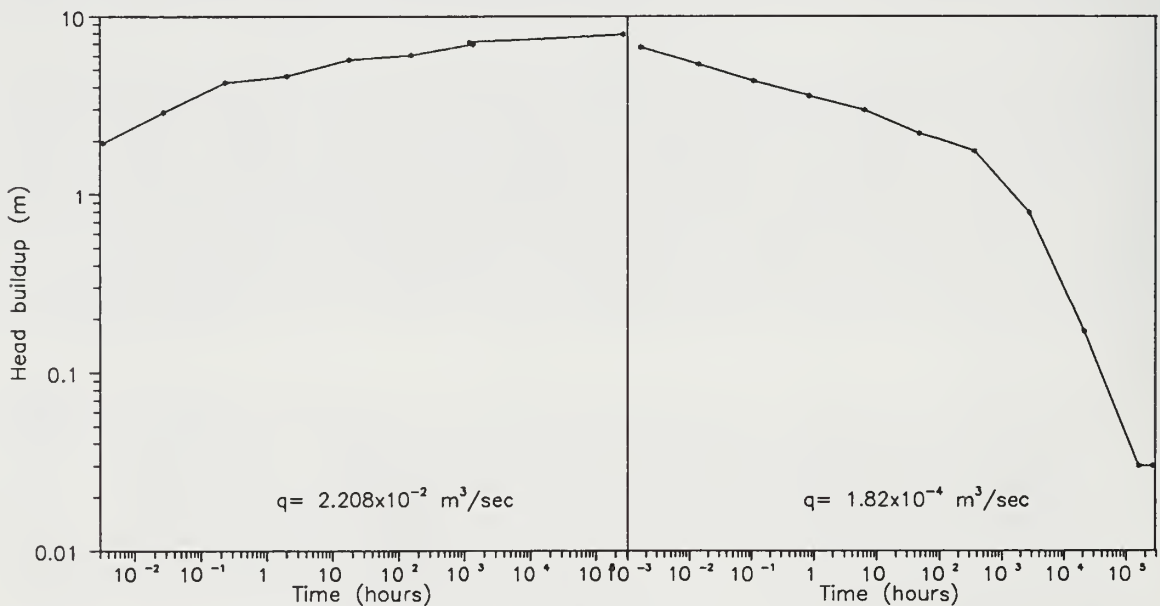


Figure 41 Injection scenario 2: head buildup and decline with time at WDW2.

In Illinois, the hydraulic fracture gradient is generally considered to be equal to 1.5×10^4 Pa/m (0.65 psi/ft). Using this value, the hydraulic pressure necessary to initiate fractures was calculated as 1.19×10^7 Pa (1,694 psi) for the bottom of the well (depth = 794.3 m) and as 1.12×10^7 Pa (1,591 psi) for the base of the confining unit (746.2 m). Thus pressures due to 30 years of continuous injection at the maximum permitted injection rate were much less than the pressure calculated to initiate hydraulic fracturing.

Hypothetical Conduits

During this final phase of modeling, the hydraulic response due to the presence of hypothetical conduits was investigated throughout the injection system. Jones and Haimson (1986) describe some hypothetical conduits pertinent to underground injection. These conduits, which allow fluid movement from the injection zone, include abandoned wells, microannuli at the injection well, and permeable fault zones. Time constraints restricted the investigation to the effect of a microannulus at the injection well. Accomplishing this task required numerical modeling to evaluate whether the pressure response in the injection system or in an overlying unit could be used to identify fluid movement from the injection zone. Three monitoring strategies were evaluated: monitoring at the injection well (WDW2), at the observation well (DOW), and in the overlying aquifer.

A new conceptual model of the site hydrogeology was developed for this task (fig. 42). A thicker sequence of geologic materials than that previously used included the Devonian limestones, the overlying New Albany Shale (a confining unit), the "Carper sand" (a permeable unit), and the Borden Siltstone (another confining unit). Since "Carper sand" lies near the base of Borden Siltstone, for purposes of modeling, it is considered the basal horizon of this formation. Hydrogeologic characteristics for these units appear on figure 42.

For this conceptual model, the head buildups at the injection and monitoring wells were slightly lower than the buildups used in the original model; however, the results were considered acceptable. The slight decrease (0.03 m at the DOW) was probably due to the greater thickness of compressible geologic materials for the conceptual model.

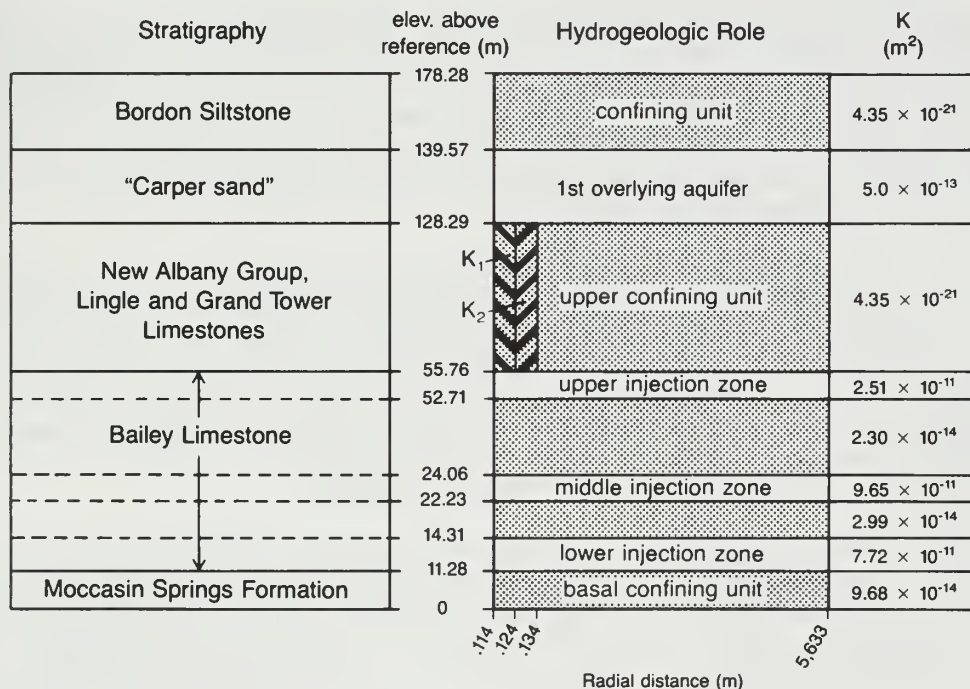


Figure 42 Conceptual model 2 of the injection system

Modeling Results: Hypothetical Conduit Scenario

In this scenario, a microannulus was assumed to have developed at the injection well. Extending from the top of the uppermost injection zone to the base of the Carper, the microannulus connected these two permeable units (fig. 42) and was input into the model as two zones. The first zone was considered the microannulus, and the second zone, a transition between the microannulus and the New Albany Shale. Both zones were 0.01 m thick and discretized using three nodes. Several runs were made, with different zone permeabilities (table 20). CT3DB1 was the baseline run used for comparison.

Table 20 Permeability (m^2) of the microannulus

Run	Microannulus (K1)	Transition zone (K2)
CT3DB1	4.35×10^{-21}	$4.35 \times 10^{-21*}$
CT3DB2	1.00×10^{-12}	1.00×10^{-14}
CT3DB3	1.00×10^{-10}	1.00×10^{-12}
CT3DB5	1.00×10^{-9}	1.00×10^{-11}
CT3DB4	1.00×10^{-8}	1.00×10^{-10}

* same permeability as New Albany shale.

For this series of model runs, the maximum permitted injection rate ($q = 2.208 \times 10^{-2} \text{ m}^3/\text{sec}$) was used to maximize the pressure gradients in the injection system. Injection continued at this rate for 365 days. Because the "Carper sand" does not produce water or hydrocarbons, hydrogeologic data for this unit are rare. On the basis of interpretations of geophysical logs from wells near Marshall, which indicated that the Carper is a permeable sandstone, permeability was assumed to be $5.0 \times 10^{-13} \text{ m}^2$.

For analysis of results, a head difference of 0.05 m, when compared with results of CT3DB1, was considered monitorable. Differences of less than 0.05 m were not considered sufficient to be monitored because of errors in measurement, head fluctuations due to earth and/or barometric tides, and related factors.

Head buildup in relation to time is shown for WDW2 (fig. 43), DOW (fig. 44), and the base of the Carper at WDW2 (fig. 45). As the permeability of the microannulus increased, the head buildup at WDW2 decreased slightly. For CT3DB4 ($K1 = 1.00 \times 10^{-8} \text{ m}^2$), difference in head buildup was -0.23 m after 1 year. Head buildup for the other cases were lower—for instance, $\Delta h = -0.10 \text{ m}$ when $K1 = 1.00 \times 10^{-10} \text{ m}^2$. A change in the head build-up of this magnitude at an operating injection well might not be monitorable because of head buildup associated with other factors, such as wellbore plugging and pipe friction increases.

For the five cases investigated, no monitorable difference in head buildup was observed at the DOW (fig. 44). For CT3DB4 ($K1 = 1.00 \times 10^{-8}$), head buildup was lower than the other cases by just 0.01 m after 365 days. Thus monitoring the DOW would not detect the leak at the microannulus. Monitorable differences in head buildup were predicted at the base of the Carper in three of the four cases. For CT3DB3, the difference after 365 days was 0.08 m. The differences after 365 days were greater for CT3DB5 (0.77 m) and CT3DB4 (3.98 m). The radial extent of head buildup at the base of the Carper varied for each of the cases. For CT3DB5, it was approximately 100 m, and for CT3DB4, more than 6,000 m (fig. 46).

In summary, monitoring the DOW would not reveal the presence of a leaky microannulus, in part because of the distance between the injection and observation wells. Monitoring the injection well might reveal a leaky microannulus, but the differences in head buildup for the cases investigated might be masked by well bore plugging, corrosion buildup in the tubing, and other related factors. Finally, monitoring in the overlying aquifer appears to be the best alternative, but it depends on the hydraulic conductivity of the microannulus. As the hydraulic conductivity of the hypothetical

conduit increases, the volume of fluid moving into the overlying aquifer and the head buildup also increases. The head buildup observed in the Carper is also a function of its hydraulic conductivity. Lower Δh would be observed if the Carper were more permeable. On the other hand, higher Δh would be observed over a smaller area if the Carper had a lower hydraulic conductivity.

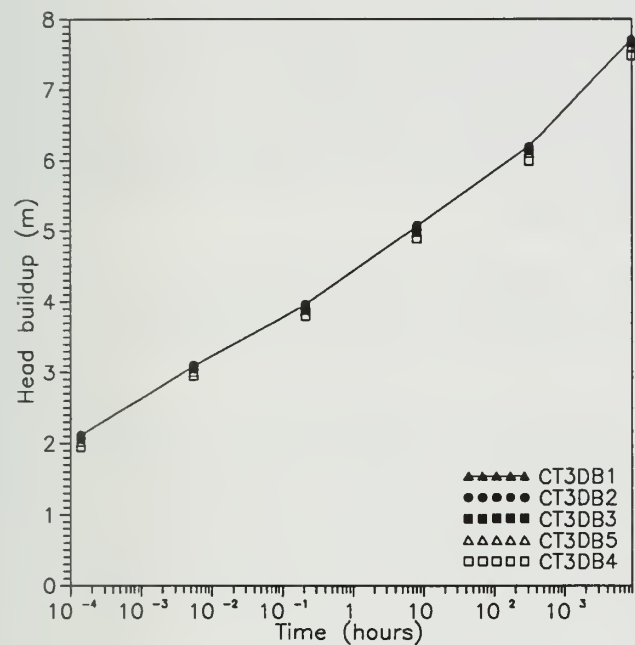


Figure 43 Effect of microannulus on the head buildup at the WDW2.

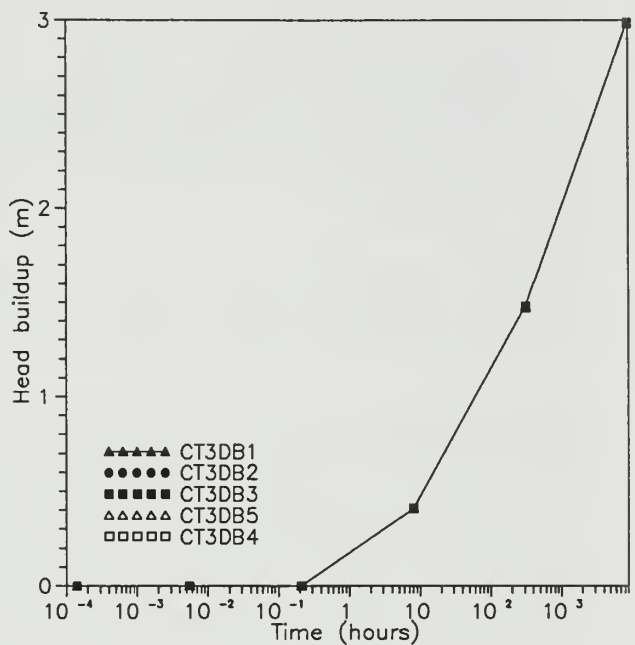


Figure 44 Effect of microannulus on the head buildup at the DOW.

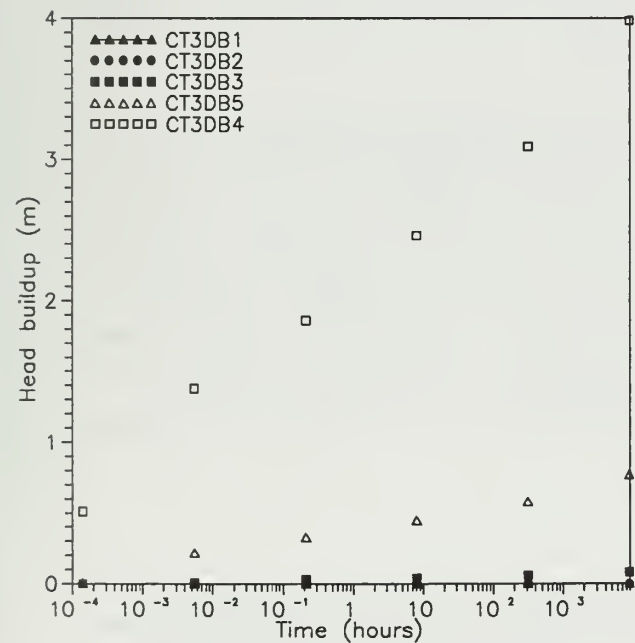


Figure 45 Effect of microannulus on the head buildup in the "Carper sand."

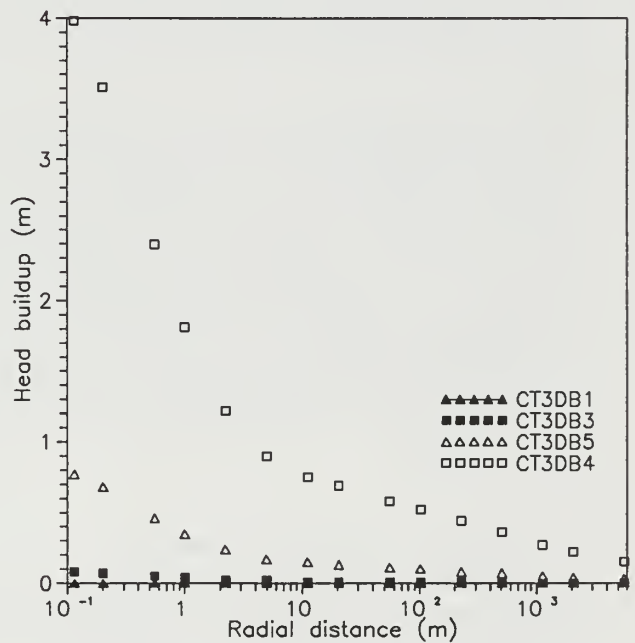


Figure 46 Head buildup in the "Carper sand" versus radial distance from WDW2.

5. SUMMARY AND CONCLUSIONS

Evaluation of Injection Scenarios

Available records and logs pertinent to the injection system were studied, hydraulic tests were conducted, geophysical logs were run, and other tests were conducted on-site to determine the hydrogeologic characteristics of the injection system. Regional and site-specific descriptions of the system's stratigraphy, structural geology, and hydrogeology were generated from analyses of these logs and test results. These descriptions formed the basis of input for the numerical groundwater flow model (HST3D) used to investigate the hydraulic effects of injection upon the injection system. Other input included data on the physical and chemical characteristics of the injected wastewater and the native brine in the injection system.

Before the effects of various injection scenarios were investigated, HST3D was verified with respect to two analytical solutions (figs. 34 and 35) and calibrated with respect to data collected during an injection test (fig. 37). Both verification and calibration were considered satisfactory.

Once calibrated, the model was used to predict the effects of various injection scenarios. The effect of long-term injection was investigated at two constant injection rates: the average historical rate ($1.150 \times 10^{-2} \text{ m}^3/\text{sec}$) and the maximum average permitted rate ($2.208 \times 10^{-2} \text{ m}^3/\text{sec}$). Under both scenarios, significant head buildup was observed at the injection well and radially from it. During the simulated 30-year injection period, steady state was approached but not obtained during either injection scenario. During the subsequent 30-year postinjection period, decrease in head buildup was fairly rapid—dropping to half in less than 2,000 hours for both scenarios. The maximum hydraulic pressures at the bottom of the well and at the base of the upper confining unit were significantly lower than the pressures calculated to initiate hydraulic fracturing.

The continuity of the regional stratigraphy and its qualitative permeability were determined from the regional and site-specific study. Numerical modeling indicated that the pressures resulting from waste injection were lower than pressures calculated to initiate hydraulic fracturing; thus new fractures would not be initiated. From a hydraulic viewpoint, therefore, waste injected within this injection system would be contained and would be considered protective of human health and the environment for the two injection scenarios investigated.

These results are based on an assumption that hydraulic conductivity remains constant. However, from available data it appears that the high pH of the injected wastewater causes it to react with the dolomite present in the injection zones, forming brucite ($\text{Mg}[\text{OH}]_2$), which reduces the hydraulic conductivity of the injection zone. Apparently, greater amounts of brucite formed in the zones where there was a greater flow of fluids; thus the zones with higher permeability were affected first. This hypothesis must be verified by additional work, which is beyond the scope of this project. At the study site, the long-term effect of this decrease in permeability on injectivity needs to be investigated. Any further decrease in the hydraulic conductivity of the injection zones will invalidate the results of the numerical modeling conducted for this study. In addition, any reduction in hydraulic conductivity of the injection zones will most likely cause an increase in hydraulic pressure if the injection rate remains constant. In such a case, hydraulic fracturing may be of concern.

Evaluation of Monitoring Strategies

The model was also used to investigate the hydraulic response throughout the injection system when a hypothetical conduit was introduced. In this scenario, a microannulus at the injection well was introduced, hydraulically connecting the uppermost injection zone and an aquifer immediately overlying the upper confining unit.

Model results were reported in terms of difference in head build-up when the microannulus was and was not present. At the WDW2, Δh (-0.23 m) was greatest for the scenario with the greatest microannulus permeability ($1 \times 10^{-8} \text{ m}^2$). A difference of this magnitude at an operating well would be considered unmonitable because of interferences such as increased Δh resulting from well bore plugging or tubing corrosion. At the DOW, Δh was considered too low to be monitorable. The difference in the overlying aquifer (Carper sand) was considered monitorable for the microannulus permeability greater than or equal to $1 \times 10^{-10} \text{ m}^2$. The head buildup in the Carper is a function of its hydraulic conductivity, the hydraulic conductivity of the microannulus, and the radial distance from the microannulus. Thus from a practical standpoint and for the scenario modeled, the overlying aquifer is the only viable location for hydraulically monitoring leakage via the microannulus.

REFERENCES

- Algermissen, S. T., January 1969, Seismic risk studies in the United States: Fourth World Conference on Earthquake Engineering, Santiago, Chile.
- Bateman, R. M., 1985a, Cased-hole log analysis and reservoir performance monitoring: International Human Resources Development Corporation, Boston, MA, 319 p.
- Bateman, R. M., 1985b, Open-hole log analysis and formation evaluation: International Human Resources Development Corporation, Boston, MA, 647 p.
- Birch, F., 1966, Compressibility: Elastic Constants, Section 7: *in* S. P. Clark Jr., editor, Handbook of Physical Constants, revised edition, Geological Society of America, Memoir 97, 173 p.
- Brock, J., 1984a, Analyzing Your Logs, v. II (Advanced Open Hole Log Interpretation): Petro-Media, Tyler, TX, 188 p.
- Brock, J., 1984b, Analyzing Your Logs, v. I (Fundamentals of Open Hole Log Interpretation): Petro-Media, Tyler, TX, 236 p.
- Brower, R. D., A. P. Visocky, I. G. Krapac, B. R. Hensel, G. R. Peyton, J.S. Nealon, and M. Guthrie, 1989, Evaluation of underground injection of industrial waste in Illinois: Illinois Scientific Surveys Joint Report 2, 184 p.
- Buschbach, T. C., 1952, The Chouteau Formation of Illinois: Illinois State Geological Survey, Circular 183, p. 108-115.
- Buschbach, T. C., and D. C. Bond, 1974, Underground storage of natural gas in Illinois 1973: Illinois State Geological Survey, Illinois Petroleum 101, 71 p.
- Cluff, R. M., M. L. Reinbold, and J. A. Lineback, 1981, The New Albany Shale Group of Illinois: Illinois State Geological Survey, Circular 518, 83 p.
- Curtis, R. M., 1966, Flow analysis with the gradiometer and flowmeter: Schlumberger Well Service, 36 p.
- Dobrin, M. B., 1976, Introduction to Geophysical Prospecting: McGraw-Hill, New York, NY, 630 p.
- Domenico, P. A., and M. D. Mifflin, 1965, Water from low-permeability sediments and land subsidence: Water Resources Research, v. 1, p. 563-576.
- Dresser Atlas, 1985a, Log Interpretation Charts: Dresser Industries, 157 p.
- Dresser Atlas, 1985b, Dresser Atlas Services Catalog: Dresser Industries, 136 p.
- Dresser Atlas, 1985c, Dresser Atlas Casing Evaluation Services: Dresser Industries, 140 p.
- Dresser Atlas, 1981, Interpretive Methods for Production Well Logs: Dresser Industries, 113 p.
- Ford, M. D., R. Piskin, M. Hagele, R. Strom, and J. Dickman, 1981, Inventory and preliminary assessment of class I and class II injection wells in Illinois: Illinois Environmental Protection Agency, 111p.
- Franke, O. L., and T. E. Reilly, 1987, The effects of boundary conditions on the steady-state response of three hypothetical ground-water systems—results and implications of numerical experiments: United States Geological Survey, Water-Supply Paper 2315, 19 p.
- Freeze, R. A., and J. A. Cherry, 1979, Groundwater: Prentice-Hall, Englewood Cliffs, N.J., 604 p.
- Gearhart, 1983, Formation Evaluation Chart Book: Gearhart Industries, Fort Worth, TX, 104 p.
- Gearhart, Well Service Systems: Gearhart Industries, Fort Worth, TX, 137 p.
- Graf, D. L., W. F. Meents, I. Friedman, and N. F. Shimp, 1966, The origin of saline formation waters, III: calcium chloride waters: Illinois State Geological Survey, Circular 397, 60 p.
- Gray, H. H., N. K. Bleuer, J. R. Hill, and J. A. Lineback, 1979, Geologic map of the 1 x 2 Indianapolis Quadrangle, Indiana and Illinois: Indiana Department of Natural Resources.
- Hallenburg, J. K., 1984, Geophysical Logging for Mineral and Engineering Applications: PennWell Publishing Co., Tulsa, OK, 254 p.
- Hantush, M. S., 1964, Hydraulics of Wells in Advances in Hydrosociences, v. 1, V.T. Chow, editor: Academic Press, New York, NY, p. 281-432.
- Heigold, P. C., 1972, Notes on the earthquake of September 15, 1972, in northern Illinois: Illinois State Geological Survey, Environmental Geology Notes 59, 15 p.
- Heigold, P. C., 1968, Notes on the earthquake of November 9, 1968, in southern Illinois: Illinois State Geological Survey, Environmental Geology Notes 24, 16 p.

- Helander, D. P., 1983, Fundamentals of Formation Evaluation: Oil and Gas Consultants International, Tulsa, OK, 332 p.
- Hilchie, D. W., 1977, Caliper and temperature logging: *in* L. W. LeRoy, D. O. LeRoy, and J. W. Raese, editors, 1977, Subsurface Geology: Petroleum, Mining, Construction, 4th edition: Colorado School of Mines Press, Colorado School of Mines, Golden, CO, p. 342-346.
- Illinois Environmental Protection Agency, 1987, Draft Underground Injection Permit for Waste Disposal Well No. 2, August 28, 46 p.
- Illinois-Indiana-Kentucky Geological Societies, 1968, Geology and petroleum production in the Illinois Basin, 32 p.
- INTERCOMP, 1976, A model for calculating effects of the liquid waste disposal in deep saline aquifers: United States Geological Survey, Water-Resources Investigations 76-61, 253 p.
- Jones, T. A., and J. S. Haimson, 1986, Demonstration of confinement: an assessment of class I wells in the Great Lakes and Gulf Coast regions: Journal of the Underground Injection Control Practices Council, p. 279-317.
- Keys, S. W., and L. M. MacCary, 1971, Application of Borehole Geophysics to Water-Resources Investigations: United States Government Printing Office, Washington, DC, 126 p.
- Kipp, K. L., Jr., 1987, HST3D: A computer code for simulation of heat and solute transport in three-dimensional ground-water flow systems: United States Geological Survey, Water Resources Investigations Report 86-4095, 515 p.
- Kipp, K. L., Jr., 1986, Adaptation of the Carter-Tracy water influx calculation to groundwater flow simulation: Water Resources Research, v. 22, n. 3, p. 423-428.
- Kovacs, G., and Associates, 1981, Subterranean Hydrology: Water Resources Publications, Littleton, CO, p. 609-713.
- Leach et al., 1974, The full bore flowmeter: Society of Petroleum Engineers of AIME, paper No. SPE 5089, Dallas, TX, 16 p.
- Leighton, M. W., D. R. Kolata, D. F. Oltz, and J. J. Eidel, editors, in press, Interior Cratonic Basins: American Association of Petroleum Geologists Memoir (World Petroleum Basins), Tulsa, OK.
- Lohman, S. W., 1972, Ground-water hydraulics: United States Geological Survey, Professional Paper 708, 70 p.
- Martin, K. I., 1982, The application of log derived transmissibility in well completion design and well performance evaluation: *in* Proceedings of the Indonesian Petroleum Association, Eleventh Annual Convention, June 1982, Jakarta, Indonesia, p. 401-414.
- Mast, R. F., 1967, The development of a reservoir data system with examples of applications in Illinois: Interstate Oil Compact Commission: Commission Bulletin, v. 9, n. 1, p. 21-28.
- Meents, W. F., 1952, Illinois oil-field brines—their geologic occurrence and chemical composition: Illinois State Geological Survey, Illinois Petroleum 66, 38 p.
- Millero, F. J., G. K. Ward, F. K. Lepple, and E. V. Hoff, 1974, Isothermal compressibility of aqueous sodium chloride, magnesium chloride, sodium sulfate, and magnesium sulfate solutions from 0 to 45 at 1 atm: Journal of Physical Chemistry, v. 78, n. 16, p. 1636-1643.
- North, W. G., 1969, The Middle Devonian strata of southern Illinois: Illinois State Geological Survey, Circular 441, 45 p.
- Peebler, B., Multipass Interpretation of the Full Bore Spinner: Schlumberger Well Service, 28 p.
- Pickett, G. R., 1977, Resistivity, radioactivity, and acoustic logs: *in* L. W. LeRoy, D. O. LeRoy, and J. W. Raese, editors, Subsurface Geology: Petroleum, Mining, Construction, 4th edition, Colorado School of Mines Press, Colorado School of Mines, Golden, CO, p. 304-336.
- Piskin, K., and R. E. Bergstrom, 1975, Glacial drift in Illinois: thickness and character: Illinois State Geological Survey, Circular 490, 36 p., 2 plates.
- Piskin, R., 1986, Letter to L. W. Eastep, Illinois Environmental Protection Agency, March 27.
- Pough, F. H., 1953, A Field Guide to Rocks and Minerals: The Riverside Press, Cambridge, MA, 137 p.
- Prasada Rao, S. V. V., 1985, Aquifer and aquiclude delineation and correlation of Quaternary sediments by borehole geophysical logs in Banganga River Basin, Rajasthan: *in* Geophysical Research Bulletin, v. 23, n. 3, National Geophysical Research Institute, Hyderabad, India, p. 169-176.

- Reeves, M., and R. M. Cranwell, 1981, User's Manual for the Sandia Waste Isolation Flow and Transport Model (SWIFT), Release 4.81: U.S. Nuclear Regulatory Commission, NUREG/CR-2324, SAND81-2516, 146 p.
- Rider, M. H., 1986, The Geological Interpretation of Well Logs: Blackie and Son, Limited, London, England, 175 p.
- Roy, W. R., S. C. Mravik, I. G. Krapac, D. R. Dickerson, and R. A. Griffin, 1989, Geochemical interactions of hazardous wastes with geological formations in deep-well systems: Illinois State Geological Survey, Environmental Geology Note 130, 52 p.
- Samson, I.E., 1989, Illinois mineral industry in 1986 and review of preliminary mineral production data for 1987: Illinois State Geological Survey, Illinois Mineral Notes 100, 40 p.
- Samson, I. E., 1983, Illinois mineral industry in 1979/1980 and review of preliminary mineral production data for 1981: Illinois State Geological Survey, Illinois Mineral Notes 84, 40 p.
- Sargent, M. L., and T. C. Bushbach, 1985, Morphology of the top of Precambrian crystalline rocks: Geological Society of America Abstracts With Program, v. 17, n. 5, p. 324.
- Schlumberger, 1985, Schlumberger Openhole Services Catalog: Schlumberger Well Services, 76 p.
- Schlumberger, 1984, Schlumberger Production Services Catalog: Schlumberger Well Services, 60 p.
- Schmoker, J. W., K. B. Krystinik, and R. B. Halley, 1985, Selected characteristics of limestone and dolomite reservoirs in the United States: American Association of Petroleum Geologists, Bulletin, v. 69, n. 5, p. 733-741.
- Stover, C. W., B. G. Reagor, and S. T. Algermissen, 1979, Seismicity map of the State of Illinois: U.S. Geological Survey, Miscellaneous Field Studies Map MF-1143.
- Student, J. D., R. Piskin, L. J. Withers, and J. Dickman, 1981, Aquifers of Illinois: Underground Sources of Drinking Water and Nondrinking Water: Illinois Environmental Protection Agency, 98 p.
- Swann, D. H., and H. B. Willman, 1961, Megagroups in Illinois: American Association of Petroleum Geologists, Bulletin, v. 45, n. 4, p. 471-483.
- Theis, C.V., 1935, The relation between the lowering of the piezometric surface and the rate and duration of discharge of a well using ground-water storage: Transactions of the American Geophysical Union, v. 16, p. 519-524.
- Todd, D. K., 1980, Groundwater Hydrology, 2nd edition: John Wiley & Sons, New York, NY, 535 p.
- Treworgy, J. D., 1981, Structural features in Illinois—a compendium: Illinois State Geological Survey, Circular 519, 22 p.
- Treworgy, J. D., 1979, Map of major structural features in Illinois: Illinois State Geological Survey.
- U.S. Environmental Protection Agency, 1986, Federal underground injection control reporting system, summary report: Office of Drinking Water, Washington, DC, August 15, 54 p.
- Velsicol, 1987, Monthly disposal well report for July 1987, sent to Illinois Environmental Protection Agency, September 10.
- Velsicol, 1984, Underground injection control permit application for Wells Nos. 1 and 2, submitted to the Illinois Environmental Protection Agency, September 10.
- Ward, D. S., M. Reeves, and L. E. Duda, 1984, Verification and Field Comparison of the Sandia Waste-Isolation Flow and Transport Model (SWIFT): Sandia National Laboratory, SAND83-1154, NUREG/CR-3316, 155 p.
- Whitaker, S. T., 1988, Silurian pinnacle reef distribution in Illinois: model for hydrocarbon exploration: Illinois State Geological Survey, Illinois Petroleum 130, 32 p.
- Whiting, L. L., J. Van Den Berg, T. F. Lawry, R. F. Mast, and C. W. Sherman, 1964, Petroleum in Illinois, 1963: Illinois State Geological Survey, Illinois Petroleum 79, 99 p.
- Willman, H. B., and J. C. Frye, 1970, Pleistocene stratigraphy of Illinois: Illinois State Geological Survey, Bulletin 94, 204 p.
- Willman, H. B., J. A. Simon, B. M. Lynch, and V. A. Langenheim, 1968, Bibliography and index of Illinois geology through 1965: Illinois State Geological Survey, Bulletin 92, 373 p.
- Willman, H. B., E. Atherton, T. C. Buschbach, C. Collinson, J. C. Frye, M. E. Hopkins, J. A. Lineback, and J. A. Simon, 1975, Handbook of Illinois stratigraphy: Illinois State Geological Survey, Bulletin 95, 261 p.

Yeh, W. W-G., 1986, Review of Parameter Identification Procedures in Groundwater Hydrology: The Inverse Problem: Water Resources Research, v. 22, n. 2, p. 95-108.

APPENDIX A. THEORY AND PRACTICAL APPLICATION OF GEOPHYSICAL LOGGING INSTRUMENTS

Geophysical logging was used in this study to investigate the site and regional hydrogeology, and this section briefly explains the basic operational theory and applications of the geophysical tools used. Comprehensive coverage of every aspect of tool theory or all possible applications is beyond the scope of this project. These tools and their many applications are discussed in greater detail in Bateman 1985a, Bateman 1985b, Helander 1983, Leach et al. 1974, Curtis 1966, Peebler, Hallenborg 1984, Dobrin 1976, Kovacs and Associates 1981, Pickett 1977, Hilchie 1977, Brock 1984a, Brock 1984b, Rider 1986, Gearhart, Gearhart 1983, Dresser Atlas 1981, Schlumberger 1984, Schlumberger 1985, Dresser Atlas 1985a, Dresser Atlas 1985b, Dresser Atlas 1985c, Prasada Rao 1985, Keys and MacCary 1971, and Martin 1982. The discussion below draws liberally from these references.

Caliper Log (CL)

The Caliper Log tool is a theoretically uncomplicated instrument. Most tools still rely on a single or a series of potentiometers (fig. A-1). The potentiometers respond to a number of arms (caliper arms), which transmit information about the borehole environment to the potentiometer actuator. This information is relayed as a series of pulses to the surface recording equipment, which then processes the data.

There are a number of different arm configurations with the CL tool. For the purposes of injection/confining interval evaluation, the one- and four-arm tools are appropriate.

For applications that utilize the numerical CL data, such as calculations involving the Flowmeter Log (FL), the more sensitive four-arm CL tool is employed. For other applications, such as mud-cake and washout location and general borehole conditions, a one-arm CL tool (usually run in mechanical combination with another device, such as a Neutron Log, Density Log, or Permeability Log) is utilized almost invariably.

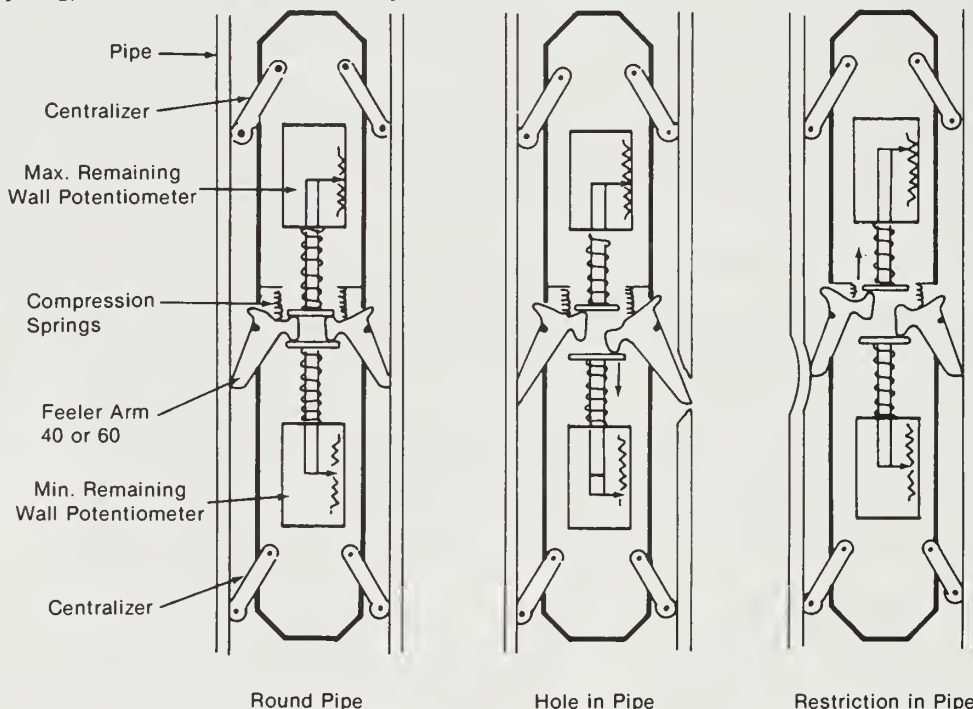


Figure A-1 Caliper Log tool that utilizes a dual potentiometer configuration (from Dresser Atlas 1985c)

Flowmeter Log (FL)

Several types of Flowmeter Log tools are available, and they all operate in a similar fashion. The tool considered in this report is the continuous variety, which would be the most appropriate at the high flow rates often encountered in waste-disposal wells.

The Continuous Spinner Flowmeter Log (CSFL) tool, shown in figure A-2, incorporates an impeller into its design. The impeller rotates in response to fluid movement. This rotation generates a series of electrical pulses that are transmitted uphole to the surface equipment for computer processing. The number of pulses generated is proportional to the number of revolutions per second of the impeller, which can be related to flow velocity. The volumetric flow rate, the measurement of most interest, can be calculated from borehole diameter data obtained from the four-arm CL tool.

The CSFL tool measures fluid velocity very satisfactorily in turbulent fluid flow. Although this flow regime is encountered most often, it nonetheless requires verification. One method of defining whether a flow regime is turbulent is to use the Reynold's Number (Re). Re is defined as

$$Re = \frac{vD\rho}{\mu} \quad [A-1]$$

where ρ = fluid density, g/cm³
 v = average fluid velocity, cm/sec
 D = hole diameter, cm
 μ = fluid viscosity, poise

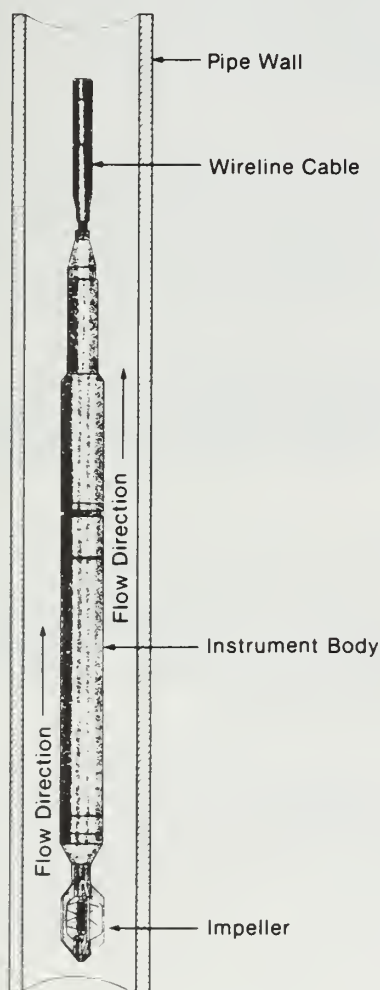


Figure A-2 Continuous Spinner Flowmeter Log tool (from Dresser Atlas 1981).

Re values of 3,000 or greater are used to represent turbulent flow in most literature dealing with fluid flow. For most applications of the CSFL tool in injection/confining interval evaluation, fluid will be injected at the surface to initiate impeller movement. A useful conversion in Re calculations is

$$v = (0.3637)Q/D^2 \quad [A-2]$$

where v = average fluid velocity, cm/sec

D = hole diameter, cm

Q = flowrate, barrels per day

This conversion is combined with the definition of the Reynold's Number to yield

$$Re = (0.3637)Q\rho/\mu D \quad [A-3]$$

Gamma Ray Log (GRL)

As its name suggests, the GRL detects gamma rays—random, high-energy electromagnetic waves emitted during the decay of unstable radioisotopes. The radioisotopes normally found in rocks are ^{40}K and the daughter products of the uranium and thorium decay series. The GRL discussed here is unable to differentiate the contribution of each individual radioisotope to the total intensity of gamma radiation.

The detector of the tool normally consists of a sodium iodide (NaI) crystal optically coupled to a photomultiplier tube. Atoms of the NaI crystal absorb gamma ray collision energy, which places the electrons of the atoms in a higher energy state. When the excited electrons lose this acquired energy and fall back into their original state, they give off light that is converted to a voltage pulse through the photomultiplier tube. These pulses are transmitted uphole and converted, on the appropriate scale, to a measure of the gamma ray intensity.

Because of the high natural concentration of ^{40}K in clay minerals, shales generally exhibit a high gamma ray intensity. On the other hand, sandstones and carbonates generally produce a lower gamma ray count because of their relatively low concentration of clays and other highly radioactive constituents. Because of this difference in gamma ray intensity, various lithologies can easily be identified (allowing correlation of lithologic units), and a rock unit's shale volume can be determined.

During phase I logging, a GRL that used a Geiger Mueller type of detector was run. The Geiger Mueller replaced the Scintillation type of detector employed in the previous GRL. This change results in a smoother, less fluctuating GR, which provides a better estimate of the formation's natural gamma ray activity (GR, measured in API units).

Sonic Log (SL)

The Sonic Log is an acoustic device that generates acoustic waves and measures reflected acoustic waves. The measurements taken from the SL tool are the direct result of the propagation of acoustic (elastic) waves through the borehole environment. The two important waves to the SL tool are the compressional (longitudinal) and the shear (transverse) waves.

The initial energy to produce the sound (acoustic) waves is generated by the transmitter (T) portion of the tool (fig. A-3). The velocity of a shear wave (V_s) is given by:

$$V_s = (\mu/\rho)^{0.5} \quad [A-4]$$

where μ = modulus of shear for the medium

ρ = density of the medium

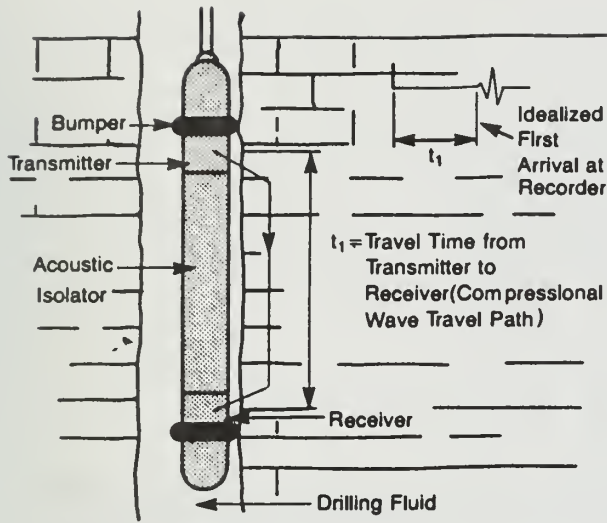


Figure A-3 (left) Generalized Sonic Log tool (from Helander 1983).

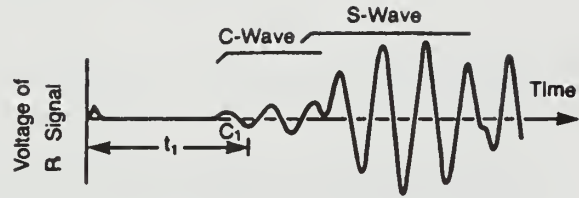


Figure A-4 Idealized schematic of receiver (R) signal (from Helander 1983).

Since the incident energy generated by the SL transmitter must first traverse a liquid medium in the borehole (where $\mu = 0$), it would appear that no shear wave would be generated, and subsequently received, by the SL tool. However, the occurrence of both shear and compressional waves in the response from the tool (fig. A-4) is a curious and useful anomaly. This apparent discrepancy can be resolved by noting that as the compressional wave strikes an interface or simply an adjacent medium with different elastic properties, a shear wave is produced. Therefore, as the compressional wave traverses from the transmitter (T) to the receiver (R) on the tool, the wave generates a shear wave that can, in this manner, be detected by the receiver circuitry. Shear waves generally are of a larger amplitude and about half as fast as compressional waves.

The transmitter-receiver array is chosen to account for abnormalities present in the borehole environment, i.e., washouts and tool tilting. The standard transmitter-receiver (T-R) arrangement is shown in figure A-5. Although other T-R configurations are available, this configuration is most nearly suited to the needs of injection/confining interval evaluation. The specific SL tool that incorporates this T-R array into its design is the Borehole Compensated Sonic Log (BCSL) tool. The main benefit of this type of T-R spacing is the compensation for washouts and tool tilting effects on travel time measurements.

Since the compressional wave has the fastest velocity of propagation, it is the one of most concern with the BCSL. If t_{fl} is the time taken to travel through the pore space (fluid travel time) and t_{ma} is the time taken to travel through the matrix, the total travel time will be t (the travel time recorded by the BCSL tool). The porosity (POR)BCS (Borehole Compensated Sonic) can be represented by the Wyllie time-average equation,

$$(POR)BCS = (t - t_{ma}) / (t_{fl} - t_{ma}) \quad [A-5]$$

The compressional wave (p-wave, also called C-wave) takes the path of least resistance. Areas of isolated (not interconnected) pockets of porosity, which would normally be found in the case of secondary porosity, will not have a pronounced effect on the travel time of the p-wave. By comparing the BCSL data with data from a tool that is influenced by the total porosity (primary and secondary), the amount of secondary porosity present can be estimated. The following equation applies to this situation,

$$(POR)_{tot} = (POR)_{sec} + (POR)_{prim} \quad [A-6]$$

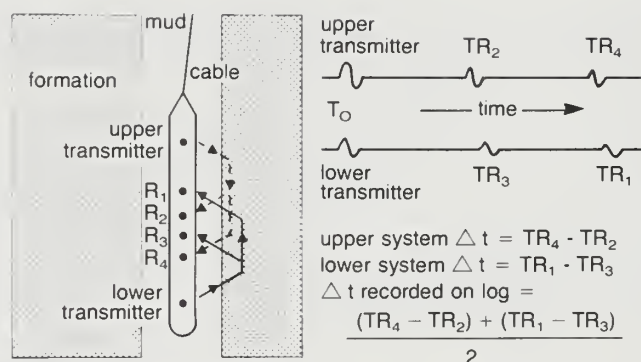


Figure A-5 Generalized Borehole Compensated Sonic Log tool (from Bateman 1985b).

During phase I logging, the BCSL was run in place of the SL. A more advanced detection system in the BCSL allows compensation for environmental factors that affect the signal transit time (t) used by the BCSL to make porosity determinations. A more accurate porosity profile results with the use of the BCSL.

One other SL tool that should be mentioned is the Long Spaced Sonic Log (LSSL) tool. It incorporates a longer T-R spacing than does the BCSL tool. In this manner, the LSSL tool is affected by a zone farther away and less disturbed by drilling operations than the zone at the borehole interface. This tool has been used for shear wave analysis, which when combined with compressional wave data results in an evaluation of some of the formation's strength characteristics, such as the pressure required to fracture the formation and the formation's elastic properties. If a hole has a large potential for washouts, this tool may be the best SL tool to use.

Neutron Log (NL)

The neutron is a fundamental particle found in the nucleus of all atoms except hydrogen, which contains only a proton. The neutron is a chargeless particle with about the same mass as the proton. The NL tool exploits these two properties of the neutron particle. The neutron source is usually a mixture of americium and beryllium, which react together to continuously emit neutrons.

Since the neutron is a small and electrically neutral particle, it passes with ease through most matter. During its passage, the neutron particle loses energy by colliding with other atoms. When the neutron's energy is reduced to a level equal to the surrounding matter (a function of absolute temperature), the neutron is called a thermal neutron. The energy of a thermal neutron is in the range of 0.025 eV.

Simple force relationships reveal that the maximum energy loss in the collision of two balls occurs when the two balls are of equal mass. Since the neutron and the hydrogen atom's proton have nearly equal masses, hydrogen dominates the behavior of neutrons and, in turn, the response of the NL tools. The thermal neutron flux is therefore controlled by the hydrogen content of the formation. Since hydrogen is found in the water molecules filling the pore space, the thermal neutron flux is a direct indication of the porosity of the formation.

Environmental factors such as hole size and mud weight influence the response of the NL tool. This influence can be corrected by taking two readings of thermal neutron flux at different spacings and using them to define the slope of the response line of the tool. This slope is relatively unaltered by environmental effects. The Compensated Neutron Log (CNL) tool utilizes this concept. The primary measurement of the CNL tool is therefore a ratio of the two count rates, far and near. Figure A-6 shows a CNL tool schematic.

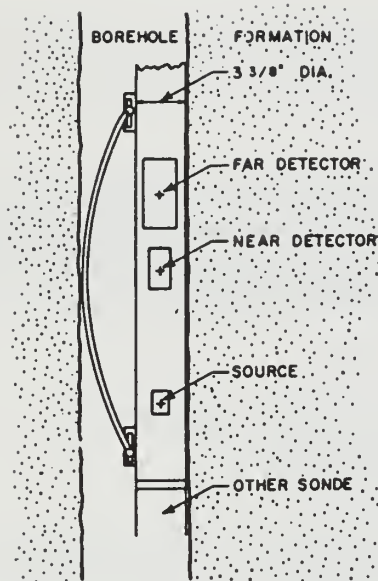


Figure A-6 Generalized Compensated Neutron Log tool (from Bateman 1985b).

The CNL displays a measurement of total porosity. Thus, it can be combined with the BCSL to provide an estimate of secondary porosity. Along with another porosity device, usually the BCSL or the Compensated Density Log (CDL), a lithologic determination may be made in addition to an accurate estimate of total porosity (cross-plotted porosity).

The CNL has replaced the Sidewall Neutron Log (SNL). The CNL utilizes a dual detector while the SNL has only one. The second detector enables the CNL to compensate effectively for environmental factors not taken into account with the SNL, such as salinity and temperature of the borehole fluid and diameter of the borehole. Accounting for these factors results in a more accurate determination of porosity with the CNL, ([POR]NIs).

Density Log (DL)

The DL utilizes a focused gamma ray source, normally cesium-137, which emits gamma rays into the formation from a pad assembly that is forced against the borehole wall via a back-up arm. The gamma rays interact with the electrons in the material opposite the focused source mainly through Compton scattering. This results in the gamma ray losing energy at each collision. The intensity of the back-scattered gamma ray is then measured by the gamma ray detectors (usually two) (fig. A-7). The measured gamma ray intensity is a function of the electron density of the formation. As the electron density of the formation increases, the probability of collision increases, resulting in reduced gamma ray intensity measured by the gamma ray detectors. The electron density, ρ_e , has been related to the bulk density, ρ_b , by the following equation,

$$\rho_e = \rho_b(2Z/A) \quad [A-7]$$

where Z = atomic number or the number of electrons per atom
 A = atomic weight

In most cases, the ratio, $2Z/A$, is approximately equal to 1.0. Therefore $\rho_e = \rho_b$, and the apparent bulk density response of the tool is a response to the bulk density, ρ_b , of the formation material opposite the tool.

A two-detector DL or Compensated Density Log (CDL), which was used for phase I logging, allows for the compensation of the mudcake's effect on CDL tool response. In this way, an accurate

total porosity measurement is obtained. CDL response can be compared to BCSL porosity to estimate secondary porosity or cross-plotted with the BCSL or CNL to produce lithologic and total porosity determinations.

Resistivity Log (RL)

The property of a material that opposes the flow of an electrical current is called electrical resistance. Resistivity is a measure of the resistance of a volume of material. Several authors have noted that formation resistivity can be determined by,

$$R = KV/I$$

[A-8]

where R = resistivity
 K = geometric factor specific for a particular tool
 V = potential across current path
 I = current.

Since the RL tool measures the potential, and K and I are known, R can be calculated. The calculated resistivity is dependent on the amount of porosity and fluid contained in the pores.

RL tools have a number of applications. For this study, the resistivity device was needed for two purposes: to determine an accurate, true formation resistivity for fluid saturation calculations, cementation factor determinations, and stratigraphic correlations; and to estimate the invasion of borehole fluids into the formation, which may affect the RL tool's response.

Two appropriate resistivity logging systems are available: the Dual Laterolog Microspherically Focused Log tool and the Dual Induction Laterolog (Spherically Focused Log) tool. Although both systems will provide the necessary results, specific borehole conditions dictate which one is appropriate. The former is used when sea water or brine mud fills the borehole and the latter when fresh or oil-based mud is present. For this discussion, the Dual Induction Laterolog (DIL) tool will be considered. (The Dual Induction Spherically Focused Log [DISFL] tool is similar in principle to the DIL.)

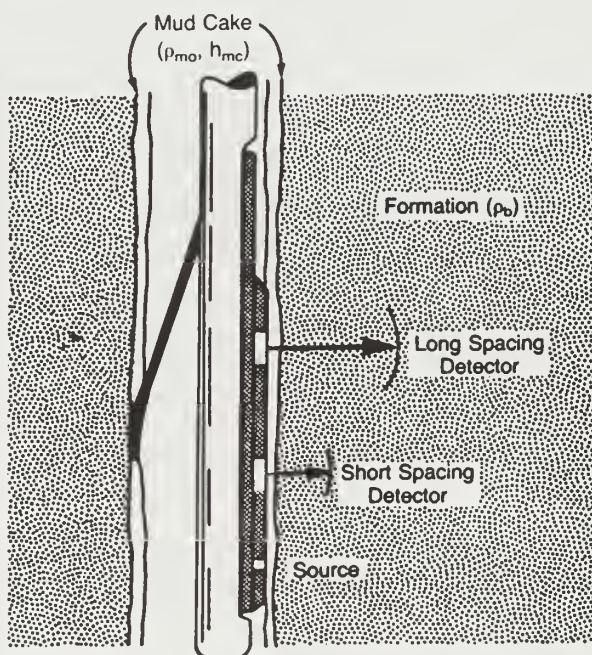


Figure A-7 Generalized two-detector Density Log tool (from Helander 1983).

The DIL tool comprises two sections: the induction and the lateral. The induction section produces two measurements, the "induction log deep" and the "induction log medium"; the lateral section yields one, the "laterolog."

The induction section, shown in schematic in figure A-8, is equipped with transmitter-receiver (T-R) coil pairs. An alternating current is applied to the transmitter, which generates a magnetic field around the tool, thereby inducing current flow in the surrounding formation. The current flow generates a magnetic field in the formation which, in turn, induces a voltage in the receiver coils. The measured voltage is proportional to the formation conductivity, which is inversely related to the formation resistivity.

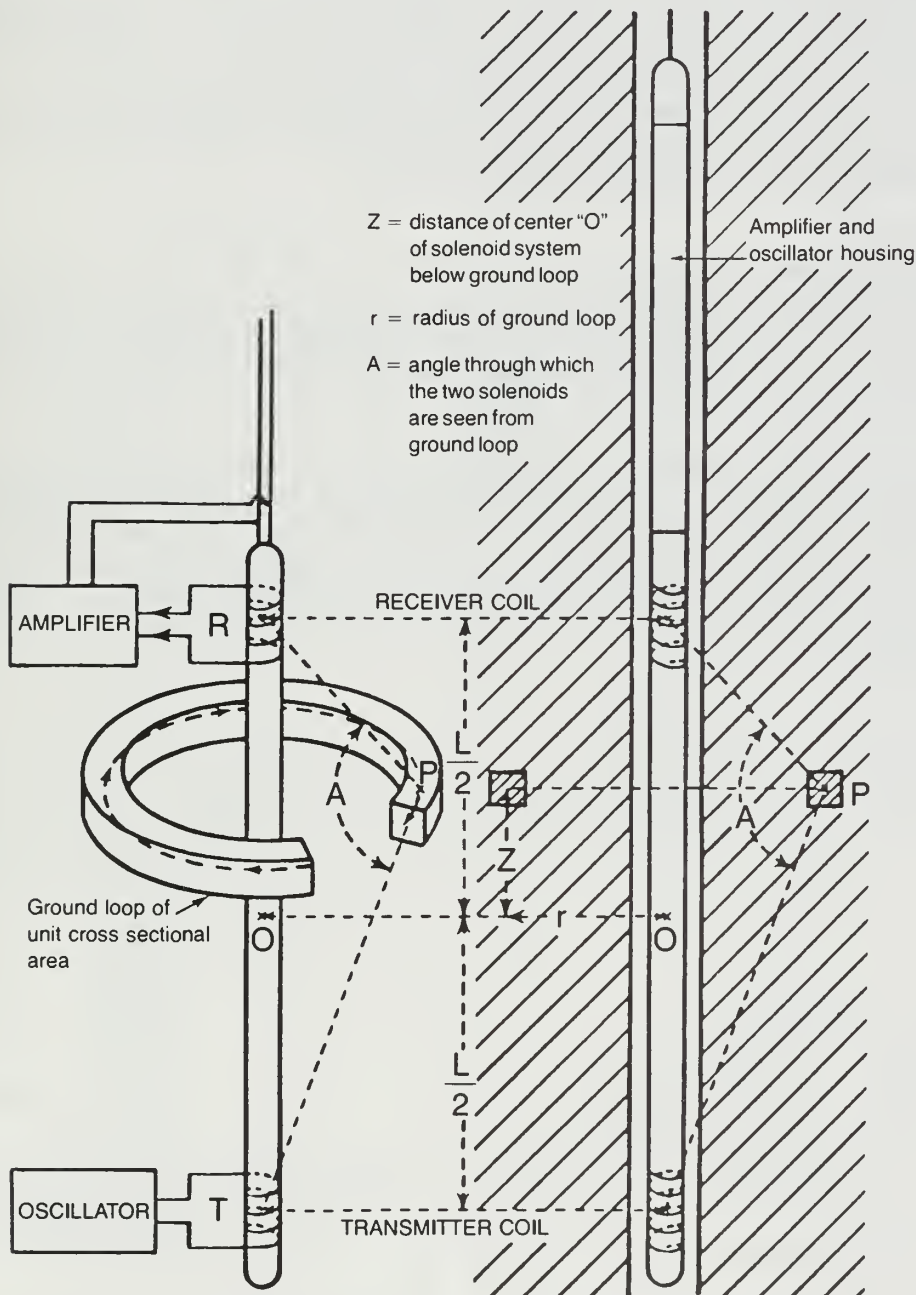


Figure A-8 Schematic diagram of induction log principles (from Hallenborg 1984).

Lateral devices pass a current of constant intensity from the tool into the formation (fig. A-9). This current flow creates equipotential spheres around the source electrode (A). Potential measuring electrodes (M, N) record the potential created by the current flow. The potential measured is then converted to formation resistivity.

The three curves generated have different depths of investigation into the formation, because of T-R spacing on the induction section and A-M,N spacing on the laterolog section. In this way, an evaluation of the amount of invasion is made, which is used to correct the deepest measurement (induction log deep) for invasion effects to produce an accurate, true formation resistivity. This resistivity can be used to obtain the cementation factor and fluid saturation of the formation.

The DISFL has replaced the Induction Electric Log (IEL). With the addition of one more resistivity curve to the output of the DISFL, the Induction Log Medium resistivity, and a deeper reading Induction Log Deep resistivity, factors that affected the resistivity response of the DISFL can be taken into account. These factors include the depth of invasion of the borehole fluids and the effect of this invasion on the determination of a true resistivity for the formation. The result is an Induction Log Deep resistivity corrected for invasion effects, which is considered more accurate than the formation's true resistivity determined by the IEL.

Permeability Log (PL)

The Permeability Log tool used most frequently today is the Minilog (MIL) tool. The MIL replaced the Microlog. Advanced electronics have increased the sensitivity of the Minilog as compared with the Microlog. Use of the Minilog results in more accurate information on permeability, mud (R_m), mud filtrate (R_{mf}), and mudcake (R_{mc}) resistivities.

The MIL, which utilizes the same resistivity theory discussed for the RL, is not discussed in detail here. The output of the MIL tool consists of two measurements: normal and lateral resistivities. The lateral configuration is described above. The normal measurement utilizes a slightly different system, shown in general schematic in figure A-10. The two arrays are housed in a nonconductive, fluid-filled rubber pad that is forced against the borehole wall by a back-up arm. This configuration is necessary to prevent the borehole fluid from short-circuiting the closely spaced current electrodes.

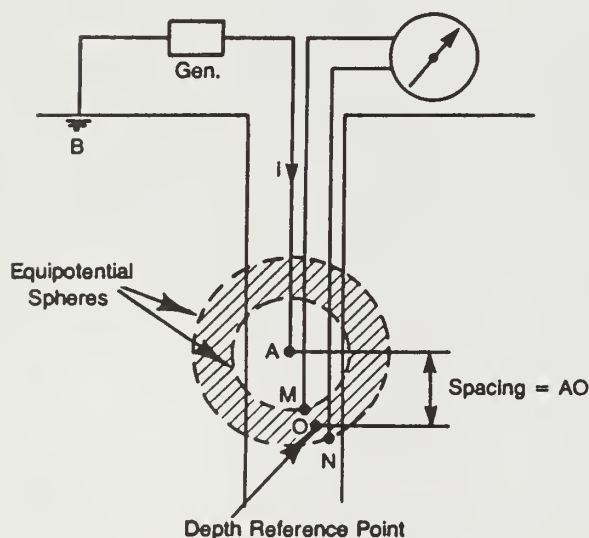


Figure A-9 (left) Schematic diagram of lateral logging system (from Helander 1983).

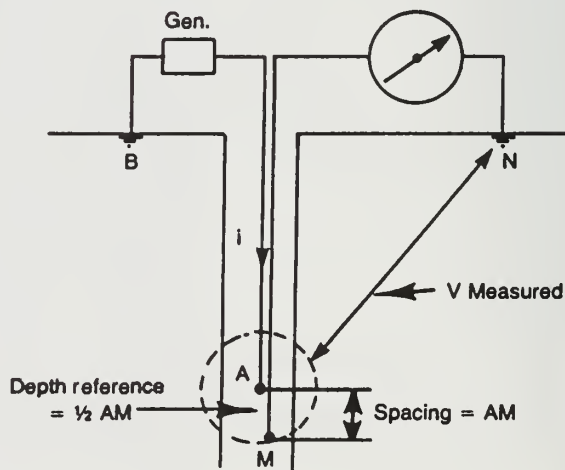


Figure A-10 Schematic diagram of normal logging system (from Helander 1983)

By utilizing two different configurations, MIL can produce varying depths of investigation. A comparison of the curves indicates the presence and magnitude of invasion of the borehole fluids into the formation. This enables a qualitative determination of the presence of permeability.

Spontaneous Potential Log (SPL)

Although the SPL system has one of the simplest physical configurations (fig. A-11), it is the result of many different factors. The SPL system records the change in naturally occurring potentials as a function of depth in the borehole. Two types of potential may contribute to the total Spontaneous Potential (E_{sp}): electrochemical (E_c) and electrokinetic (E_k). In well log analysis it is assumed that the measured SP response is due solely to the electrochemical component; therefore, $E_{sp} = E_c$.

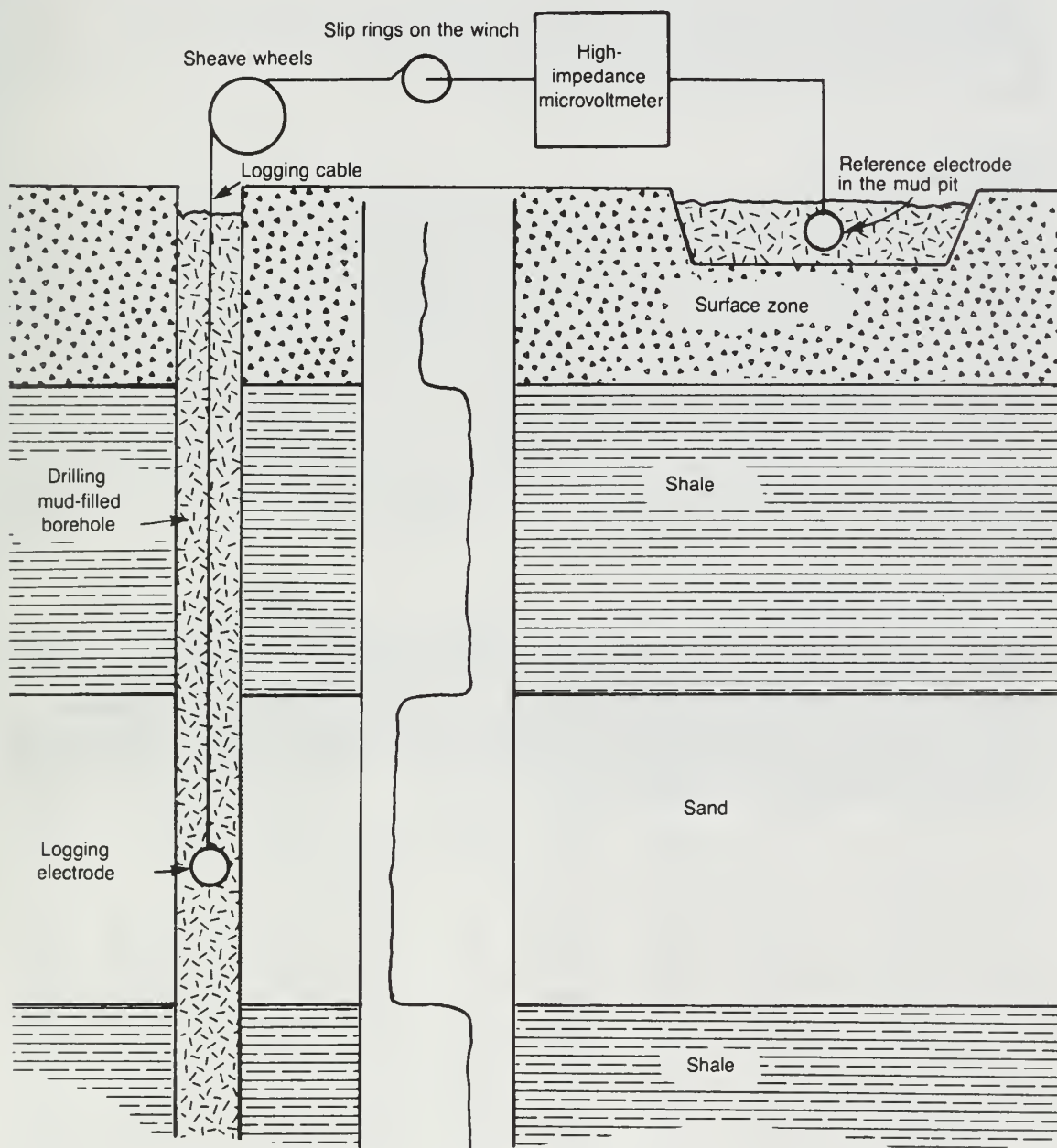


Figure A-11 Schematic diagram of spontaneous potential circuit.

The electrochemical potential is composed of the membrane potential (E_m) and the liquid junction potential (E_j). The membrane potential is caused by the separation of two fluids of different activity by a permeable, charged membrane. An analogy might be mud and formation water separated by shale. The liquid junction potential is the result of the contact of two solutions of differing activity, such as mud filtrate and formation water.

The E_{sp} is commonly written as

$$E_{sp} = -K_c \log(R_{mf}/R_w) \quad [A-9]$$

where $K_c = 61 + 0.133T(^{\circ}F)$
 R_{mf} = mud filtrate resistivity
 R_w = formation water resistivity.

This equation illustrates one application of the SPL system, namely R_w determination. The other applications relevant to this study are stratigraphic correlation and qualitative permeability estimation. The latter two are available through a consideration of the fluids and formation materials that give rise to the membrane and liquid junction potentials.

Temperature Log (TL)

The TL tool is simply a device that records the magnitude of the subsurface temperature. This is accomplished by incorporating into the tool's design a sensor element that provides ultrasensitive, stable readings over a suitable temperature range. A temperature probe in contact with the borehole environment transmits the thermal energy to the sensor, which converts the energy to a signal covered by the surface equipment to absolute and differential temperature. These data can be useful to injection/confining interval evaluation in several ways. First, in many injection wells the temperature of the injection fluid is anomalously cooler than the native formation temperature. This anomaly can often be detected by the TL, providing another method, along with the CSFL, for delineating the location of fluid infiltration into a formation. Also, data from the TL provide temperature values to be used in the selection of appropriate temperature-corrected fluid and formation parameters (such as fluid density and water compressibility) necessary in many calculations.

Radioactive Tracer Log (RATL)

The Radioactive Tracer Log tool "traces" the movement of a radioactive source. This is accomplished by injecting a short-lived, radioactive isotope (usually ^{131}I) from one section of the tool and recording its movement with a detection gamma ray package housed in another section of the tool. As the radioactive isotope decays, it emits gamma rays that are detected by the gamma ray apparatus. It is in this way that the position of the radioactive "slug" can be monitored as it makes its way through the cased and uncased borehole. Thus it is another technique for delineating fluid flow within the injection zone.

APPENDIX B. REDUCTION AND ANALYSIS OF GEOPHYSICAL LOG DATA

Improved modeling techniques (correction charts) were used to interpret the advanced suite of logs run during phase I and II. Use of these charts generally improved the accuracy of data obtained from the phase I and II logs, compared with logs run during WDW2 construction. Figures B-1, B-2, and B-3 are examples of the correction charts used. By using these modern logging tools and incorporating improved analytical techniques, we were able to determine more accurately the following hydrogeologic data on geologic materials constituting the injection interval: the formation's matrix-corrected CNL porosity ([POR]Ncor), matrix corrected BCS porosity ([POR]BCScor), cross-plotted porosity ([POR]xp), secondary porosity ([POR]sec), true resistivity (R_t), matrix lithology (MA), water saturation (SW), shale volume (Vsh), and qualitative permeability (k). These values, computed at 2-foot intervals throughout the injection zone, are reported in table B-1. The same parameters for geophysical logs run down WDW2 are reported in table B-2.

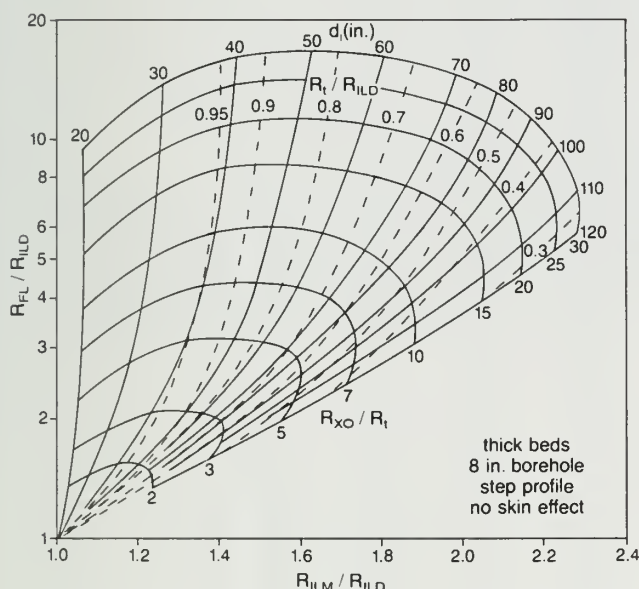


Figure B-1 (left) "Tornado" chart for Dual Induction-Focused Log analysis (Dresser Atlas 1981).

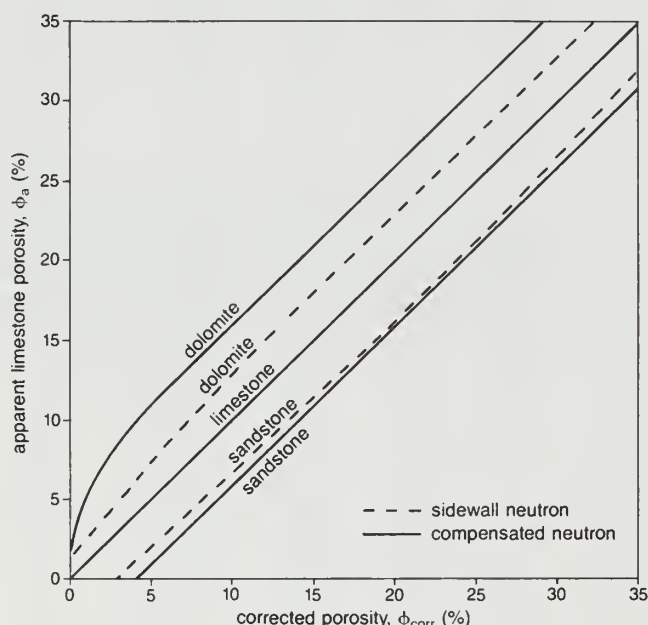


Figure B-2 Neutron porosity lithologic correction chart (Dresser Atlas 1981).

Table B-1 Data from geophysical logs run in the Devonian Observation Well

Depth GL (ft)	GR (API)	(POR) Nls (%)	(POR) ¹ Ncor (%)	t (sec)	(POR) ² BCScor (%)	(POR) ³ xp (%)	(POR) ⁴ sec (%)	RT ⁵ (ohm-m)	MA ⁶	SW ⁷ (%)	Vsh ⁸ (%)	k ⁹
2,434	28	4.3	4.3	53	3.8	4.3	0.5	50.0	LS	100	6.2	N
36	40	5.0	5.0	53	3.8	5.0	1.2	65.0	LS	100	15.4	N
38	35	12.0	12.0	60	8.8	10.0	3.2	20.0	LS	100	11.5	N
40	25	18.0	18.0	69	15.1	16.4	2.9	11.0	LS	100	3.8	N
42	30	19.0	19.0	69	15.1	16.7	3.9	7.0	LS	100	7.7	Y
44	25	23.8	23.8	77	20.8	21.7	3.0	5.0	LS	100	3.8	Y
46	22	22.6	22.6	76	20.1	21.1	2.5	4.8	LS	100	1.5	Y
48	23	23.0	17.0	70	18.2	18.2	0.0	7.0	DOL	100	2.3	N
50	30	16.0	10.0	62	12.7	12.0	0.0	10.0	DOL	100	7.7	N
52	30	17.5	11.5	57	9.3	9.7	2.2	16.0	DOL	100	7.7	N

Table B-1 *continued*

Depth GL (ft)	GR (API)	(POR) Nls (%)	(POR) ¹ Ncor (%)	t (sec)	(POR) ² BCScor (%)	(POR) ³ xp (%)	(POR) ⁴ sec (%)	RT ⁵ (ohm-m)	MA ⁶	SW ⁷ (%)	Vsh ⁸ (%)	K ⁹
54	22	19.0	13.0	60	11.3	11.7	1.7	13.0	DOL	100	1.5	N
56	17	22.0	16.0	62	12.7	13.3	3.3	9.0	DOL	100	0.0	N
58	20	20.6	14.6	63	13.4	13.6	1.2	10.0	DOL	100	0.0	N
60	28	21.8	15.8	61	12.0	12.7	3.8	9.0	DOL	100	6.2	N
62	27	24.6	18.6	65	14.8	15.6	3.8	7.0	DOL	100	5.4	Y
64	32	24.0	18.0	66	15.5	16.0	2.5	5.5	DOL	100	9.2	Y
66	22	25.5	19.5	70	18.2	18.5	1.3	4.8	DOL	100	1.5	Y
68	23	28.5	22.5	78	23.7	23.5	0.0	4.0	DOL	100	2.3	Y
70	17	29.2	23.2	82	26.5	26.0	0.0	3.3	DOL	100	0.0	Y
72	18	28.0	28.0	82	24.3	25.7	3.7	3.0	LS	100	0.0	Y
74	17	30.0	30.0	87	27.9	28.8	2.1	3.2	LS	100	0.0	Y
76	17	28.0	28.0	83	25.0	26.3	3.0	3.5	LS	100	0.0	Y
78	19	26.8	20.8	78	23.7	23.2	0.0	3.9	DOL	100	0.0	Y
80	17	26.3	20.3	77	23.0	22.6	0.0	4.4	DOL	100	0.0	Y
82	20	29.0	23.0	74	21.0	21.4	2.0	4.0	DOL	100	0.0	Y
84	24	23.5	17.5	71	18.9	18.5	0.0	4.6	DOL	100	3.1	Y
86	26	21.3	15.3	63	13.4	13.7	1.9	7.1	DOL	100	4.6	N
88	23	22.3	16.3	64	14.1	14.5	2.2	10.0	DOL	100	2.3	N
90	23	16.5	10.5	60	11.3	11.1	0.0	11.0	DOL	100	2.3	N
92	30	16.4	10.4	56	8.6	8.9	1.8	16.0	DOL	100	7.7	N
94	29	19.8	13.8	57	9.3	10.2	4.5	21.0	DOL	100	6.9	N
96	60	19.0	13.0	60	11.3	11.6	1.7	20.0	DOL	100	30.8	N
98	84	18.5	12.5	60	11.3	11.5	1.2	15.0	DOL	100	49.2	N
50	52	19.3	13.3	62	12.7	12.7	0.6	14.0	DOL	100	24.6	N
2	37	18.2	12.2	57	9.3	9.8	2.9	14.0	DOL	100	13.1	N
4	33	22.0	16.0	59	10.7	11.8	5.3	11.0	DOL	100	10.0	N
6	45	23.0	17.0	64	14.1	15.1	2.9	8.0	DOL	100	19.2	N
8	30	19.8	13.8	60	11.3	12.1	2.5	9.0	DOL	100	7.7	N
10	23	20.0	14.0	58	10.0	11.3	4.0	8.5	DOL	100	13.1	N
12	20	22.8	16.8	60	11.3	13.2	5.5	8.2	DOL	100	0.0	N
14	32	20.7	14.7	64	14.1	14.4	0.6	9.0	DOL	100	9.2	N
16	30	20.1	14.1	60	11.3	12.4	2.8	10.5	DOL	100	7.7	N
18	42	20.8	14.8	62	12.7	13.6	2.1	8.5	DOL	100	16.9	N
20	38	19.0	13.0	60	11.3	12.1	1.7	10.0	DOL	100	13.8	N
22	30	20.3	14.3	56	8.6	10.4	5.7	11.0	DOL	100	15.4	N
24	23	21.7	15.7	61	12.0	13.3	3.7	10.0	DOL	100	2.3	N
26	24	20.0	14.0	60	11.3	12.2	2.7	8.0	DOL	100	3.1	N
28	23	16.0	10.0	57	9.3	9.7	0.7	9.0	DOL	100	2.3	N
30	23	19.0	13.0	61	12.0	12.5	1.0	10.0	DOL	100	2.3	N
32	21	20.4	14.4	63	13.4	13.8	1.0	12.0	DOL	100	0.8	Y
2,534	33	22.5	16.5	60	11.3	12.2	5.2	10.0	DOL	100	10.0	Y
36	27	22.0	16.0	63	13.4	13.9	2.6	7.5	DOL	100	5.4	Y
38	28	24.3	18.3	65	14.8	15.5	3.5	6.5	DOL	100	6.2	Y
40	29	24.0	18.0	63	13.4	14.2	4.6	5.8	DOL	100	6.9	Y
42	35	17.3	11.3	61	12.0	11.8	0.0	7.1	DOL	100	11.5	N
44	40	16.5	10.5	59	10.7	10.6	0.0	9.0	DOL	100	15.4	N
46	42	21.3	15.3	63	13.4	13.7	1.9	8.5	DOL	100	16.9	Y
48	40	22.5	16.5	70	18.2	17.7	0.0	6.7	DOL	100	15.4	Y
50	40	20.6	14.6	66	15.5	15.1	0.0	6.7	DOL	100	15.4	Y
52	38	15.6	15.6	65	12.3	13.3	3.3	10.0	LS	100	13.8	N
54	29	8.6	8.6	57	6.6	7.4	2.0	20.0	LS	100	6.9	N

Notes for table B-1

1. Matrix corrected using figure B-2.
2. Matrix corrected using (POR)BCScor = $(t_{log} - t_{ma}) / (t_{f1} - t_{ma}) \times 1/C_p$,
 where $t_{ma} = 47.6 \times 10^{-6}$ sec/ft for limestone
 $t_{ma} = 43.5 \times 10^{-6}$ sec/ft for dolomite
 $t_{f1} = 189 \times 10^{-6}$ sec/ft
 t_{log} = transit time from log
 t_{ma} = transit time of the matrix
 C_p = constant for shale correction
 assume $C_p = 1$, since no shale correction is needed
3. See figure B-3
4. $(POR)_{sec} = (POR)_{Ncor} - (POR)_{BCScor}$
5. Since R_{ilm} and R_{ild} are approximately equal, a correction for invasion was not necessary; see figure B-1
6. Taken from $(POR)N$ versus t crossplot, figure B-3
7. Using $SW^2 = R_o/R_t = FR_w/R_t = R_w/(por)^2 R_t = R_w/(por) \times p^2 R_t$,
 from this, all zones were 100% water saturated.
8. Using $V_{sh} = (GR_{log} - GR_{cl}) / (GR_{sh} - GR_{cl})$,
 where GR_{log} = GR reading taken off log.
 GR_{cl} = GR reading from the zone with the lowest GR (10 @ 2,474 ft).
 GR_{sh} = GR reading from nearest shale zone (140 @ 2,242 ft).
9. Based on interpretation of MIL, Y denotes zone interpreted as having "significant" permeability. N denotes zone interpreted as not having "significant" permeability. MIL response is adversely affected by unevenness of borehole. A 4-arm caliper run indicated a very even borehole: 6.3-inch diameter from 2,424 to 2,524 ft, 6.2-inch diameter from 2,525 to 2,556 ft, and 5.8-inch diameter from 2,557 to 2,560 ft.

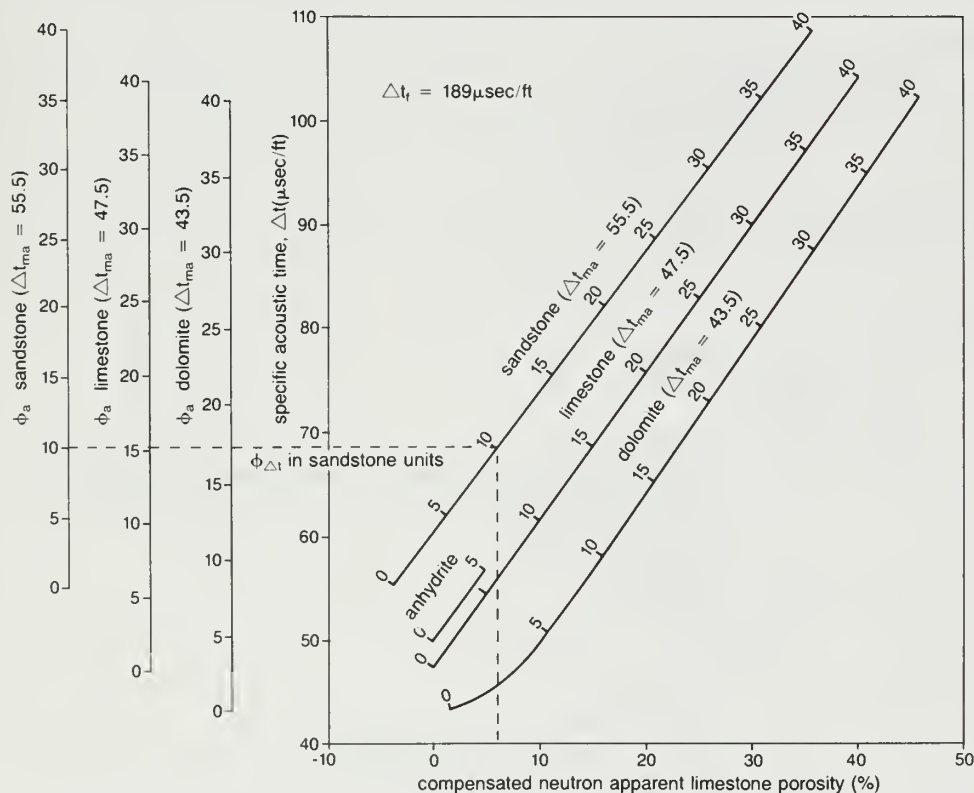


Figure B-3 Compensated Neutron Log and Borehole Compensated Acoustilog porosity crossplot (Dresser Atlas 1983).

Table B-2 Data from existing geophysical logs run in WDW2**

DEPTH GL (ft)	GR (API)	(POR) Nls (%)	(POR) Ncor (%)	(POR) t (sec)	(POR) BCScor (%)	(POR) xp (%)	(POR) sec (%)	RT (ohm-m)	MA	SW (%)	Vsh (%)	k
2582	26	8.1	8.1	63	10.9	10.1	0.0	30.0	LS	90	4.6	N
84	30	10.0	10.0	66	13.0	12.2	0.0	28.0	LS	77	7.7	N
86	34	15.0	15.0	71	16.5	16.3	0.0	17.0	LS	74	10.8	N
88	38	14.7	14.7	73	18.0	17.1	0.0	13.0	LW	81	13.8	Y
90	37	13.5	13.5	73	18.0	16.9	0.0	13.0	LS	82	13.1	Y
92	26	7.8	11.1	68	8.8	10.0	2.3	20.0	SS	100	4.6	Y
94	29	6.1	9.3	65	7.1	8.2	2.2	38.0	SS	98	6.9	N

* For explanation of column headings, see table B-1.

** All logs used for study were run during well installation, and all were from WDW2 except the sonic log (SL), which was from WDW1. Analysis methods used were those described in table B-1. All depths measured are from Kelly Bushing (KB), which is 12 ft above ground level.

A brief discussion of the computation of the correction factors and assumptions used to analyze the logging data follows. The analysis focused on data from intervals with higher relative permeabilities (as displayed by the Minilog and higher porosities from the CNL). These zones were 2,440 to 2,506 ft GL, 2,532 to 2,552 ft GL, and 2,572 to 2,582 ft GL as logged in DOW.

From figure B-4:

$m = 1.54$ or 1.76 ; this value is in close agreement with an assumed value of $m = 2$ for limestone (Ls) and dolomite (Dol).

From Minilog:

$R_m = 0.30$ ohm-m

Therefore, from figure B-5,

$R_{mf} = 0.23$ ohm-m and

$R_{mc} = 0.41$ ohm-m

From temperature log on WDW2,

Temperature @ 2,460 ft = 75.6° F.

Determine R_w :

Using Archie's Equation:

$F = a/(\text{por})^2 = R_o/R_w$ and

$SW^n = R_o/R_t$

where F = formation factor

R_o = true resistivity of the formation at 100% water saturation
(when $SW = 100\%$)

n = saturation exponent

a = constant

For limestone and dolomite,

Assume $a = 1$, $m = n = 2$

Therefore,

$F = 1/(\text{por})^2$

$SW^2 = R_o/R_t$

@ 2473 ft assume $SW = 100\%$

$SW^2 = R_o/R_t$

$R_o = R_t$

Assume $R_t = R_{ildcorr}$

Correct Rild for invasion, figure B-1
 $R_{ildcorr} = 3 \text{ ohm-m}$
 $R_t = 3 \text{ ohm-m}$
 $R_o = 3 \text{ ohm-m}$
 $R_o = F \times R_w = R_w / (\text{por})^2$
 $R_w = R_o \times (\text{por})^2$
 Porosity is needed; assume $\text{por} = \text{porxp of Sonic vs CNS}$
 $\text{porxp} = 28.7\%$
 Therefore,
 $R_w = 0.247 \text{ ohm-m}$

These factors were used to analyze the logging data reported in tables B-1 and B-2. Important hydrogeologic parameters of the injection zones are summarized in table B-3.

Table B-3 Summary of important formation characteristics

(POR)xp,ave = 16%	(POR)xp,max = 28.8%	(POR)xp,min = 8.9%
(POR)sec,ave = 1.98%	(POR)sec,max = 5.7%	
tave = $66.7 \times 10^{-6} \text{ sec/ft}$		
tmax = $87 \times 10^{-6} \text{ sec/ft}$		
tmin = $56 \times 10^{-6} \text{ sec/ft}$		
Rt,ave = 8.6 ohm-m	Rt,max = 21 ohm-m	Rt,min = 3 ohm-m
Vsh,ave = 8.05%	Vsh,max = 49.2%	Vsh,min = 0.0%
Formation lithology (based on 98 ft of "higher permeability, higher porosity" zone), 61.0% dolomite, 35.0% limestone, and 4.0% sandstone.		

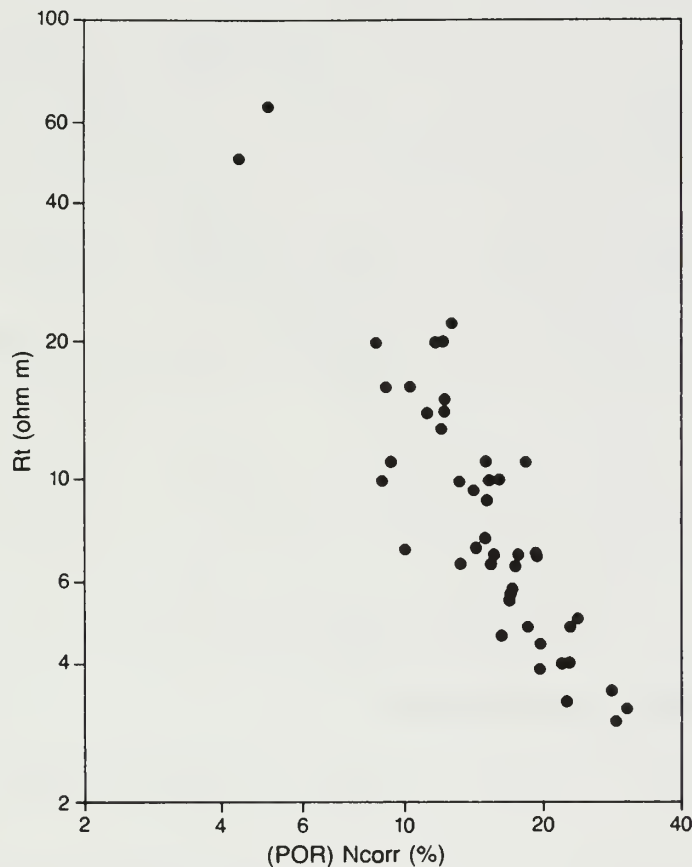


Figure B-4 Determination of the cementation factor.

After reviewing the data, we concluded that the host formation, the Bailey Limestone, is composed mainly of a clean dolomite with less than 20 percent shale throughout most of the interval logged. Since the Bailey Limestone is predominantly a dolomite, secondary porosity is always a consideration. A comparison of CNL and BCSL data suggests that secondary porosity may account for up to 10 percent of the total porosity. The intervals with higher relative permeability have a slightly higher secondary porosity and therefore a higher total porosity.

The entire interval is primarily 100 percent water saturated and has a fluid resistance of approximately 0.247 ohm-m. At a formation temperature of about 80°F and depth of 2,460 feet GL, the fluid composition is estimated to be approximately 24,000 ppm NaCl (fig. B-6).

As stated in chapter 3, one use of the core data was to verify data obtained from the geophysical logs. Figure B-7 shows good agreement between the two methods for porosity data. Figure B-8 indicates a close correlation between the two methods for true formation resistivity values (R_t); this correlation becomes more apparent when the equation used to derive water saturation (S_w) is reviewed,

$$S_w^2 = \frac{R_w}{(\text{por}) \times \frac{1}{R_t}} \quad (1/R_t)$$

S_w is shown to be indirectly proportional to the square root of R_t .

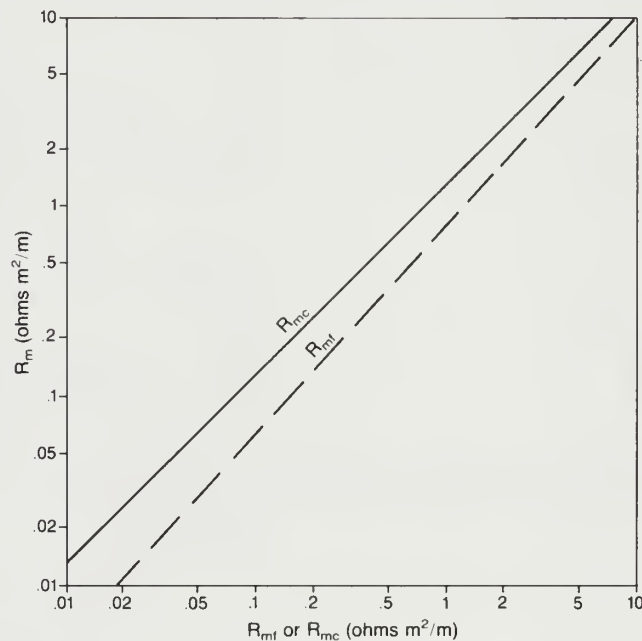


Figure B-5 R_m - R_{mf} - R_{mc} relationships (Gearhart).

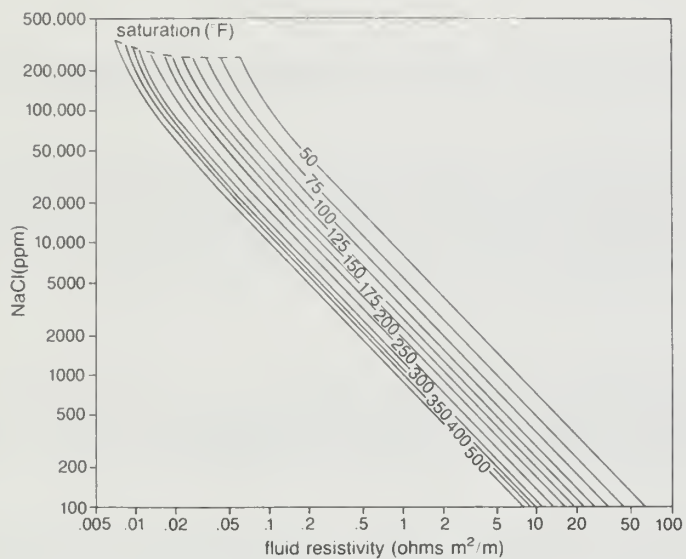


Figure B-6 NaCl concentration for different temperatures and fluid resistivities (Gearhart).

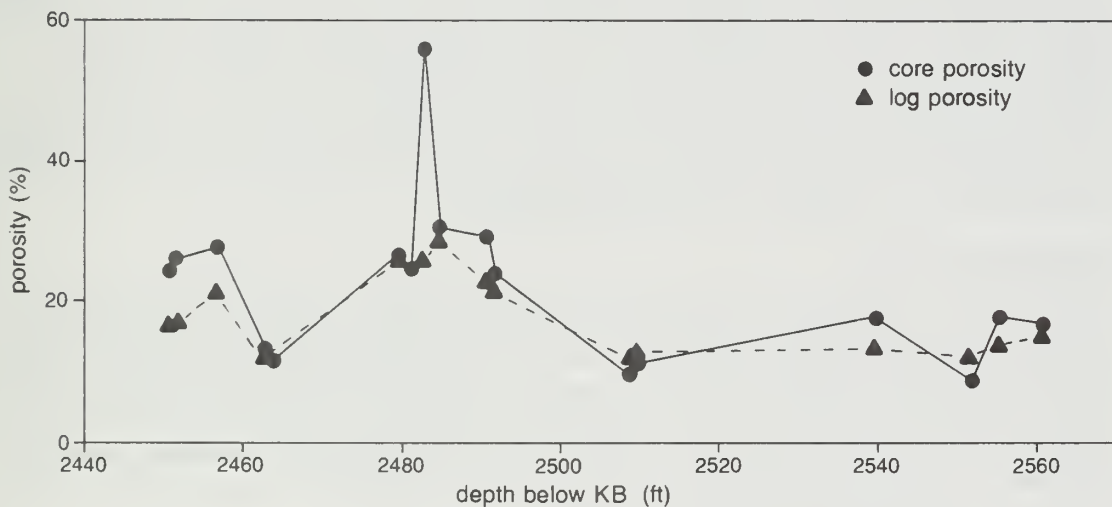


Figure B-7 Core porosity versus log porosity (phase I, cross-plotted porosity) for WDW2.

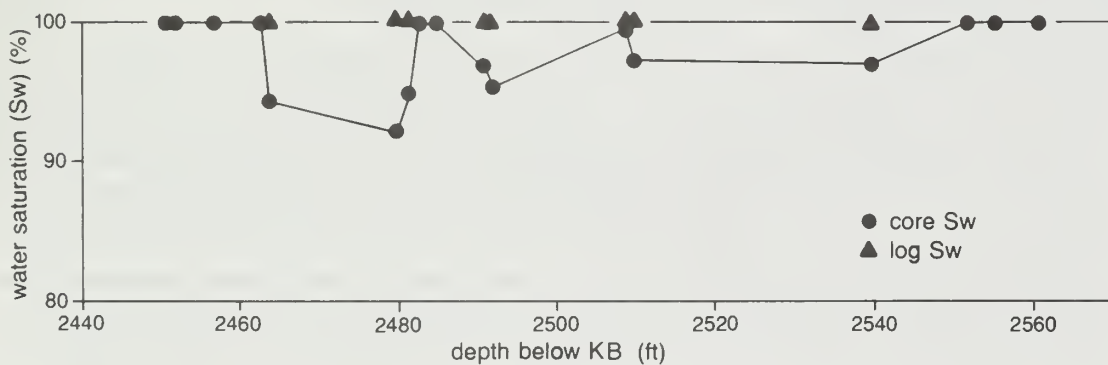


Figure B-8 Core water saturation versus log water saturation for WDW2 at designated depths. Log Sw obtained from phase I logging on the DOW.

APPENDIX C. BRUCITE FORMATION: PROPOSED MECHANISM OF FORMATION

The hydrogeologic site descriptions developed from phase I and phase II data (see chapter 3) differed from each other significantly; however, the reason for these differences was not readily apparent. To develop a hypothesis to explain the results and increase our understanding of the site hydrogeology, we conducted additional analyses.

Core Analysis

Analysis of sidewall core obtained during phase II was critical to the development of a hypothesis to explain the discrepancies described in chapter 3. Our core analysis included hydraulic testing, mineralogic analysis, and scanning electron microscope (SEM) investigation.

Hydraulic Testing

Hydraulic testing provided no hard evidence to resolve the discrepancies between phase I and phase II data. Injection zones 1, 2, and 3 (fig. C-1) had abnormally high porosities and permeabilities, but core analysis data did not agree with the results from the CSFL. First, the zone from 2,468 to 2,496 feet KB showed some injection potential. Core analysis indicated that at least some portions of this zone (e.g., 2,481.0 ft KB) were not permeable enough to allow fluid flow; however, most of this zone appeared to have sufficient permeability. Second, the core from 2539.5 feet KB seemed to have sufficient porosity and permeability to allow fluid flow, but the CSFL did not show any flow at this location. On the basis of CSFL results, zone 3 should have had the highest porosity and permeability, zone 2 the next highest, and zone 1 the lowest; however, core analysis indicated just the opposite. Therefore, the same discrepancies were encountered with core analysis as with geophysical logging.

Mineralogic Analysis

Cores were also analyzed for their mineralogical content. Brucite was found in the anomalous zones, and its presence was confirmed by x-ray diffraction (XRD) analysis. Brucite was not expected to be present in the injection system environment of WDW2. Brucite is normally found in veins in serpentine and basic rocks and as flakes scattered through some marbles (Pough 1953). Roy et al. (1989) analyzed a sample of the native formation brine taken from the DOW. The sample was vastly undersaturated with respect to brucite, $\text{Mg}(\text{OH})_2$. The ion activity product of Mg^{2+} and OH^- (brucite) in the sample was 3 percent of that predicted by the solubility of brucite determined by thermodynamic modeling (Roy 1987).

Mineralogical analysis conducted on a few representative samples of the original well cuttings collected during the drilling of WDW2 indicated that none of these samples contained brucite. Downhole geophysical data (table 2) also confirmed the absence of brucite and indicated that prior to injection, the disposal horizon was predominantly dolomitic.

Apparently the injected waste, which consisted of a number of organics in a very alkaline ($\text{pH} > 12$), brinelike solution, created an environment in the injection system that promoted the formation of brucite. Although the waste had a component of Mg^{2+} , dolomite (from injection zone rock) was the most likely source of Mg^{2+} for two reasons. First, an increase in the brucite concentration accompanied a corresponding decrease in the dolomite concentration (fig. C-2). Second, the porosity throughout the injection zone subsequent to brucite precipitation should have been lower than the original (pre-injection) porosity if the brine was the source of the Mg^{2+} . Data from log analysis did not indicate a decrease in porosity. Therefore, on the basis of available data, the most plausible hypothesis is that dissolution of dolomite from injection zone rock released magnesium, which then combined with the OH^- in the waste stream to form brucite.

If this hypothesis is correct, the zones that originally had the highest porosities and permeabilities would accept the greatest volume of waste fluid and thus would show the highest brucite con-

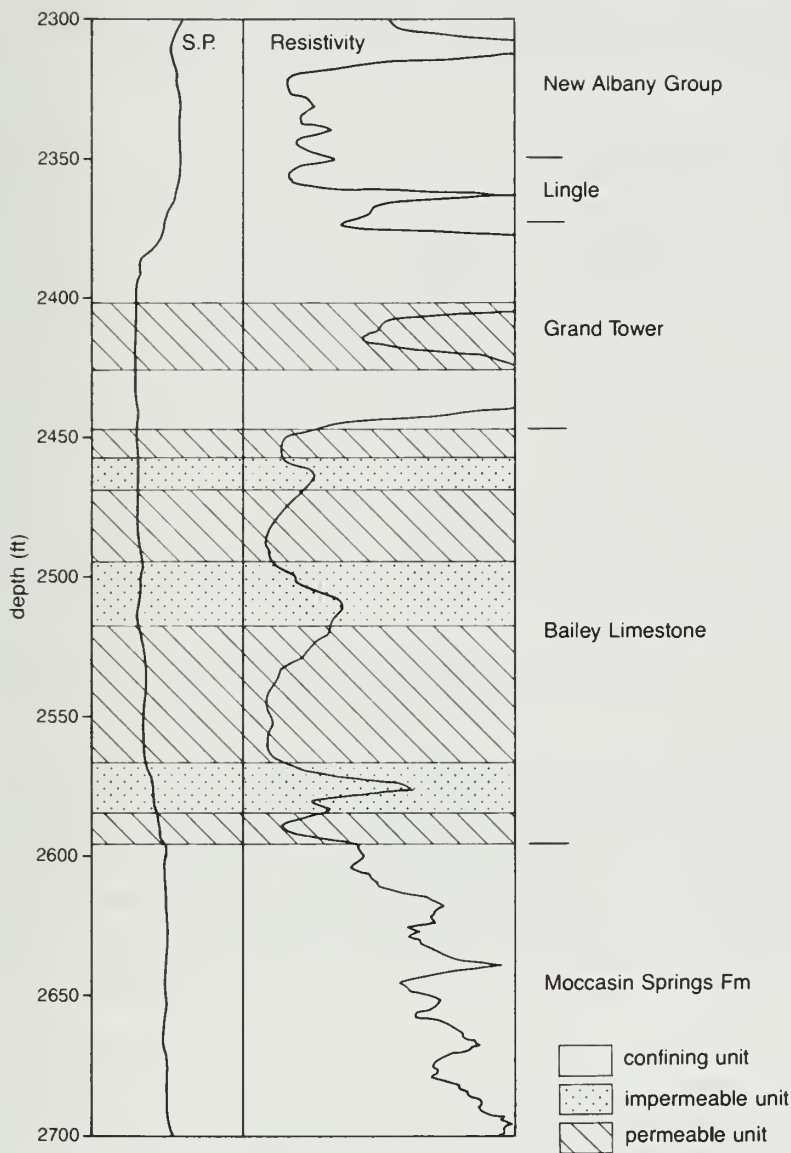


Figure C1 Injection system in WDW2 indicating permeable and nonpermeable zones delineated with the aid of geophysical logging.

centrations. Table C-1 gives porosity and brucite percentages for the cored intervals. For comparison, the Sidewall Neutron Log run during well construction was used to obtain original porosity data. Five intervals were identified and ranked on the basis of porosity characteristics. Zones with higher average porosity were given a higher porosity ranking.

Table C-2 shows the five highest ranked zones with their corresponding average brucite concentrations, air permeabilities (k_a), and percentages of total flow (from the CSFL). These data indicate that the presence of brucite has a profound effect on fluid movement. However, laboratory permeability values for zones with higher brucite concentrations were greater than the values for zones with lower brucite concentrations, and laboratory porosity values for zones with higher brucite concentrations were similar to the pre-injection porosities.

In an attempt to explain this finding, we reviewed the analytical procedure used to determine permeability. Laboratory permeabilities were performed on dried samples. If the cations (Na+) that may have been lodged between the brucite layers were lost during drying, a volume reduction in brucite would occur. Therefore, in samples with high brucite concentrations, abnormally high permeability measurements could be encountered, and the cores at 2,479.5, 2,481.0, 2,490.5, 2,491.5, 2,439.5, and 2,560.5 ft KB should have higher permeabilities than expected. These depths corresponded to the zones in which discrepancies were noted between core and CSFL analysis. The anomalously high core permeabilities appeared to be the result of a volume reduction of the brucite upon drying.

Table C-1 Core porosities and brucite concentrations

Depth (KB) (ft)	Original porosity (%)	Porosity ranking	Brucite (wt %)
2450.5	23	3	9
2451.5	25	3	21
2456.5	24	3	0
2462.5	17	-	18
2463.5	19	-	22
2479.5	30+	1	45
2481	30+	1	45
2484.5	30+	1	12
2490.5	30+	1	39
2491.5	30	1	31
2508.5	18	-	26
2509.5	19	-	35
2539.5	27	2	41
2551.5	20	2	38
2555	24	4	7
2556.5	28	2	45
2560.5	28	2	45
2572.5	4	-	2
2573.5	5	-	0
2588.5	15	5	0
2605	6	-	0
2606	6	-	0

Table C-2 Effect of brucite concentration on total flow

Porosity ranking	Brucite (wt %)	Ave ka (md)	Total Flow (vol %)
1	40	1	0
2	42.3	0.1	0
3	10	0.6	14
4	7	0.06	36
5	0	0.02	50

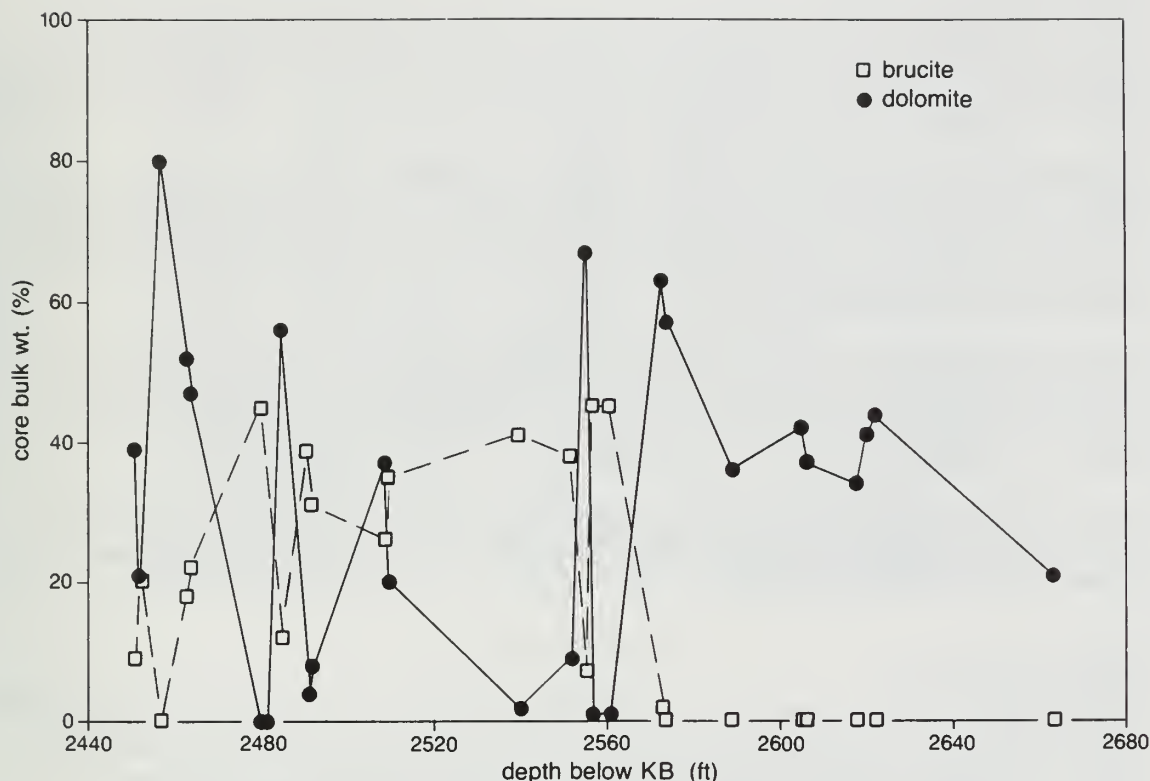


Figure C-2 Core composition: dolomite and brucite in WDW2.

On the basis of available data, this explanation appeared to be reasonable, but two problems with the results remained unresolved: (1) the cores at 2,462.5, 2,463.5, 2,508.5, and 2,509.5 ft KB showed slightly higher than expected brucite concentrations (approximately 25% brucite), and (2) the core at 2,484.5 ft KB had an extremely high core permeability ($k_a = 14.97$ md) but a relatively low concentration of brucite (12%). Scanning Electron Microscope (SEM) analysis was performed on selected core samples in an attempt to resolve these discrepancies, gain additional information on the factors affecting fluid flow, and confirm some of the assumptions inherent in the previous discussion.

SEM Analysis

Eight cores chosen for analysis represented the three injection zones and the major areas where anomalous results were encountered by various analytical procedures (e.g., core analysis, CSFL, and standard geophysical logging). Generally, two magnifications were used per sample: approximately 100x to show the general porosity type and any large-scale features such as fracturing, and 1,000x to show the pore geometry and other small-scale features. Although a detailed discussion of SEM analysis results is beyond the scope of this project, a few generalizations can be made to help resolve the discrepancies noted.

SEM analysis was performed on dried samples; therefore, the effect of cation adsorption into the crystal lattice of brucite was assumed to be unrecognizable.

Data from historical and phase I logging indicated that the core at 2,484.5 ft KB should have had a high injection potential. When the CSFL indicated a lack of fluid flow into this zone, we reasoned—on the basis of core analysis—that the lack of flow into this zone could have been due to the presence of brucite in the sample. However, only 12 percent brucite was found in this core,

compared with an average of 40 percent in the other adjacent samples. Another explanation for the lack of flow was obviously needed. Figures C-3 and C-4 indicate that the predominant type of porosity in this sample is fracture porosity. Figure C-3 shows that the fracturing is discontinuous on a large scale. Figure C-4 is a close-up of the fracture depicted in figure C-3. The platy material on the fracture walls was interpreted to be brucite.

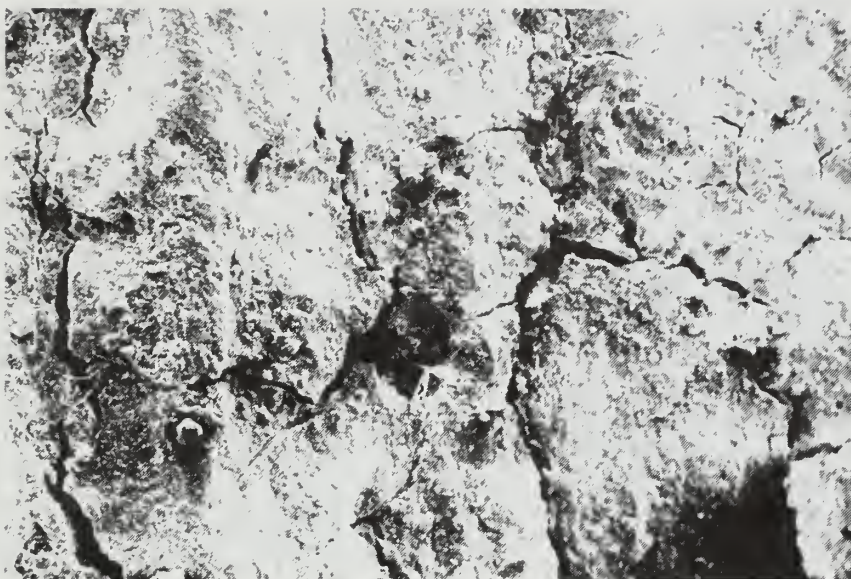
Another sample selected was the core at 2,479.5 feet KB, which is from the same zone as the previous sample. No fractures can be seen in figures C-5 and C-6, and the crystals and matrix of the sample are coated. Core analysis indicated that this sample was 45 percent brucite, so this coating was assumed to be brucite. With such a widespread occurrence of brucite, the decrease in permeability seems reasonable.

A sample from the uppermost injection zone (2,456.5 ft KB) (figs. C-7 and C-8) is free of the coating present in the previous samples. Core analysis indicated that this sample had no brucite, which agrees with SEM analysis and the supposition that brucite has not affected fluid flow in the uppermost injection zone.

The hypothesis used to resolve the brucite formation explains the available data and was confirmed to some extent by SEM analysis. But to evaluate this hypothesis more fully, additional work beyond the scope of this project is necessary.

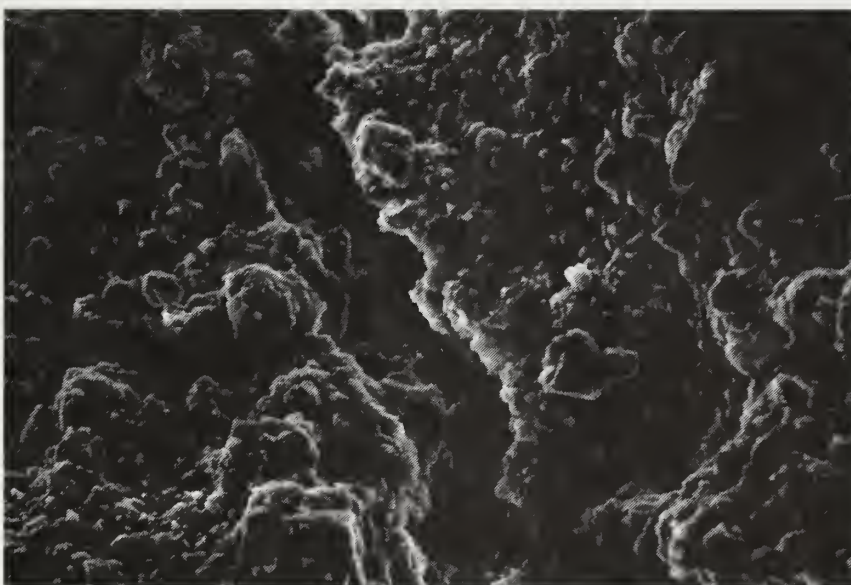
Additional Research

To support the hypothesis developed regarding brucite formation, the following work should be done. A hydrogeochemical investigation of the Velsicol waste stream and the Devonian limestone, similar to that of Roy et al. (1989), should be conducted. Core from the DOW could be used in this type of investigation. This type of work would help define the conditions favorable for brucite formation.



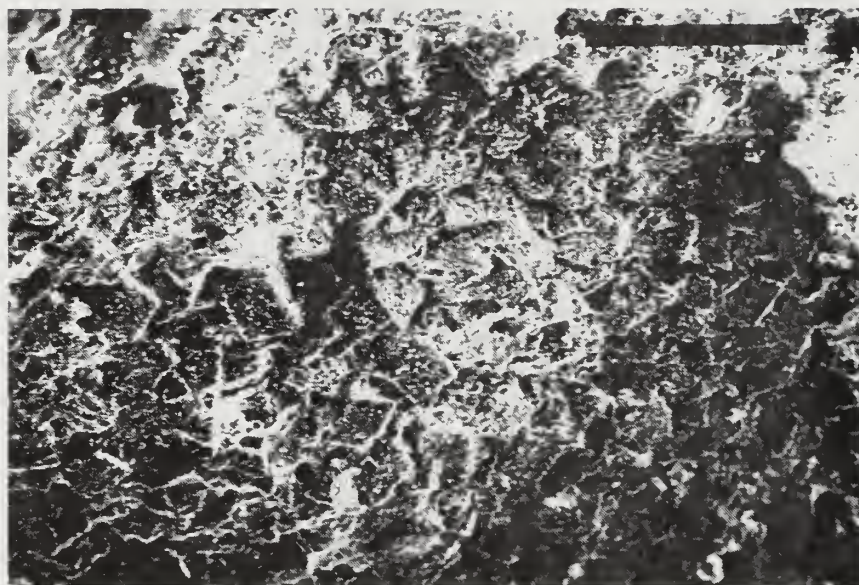
0.5mm

Figure C-3 SEM photograph of core at 2,484.5 feet KB (x58.5).



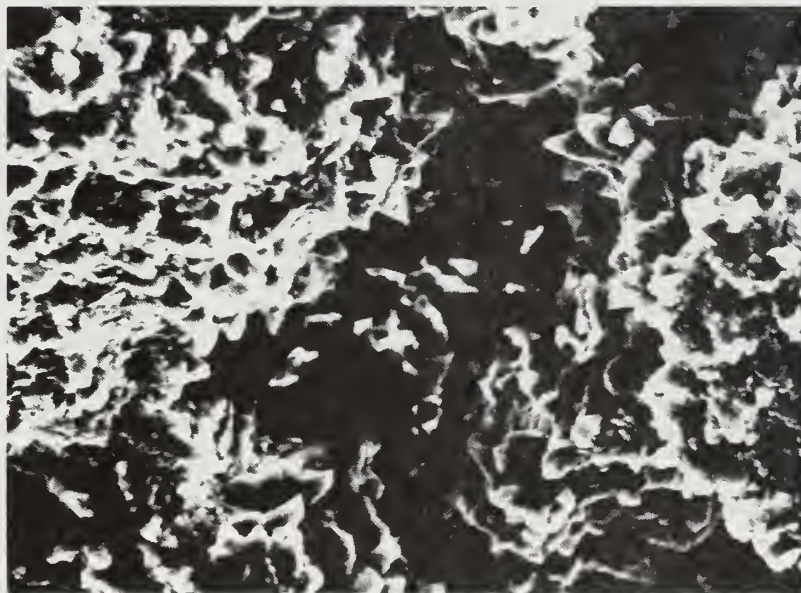
20 μ m

Figure C-4 SEM photograph of core at 2,484.5 ft KB (x 1,050).



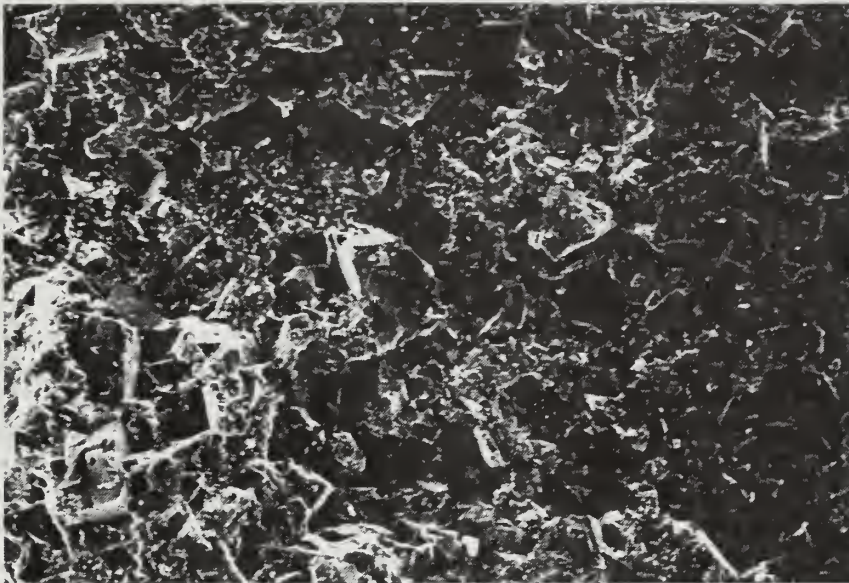
0.5mm

Figure C-5 SEM photograph of core at 2,479.5 KB (x80).



20 μm

Figure C-6 SEM photograph of core at 2,479.5 KB (x1,080).



200 μm

Figure C-7 SEM photograph of core at 2,456.5 KB (x113).



20 μm

Figure C-8 SEM photograph of core at 2,456.5 feet KB (x1,160).

APPENDIX D. SENSITIVITY ANALYSIS

A rigorous sensitivity analysis as described by Yeh (1986) was not conducted. The sensitivity analysis conducted for this project involves the variation of significant parameters and the effect of this variation on head buildup (Δh) at the DOW, the parameter of interest. The significance of various parameters (injection rate, hydraulic conductivity, etc.) was observed during the validation and calibration stages of modeling. On the basis of these observations, sensitivity analysis was conducted for the following parameters: boundary conditions, injection rate, rock compressibility, fluid compressibility, hydraulic conductivity, and anisotropy.

Throughout this phase of the project, the same conceptual model as depicted in figure D-1 was used unless otherwise noted. The injection system was modeled using cylindrical coordinates with 60 nodes in the r-direction and 22 nodes in the z-direction. A no-flow boundary condition was applied at the upper and lower boundaries, while an aquifer influence function (AIF) condition was applied at the radial boundary.

Boundary Conditions

Boundary conditions (BC) are the most difficult and critical issue in the development of a conceptual model for a numerical modeling study and must be selected carefully (Franke and Reilly 1987). In all cases, the upper and lower boundaries were modeled as no-flow boundaries.

The type and distance of the radial boundary from the injection well were varied. For the purposes of comparison, VELS14I was considered the baseline run. Five other runs were made in order to note the effect of the boundary condition on head buildup at various locations within the injection system. Table D-1 summarizes the types of boundary conditions and results.

The results of VELS14G2 indicate that the no-flow boundary condition did not cause an increase in head buildup at the DOW during the 14-day period investigated, but a slight increase in Δh occurred at the radial boundary. For VELS14H, the radial boundary is located farther from the injection well than in VELS14G2; no Δh was observed at the radial boundary. These two runs and the other runs of the VELS14 series show that the radial boundary exerted no real influence on the head buildup at the DOW ($r = 505.95$ m) during the time period investigated.

VELS14I and VELS14I2 indicate the effect of the intrinsic permeability of the aquifer influence region (k_{AIF}). A reduction in k_{AIF} may increase the Δh observed at the radial boundary. Although

Stratigraphy	elev. above reference (m)	Hydrogeologic Role	K (m ²)
New Albany Group, Lingle and Grand Tower Limestones	128.29	upper confining unit	4.35×10^{-21}
Bailey Limestone	55.76	upper injection zone	2.51×10^{-11}
	52.71		2.30×10^{-14}
	24.06	middle injection zone	9.65×10^{-11}
Moccasin Springs Formation	22.23		2.99×10^{-14}
	14.31	lower injection zone	7.72×10^{-11}
	11.28	basal confining unit	9.68×10^{-14}
	0		

Figure D-1 Conceptual model 1 of the injection system.

Table D-1 Effect of boundary conditions on head buildup

Run	No. of r-nodes	Radius (m)	Type ¹ of BC	k_{AIF}^2 (m ²)	Δh @ DOW ³ (m)	Δh @ radial boundary (m)
VELS14I	60	15870.9	AIF	1.00×10^{-11}	1.28	0.01 t = 14.0 days
VELS14G2	60	15870.9	NF	—	1.28	0.02 t = 7.16 days
VELS14H	60	35703.0	NF	—	1.28	0.00 t < 14.0 days
VELS14I2	60	15870.9	AIF	1.00×10^{-12}	1.28	0.02 t = 14.0 days
VELS18H2	60	15870.9	AIF	1.00×10^{-11}	1.25	—
VELS18J	50	2090.8	AIF	1.00×10^{-11}	0.75	—

Notes: (1) AIF = aquifer influence boundary condition; NF = no-flow boundary condition; (2) k_{AIF} = intrinsic permeability of aquifer influence region; (3) all values given at t = 14.00 days.

not shown in Table D-1, if k_{AIF} were reduced, the cumulative fluid outflow via the AIF boundary also would be reduced. In this case, the cumulative fluid outflow across the radial boundary, in terms of the total volume of fluid injected, was reduced from 3.0 percent (VELS14I) to 0.69 percent (VELS14I2) when k_{AIF} was reduced one order of magnitude.

Over longer periods, the radial boundary would certainly influence the head buildup at the DOW. Thus the use of an AIF BC appeared to be a better choice for the radial boundary, especially when the model is used as a tool to predict long-term (30-year) effects of injection upon the system. In addition, the regional hydrogeologic investigation covered a 10-mile (16,000-m) radius from the well; thus use of a radius larger than 10 miles was considered speculative.

Two runs from the VELS18 series are included to show the effect of the position of the AIF BC. The conceptual model for the VELS18 series is more complex than the VELS14 series and includes a thicker sequence of geologic materials (fig. D-2). The results from VELS18H2 are in agreement with VELS14I, allowing for a slightly lower head buildup for VELS18H2 due to the greater thickness of compressible geologic materials. For VELS18J, distance to the radial

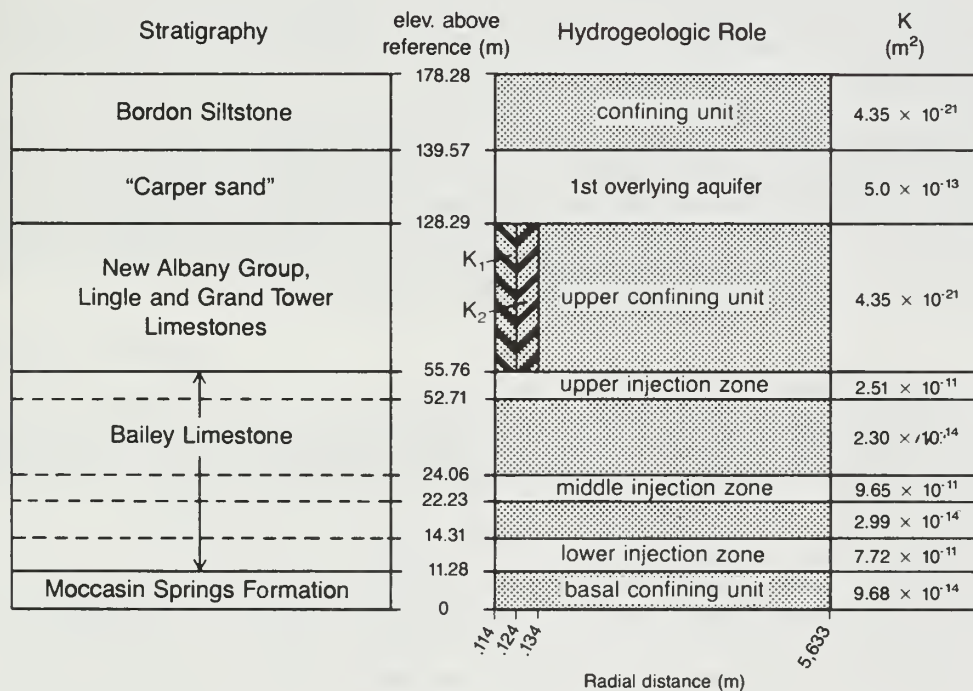


Figure D-2 Conceptual model 2 of the injection system.

boundary was much closer than for VEL18H2. In addition, the head buildup at the DOW was much lower, although k_{AIF} is the same for both runs. For both VEL18H2 and VEL18J, the AIF zone is more transmissive than the inner discretized zone; therefore, decreasing the radial distance of this zone from the injection well allows fluid to move more readily and with less head buildup. The results of VEL18H2 and VEL18J indicate the effect of the location of the boundary and the need to properly define the intrinsic permeability of the aquifer influence region.

Injection Rate

Three runs were made to investigate the effect of the injection rate upon head buildup at the DOW. VEL14I ($q = 1.820 \times 10^{-2} \text{ m}^3/\text{sec}$) is the baseline run. For VEL15A, the injection rate was increased 10 percent, $q = 2.002 \times 10^{-2} \text{ m}^3/\text{sec}$. For VEL15B, the injection rate was decreased 10 percent to $1.638 \times 10^{-2} \text{ m}^3/\text{sec}$. Figure D-3 shows the Δh at the DOW with time. Increasing the q by 10 percent resulted in a 10.2-percent increase in Δh . The increase in Δh was noticeable after several hours of injection. In a similar fashion, a 10-percent reduction in the injection rate resulted in a 9.4-percent decrease in Δh . This decrease was also noticeable after several hours of injection. Round-off error for the percentage increase/decrease of Δh was responsible for these values not being equal and the deviation of these values from 10 percent as predicted by Darcy's Law.

Rock Compressibility

Storativity may be defined according to the following equation (Lohman 1972).

$$S = \gamma b(\beta + \alpha/n) \quad [D-1]$$

where S = storativity (-)
 n = porosity (-)
 γ = unit weight of fluid (kg/m^3)
 b = aquifer thickness (m)
 β = fluid compressibility (Pa^{-1})
 α = rock compressibility (Pa^{-1})

Rock compressibility (α) is one of two major components of storativity. For HST3D, Kipp (1987) indicated that it is more convenient to use rock and fluid compressibility than a storativity term, since fluid density (i.e., unit weight) may be variable.

Three runs were used to investigate the effects of rock compressibility. VEL14I was the baseline run with $\alpha = 4.50 \times 10^{-10} \text{ Pa}^{-1}$. For VEL15C, rock compressibility was reduced 10 percent to $\alpha = 4.05 \times 10^{-10}$. For VEL15D, α was increased 10 percent, $\alpha = 4.95 \times 10^{-10}$. Figure D-4 shows the results of the runs. Decreasing α by 10 percent resulted in a 1.6-percent increase in Δh at the DOW. Similarly, a 10-percent increase in α resulted in a 1.6-percent decrease in Δh . The increase and decrease in Δh were evident after several hours of injection.

Fluid Compressibility

Fluid compressibility (β) is the other major component of storativity. VEL14I, VEL15G, and VEL15H were used to investigate the effect of varying fluid compressibility on the head buildup at the DOW. For VEL14I, $\beta = 4.00 \times 10^{-10} \text{ Pa}^{-1}$. A 10-percent reduction in β was used for VEL15G, $\beta = 3.60 \times 10^{-10}$. For VEL15H, β was increased to $\beta = 4.40 \times 10^{-10}$.

Figure D-5 shows the results from these runs. Decreasing β did not cause any change in Δh . Increasing β produced a negligible change in Δh , which was probably due to round-off error. The lack of sensitivity of Δh to β can easily be explained. Referring back to equation D-1, one can see that S is proportional to the quantity $(\beta + \alpha/n)$. For the situation investigated here, α/n was approximately 8 times larger than β ; thus minor changes in β did not affect S and did not affect Δh .

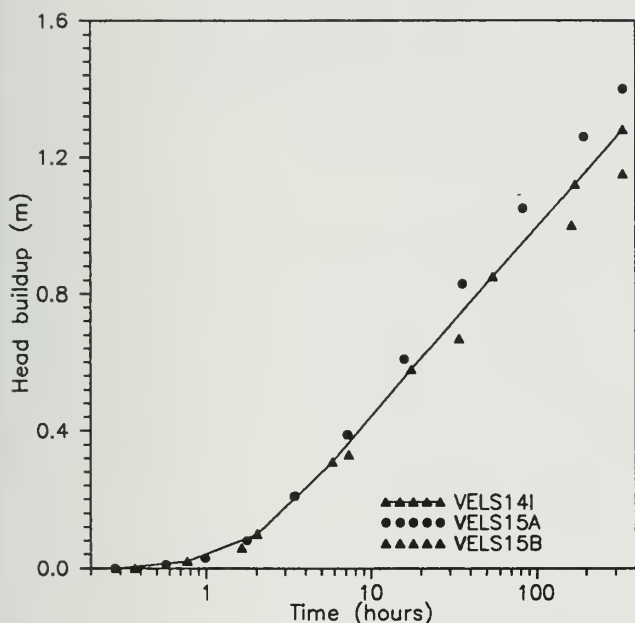


Figure D-3 (left) Sensitivity analysis: effect of injection rate.

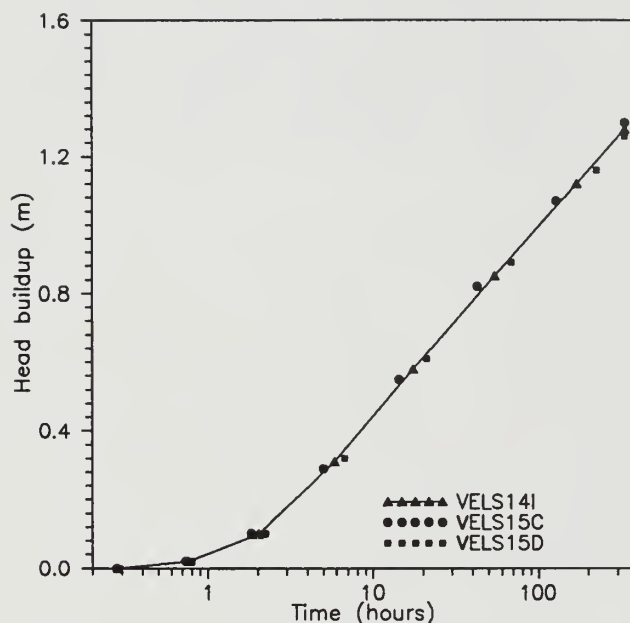


Figure D-4 Sensitivity analysis: effect of rock compressibility.

Hydraulic Conductivity

The results from VEL14I, VEL15I, and VEL15J were used to demonstrate the effect of hydraulic conductivity on Δh . For VEL15I, the hydraulic conductivity of each of the 7 layers was reduced by 10 percent, compared with the hydraulic conductivity values used for VEL14I. Similarly, the hydraulic conductivity values used in VEL15J were all increased by 10 percent.

Figure D-6 shows the results for all runs. As expected, decreasing the hydraulic conductivity resulted in an increase in Δh observed at the DOW. A 10-percent decrease in hydraulic conductivity resulted in a 9.4-percent increase (within round-off error of 10 percent) in Δh at the DOW. Increasing the hydraulic conductivity by 10 percent caused only a 7-percent decrease in Δh at the DOW. The deviation of this value from 10 percent, as predicted by Darcy's Law, is due to the KAIF. The KAIF for VEL15J was not increased from the value used for VEL14I, causing the head build-up within the inner aquifer region to be higher than anticipated.

Anisotropic Conditions

To this point, isotropic conditions have been assumed. On the basis of the hydrogeologic and geophysical tests conducted at the site during the project, it was not possible to establish the predominance of isotropic or anisotropic conditions. Thus, this series of runs was conducted to investigate the effect of this assumption.

Two runs were used to investigate this effect, VEL14I and VEL15K. Isotropic conditions (i.e., $k_r/k_z = 1$) were assumed for VEL14I. For VEL15K, k_z was decreased so that k was 10 times greater in the radial direction than in the vertical direction (i.e. $k_r/k_z = 10$). Figure D-7 indicates that under anisotropic conditions, Δh observed at the DOW was lower by approximately 2 percent than under isotropic conditions. Thus, if the assumption of isotropic conditions is not correct, the hydraulic conductivity of the geologic materials determined during model calibration may need to be reduced by nearly 2 percent.

Summary of Sensitivity Analysis

On the basis of the preceding sensitivity analysis, injection rate and hydraulic conductivity were the most sensitive input parameters. That is, a given change in injection rate or hydraulic conductivity produced the largest change in Δh observed at the DOW. The type of boundary condition and the location of the boundary can also have a significant effect on the head buildup predicted by the model. In decreasing order, the most sensitive parameters were injection rate and hydraulic conductivity, rock compressibility, anisotropy, and fluid compressibility.

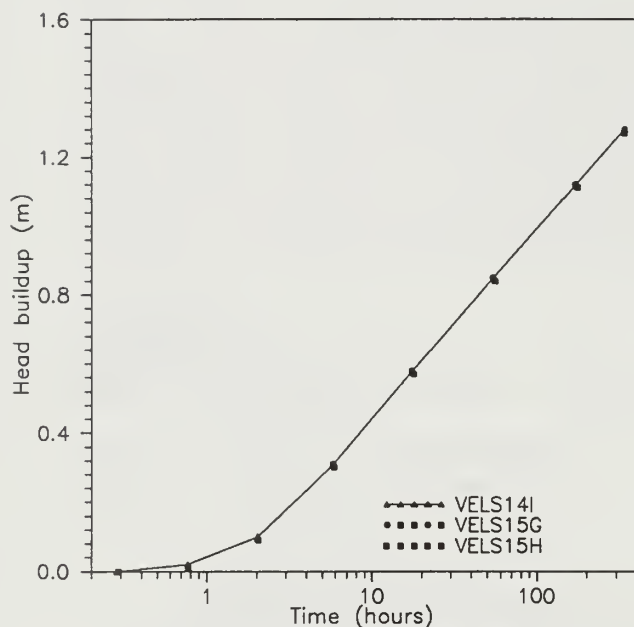


Figure D-5 (left) Sensitivity analysis: effect of fluid compressibility.

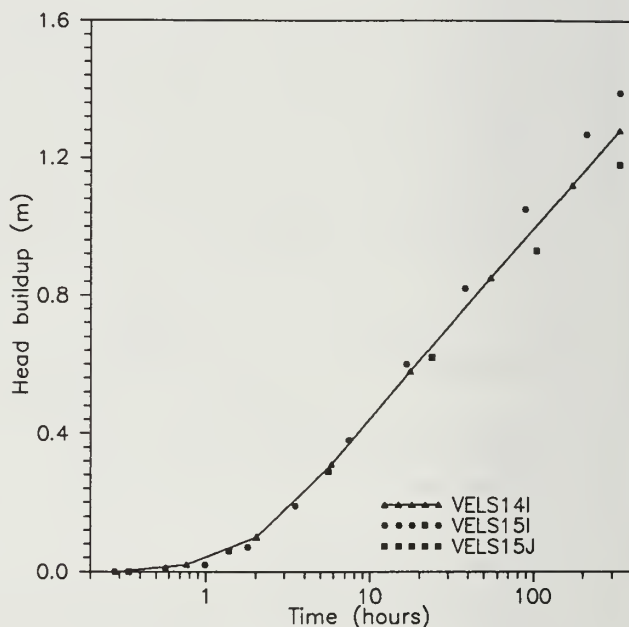


Figure D-6 Sensitivity analysis: effect of hydraulic conductivity.

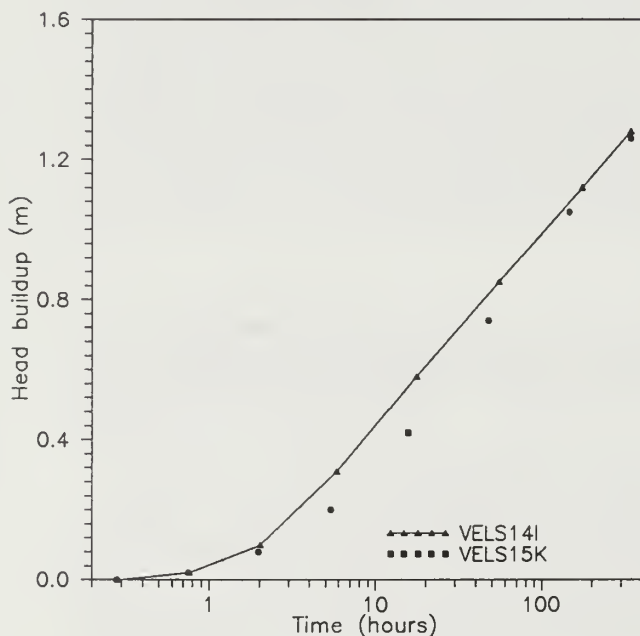


Figure D-7 Sensitivity analysis: effect of anisotropy.

HECKMAN
BINDERY INC.



JUN 97

Bound-To-Pleas[®] N. MANCHESTER,
INDIANA 46962

